FOR UNRESTRICTED DISTRIBUTION
DATE _____ WEC

Westinghouse Energy Systems

ERRATA

WCAP-12811

Page 4-8

Figure 4-2 is a simplified version of earlier drawings of the surveillance capsule design; e.g., Figure 2-5 on pages 2-7/2-8 of WCAP-8783, Reference 1 to this report. In the simplification process, the actual positions of the three thermal monitors and neutron dosimeters were inadvertently omitted from Figure 4-2. See the earlier drawings for the actual positions.

Page 6-26

The time averaged exposure rate for the lowest energy range of the neutron spectrum in Table 6-9 has an error in its exponent. The correct value for the flux is 8.17×10^{10}.

WESTINGHOUSE CLASS 3

WCAP-12811

ANALYSIS OF CAPSULE X FROM THE PACIFIC GAS AND ELECTRIC COMPANY DIABLO CANYON UNIT 2 REACTOR VESSEL RADIATION SURVEILLANCE PROGRAM

E. Terek
S. L. Anderson
L. Albertin

December 1990

Work Performed Under Shop Order LSFP-106

Prepared by Westinghouse Electric Corporation
for the Pacific Gas and Electric Company

Approved by: T. A. Meyer

T. A. Meyer, Manager
Structural Reliability
and Life Optimization

WESTINGHOUSE ELECTRIC CORPORATION
Nuclear and Advanced Technology Division
P.O. Box 2728
Pittsburgh, Pennsylvania 15230-2728

PREFACE

This report has been technically reviewed and verified.

	Reviewer	
Sections 1 through 5, 7, and 8	J. M. Chicots	J. M. Chicots
Section 6	E. P. Lippincott	E. P. Lippincott

TABLE OF CONTENTS

LIST OF ILLUSTRATIONS

LIST OF ILLUSTRATIONS (Cont)

LIST OF ILLUSTRATIONS (Cont)

LIST OF ILLUSTRATIONS (Cont)

LIST OF TABLES

LIST OF TABLES (Cont)

LIST OF TABLES (Cont)

SECTION 1.0
SUMMARY OF RESULTS

The analysis of the reactor vessel materials contained in surveillance Capsule X, the second capsule to be removed from the Pacific Gas and Electric Company Diablo Canyon Unit 2 reactor pressure vessel, led to the following conclusions:

- The capsule received an average fast neutron fluence (E > 1.0 MeV) of 8.87×10^{18} n/cm^2 after 3.11 EFPY of plant operation.

- Irradiation of the reactor vessel intermediate shell plate B5454-1 Charpy specimens, oriented with the longitudinal axis of the specimen parallel to the major working direction (Longitudinal Orientation), to 8.87×10^{18} n/cm^2 (E > 1.0 MeV) resulted in 30 and 50 ft-lb transition temperature increases of 101 and 121 °F, respectively.

- Irradiation of the reactor vessel intermediate shell plate B5454-1 Charpy specimens, oriented with the longitudinal axis of the specimen perpendicular to the major working direction (Transverse Orientation), to 8.87×10^{18} n/cm^2 (E > 1.0 MeV) resulted in a 30 and 50 ft-lb transition temperature increase of 99 °F.

- Weld metal Charpy specimens irradiated to 8.87×10^{18} n/cm^2 (E > 1.0 MeV) resulted in 30 and 50 ft-lb transition temperature increases of 204 and 214 °F, respectively.

- Irradiation of the reactor vessel weld Heat-Affected-Zone (HAZ) metal Charpy specimens to 8.87×10^{18} n/cm^2 (E > 1.0 MeV) resulted in 30 and 50 ft-lb transition temperature increases of 252 and 247 °F, respectively.

- Irradiation of the intermediate shell plate to 8.87×10^{18} n/cm^2 (E > 1.0 MeV) resulted in a decrease of 30 ft-lbs (longitudinal orientation) and a decrease of 10 ft-lb (transverse orientation) in upper shelf energy.

- The average upper shelf energy of the weld metal showed a decrease in energy of 47 ft-lbs after irradiation to 8.87×10^{18} n/cm^2 (E > 1.0 MeV).

- Both the weld and plate metal Charpy test results are in close agreement with Regulatory Guide 1.99, Revision 2 predictions.

- The calculated End-of-Life (EOL) (32 EFPY) maximum neutron fluence (E > 1.0 MeV) for the Diablo Canyon Unit 2 reactor vessel is as follows:

  Vessel inner radius* - 1.70×10^{19} n/cm^2
  Vessel 1/4 thickness - 9.14×10^{18} n/cm^2
  Vessel 3/4 thickness - 1.84×10^{18} n/cm^2

  * clad/base metal interface

- The surveillance capsule data presented in this report may be considered in the development of heatup and cooldown curves. However, in selecting the limiting material(s), the entire belt line components should be considered (Reference 5).

SECTION 2.0
INTRODUCTION

This report presents the results of the examination of Capsule X, the second capsule to be removed from the reactor in the continuing surveillance program which monitors the effects of neutron irradiation on the Pacific Gas and Electric Company Diablo Canyon Unit 2 reactor pressure vessel materials under actual operating conditions.

The surveillance program for the Diablo Canyon Unit 2 reactor pressure vessel materials was designed and recommended by the Westinghouse Electric Corporation. A description of the surveillance program and the preirradiation mechanical properties of the reactor vessel materials is presented by Davidson and Yanichko in Reference 1. The surveillance program was planned to cover the 40-year design life of the reactor pressure vessel and was based on ASTM E185-73, "Standard Recommended Practice for Surveillance Tests for Nuclear Reactor Vessels". Westinghouse Power Systems personnel were contracted to aid in the preparation of procedures for removing capsule "X" from the reactor and its shipment to the Westinghouse Science and Technology Center Hot Cell. The postirradiation mechanical testing of the Charpy V-notch impact and tensile surveillance specimens was performed at the remote metallographic hot cell facility.

This report summarizes the testing of and the postirradiation data obtained from surveillance Capsule "X" removed from the Diablo Canyon Unit 2 reactor vessel and discusses the analysis of these data.

SECTION 3.0
BACKGROUND

The ability of the large steel pressure vessel containing the reactor core and its primary coolant to resist fracture constitutes an important factor in ensuring safety in the nuclear industry. The beltline region of the reactor pressure vessel is the most critical region of the vessel because it is subjected to significant fast neutron bombardment. The overall effects of fast neutron irradiation on the mechanical properties of low alloy, ferritic pressure vessel steels such as SA533 Grade B Class 1 (base material of the Pacific Gas and Electric Company Diablo Canyon Unit 2 reactor pressure vessel intermediate shell plate B5454-1) are well documented in the literature. Generally, low alloy ferritic materials show an increase in hardness and tensile properties and a decrease in ductility and toughness under certain conditions of irradiation.

A method for performing analyses to guard against fast fracture in reactor pressure vessels has been presented in "Protection Against Nonductile Failure," Appendix G to Section III of the ASME Boiler and Pressure Vessel Code[6]. The method uses fracture mechanics concepts and is based on the reference nil-ductility temperature (RT_{NDT}).

RT_{NDT} is defined as the greater of either the drop weight nil-ductility transition temperature (NDTT per ASTM E-208[7]) or the temperature 60°F less than the 50 ft-lb (and 35-mil lateral expansion) temperature as determined from Charpy specimens oriented normal (transverse) to the major working direction of the material. The RT_{NDT} of a given material is used to index that material to a reference stress intensity factor curve (K_{IR} curve) which appears in Appendix G of the ASME Code. The K_{IR} curve is a lower bound of dynamic, crack arrest, and static fracture toughness results obtained from several heats of pressure vessel steel. When a given material is indexed to the K_{IR} curve, allowable stress intensity factors can be obtained for this material as a function of temperature. Allowable operating limits can then be determined using these allowable stress intensity factors.

RT_{NDT} and, in turn, the operating limits of nuclear power plants can be adjusted to account for the effects of radiation on the reactor vessel material properties. The radiation embrittlement changes in mechanical properties of a given reactor pressure vessel steel can be monitored by a reactor surveillance program such as the Diablo Canyon Unit 2 Reactor Vessel Radiation Surveillance Program[1], in which a surveillance capsule is periodically removed from the operating nuclear reactor and the encapsulated specimens tested. The increase in the average Charpy V-notch 30 ft-lb temperature (ΔRT_{NDT}) due to irradiation is added to the original RT_{NDT} to adjust the RT_{NDT} for radiation embrittlement. This adjusted RT_{NDT} (RT_{NDT} initial + ΔRT_{NDT}) is used to index the material to the K_{IR} curve and, in turn, to set operating limits for the nuclear power plant which take into account the effects of irradiation on the reactor vessel materials.

SECTION 4.0
DESCRIPTION OF PROGRAM

Six surveillance capsules for monitoring the effects of neutron exposure on the Diablo Canyon Unit 2 reactor pressure vessel core region material were inserted in the reactor vessel prior to initial plant start-up. The six capsules were positioned in the reactor vessel between the neutron pads and the vessel wall as shown in Figure 4-1. The vertical center of the capsules is opposite the vertical center of the core.

Capsule X was removed after 3.11 effective full power years of plant operation. This capsule contained Charpy V-notch, tensile, 1/2 T compact tension (CT), and bend bar specimens (see Figure 4-2) from intermediate shell plate B5454-1. Capsule X, also, contained Charpy V-notch, tensile, and 1/2 T compact tension (CT) specimens from weldment which was made from sections of intermediate shell plate B5454-1 and adjoining intermediate shell plate B5454-2 using weld wire representative of that used in the original fabrication and Charpy V-notch specimens from weld Heat-Affected-Zone (HAZ) material. All weld HAZ specimens were obtained from within the weld HAZ of intermediate shell plate B5454-1.

The chemical composition and heat treatment of the surveillance material is presented in Table 4-1. The chemical analyses reported in Table 4-1 were obtained from unirradiated material used in the surveillance program. In addition, a chemical analysis using Inductively Coupled Plasma Spectrometry (ICPS) was performed on one irradiated Charpy specimen from intermediate shell plate B5454-1 and three weld metal Charpy specimens and is reported in Table 4-2. The chemistry results from the NBS certified reference standards are reported in Table 4-3.

Test material was obtained from the intermediate shell course plate after thermal heat treatment and forming of the plate. All test specimens were machined from the 1/4 thickness location of the plate after performing a simulated postweld stress-relieving treatment on the test material. The test specimens represent material taken at least one plate thickness (9 5/8 inches) from the quenched end of the plate.

Base metal Charpy V-notch impact specimens from intermediate shell plate B5454-1 were machined in both the longitudinal orientation (longitudinal axis of the specimen parallel to the major working direction of plate B5454-1) and transverse orientation (longitudinal axis of the specimen perpendicular to the major working direction of plate B5454-1). The core region weld Charpy V-notch impact specimens were machined from the weldment such that the long dimension of the Charpy specimen was normal to the weld direction; the notch was machined such that the direction of crack propagation in the specimen will be in the weld direction.

Base metal tension specimens from the intermediate shell plate B5454-1 were machined so as to produce some with the longitudinal axis of the specimen normal to and some perpendicular to the major rolling direction of the plate. The core region weld tension specimens were machined from the weldment such that the long dimension of the specimen was oriented normal to the weld direction.

The bend bar specimen, contained in Capsule X, was machined from plate B5454-1 with the longitudinal axis of the specimen oriented normal to the rolling direction of the plate such that the simulated crack would propagate in the rolling direction of the plate. The bend bar specimen was fatigue precracked according to ASTM E399.

The 1/2T Compact Tension (CT) test specimens in Capsule X from intermediate shell plate B5454-1 were machined in both the longitudinal and transverse orientations. Thus, these CT specimens will generate fracture toughness data both normal and parallel to the rolling direction of plate B5454-1. CT specimens from the weld metal were machined normal to the weld direction, with the notch oriented in the direction of the weld. All 1/2T CT specimens were fatigue precracked according to ASTM E399.

Capsule X contained dosimeters of pure copper, iron, nickel, and aluminum-0.15 weight percent cobalt wire (cadmium-shielded and unshielded). In addition, cadmium shielded dosimeters of neptunium (Np^{237}) and uranium (U^{238}) were included to measure the integrated flux at specific neutron energy levels.

The capsule contained two low-melting-point eutectic alloy thermal monitors. These thermal monitors were used to more accurately define the maximum temperature attained by the test specimens during irradiation. The thermal monitors were sealed in Pyrex tubes and inserted in spacers located at three axial locations throughout the capsule The composition of the two low-melting-point eutectic alloys and their melting points are as follows:

2.5% Ag, 97.5% Pb	Melting Point: 579°F (304°C)
1.75% Ag, 0.75% Sn, 97.5% Pb	Melting Point: 590°F (310°C)

The arrangement of the various mechanical specimens, dosimeters and thermal monitors contained in Capsule X are shown in Figure 4-2.

TABLE 4-1

CHEMICAL COMPOSITION AND HEAT TREATMENT OF THE

DIABLO CANYON UNIT 2 REACTOR VESSEL SURVEILLANCE MATERIALS

Element	Chemical Composition (wt%)* Intermediate Shell Plate B5454-1	Weld Metal
C	0.23	0.13
S	0.010	0.010
N_2	0.008	0.008
Co	0.002	0.012
Cu	0.15	0.22
Si	0.22	0.22
Mo	0.43	0.47
Ni	0.67	0.83
Mn	1.28	1.32
Cr	0.071	0.031
V	0.001	0.001
P	0.012	0.017
Sn	0.010	0.010
Al	0.031	0.009

* Westinghouse Analysis

HEAT TREATMENT

Intermediate Shell Plate B5454-1 (Heat C5161-1)	1550-1650°F	4 hr - Water Quench
	1225±25 °F	4 hr - Air Cool
	1150±25 °F	40 hr - Furnace Cool
Weld	1150±25 °F	40 hrs

TABLE 4-2

CHEMICAL COMPOSITION OF DIABLO CANYON UNIT 2 CAPSULE X
IRRADIATED CHARPY IMPACT SPECIMENS

Material ID.	Diablo Canyon Unit 2: Irradiated Low Alloy Steel			
Specimen No.	PT-56	PW-55	PW-56	PW-58
Metals	Concentration in Weight Percent			
Fe	MATRIX ELEMENT: Remainder by Difference			
Co	0.003	0.018	0.004	0.010
Cu	0.137	0.225	0.213	0.225
Cr	0.070	0.043	0.071	0.043
Mn	1.226	1.432	1.355	1.391
Mo	0.453	0.545	0.484	0.506
Ni	0.656	0.875	0.856	0.877
P	<0.0050	0.0131	0.0105	0.0118
V	0.002	0.006	0.009	0.006
C	0.237	0.152	0.134	0.066
S	0.0115	0.0054	0.0026	0.0025
Si	0.134	0.157	0.155	0.155

Analyses	Method of Analysis
Metals	ICPS, Inductively Coupled Plasma Spectrometry
Carbon	EC-12, LECO Carbon Analyzer
Sulfur	Combustion/titration
Silicon	Dissolution/gravimetric
Iron	(Matrix Element: Remainder by Difference)

TABLE 4-3
CHEMISTRY RESULTS FROM THE NBS
CERTIFIED REFERENCE STANDARDS

Material ID: Low Alloy Steel: NBS Certified Reference Standards

	NBS 361		NBS 362	
	Certified	Measured (a)	Certified	Measured (a)
Metals	Concentration in Weight Percent			
Fe *	95.60	(matrix)	95.30	(matrix)
Co	0.072	0.033	0.300	0.318
Cu	0.042	0.043	0.500	0.514
Cr	0.694	0.663	0.300	0.297
Mn	0.660	0.644	1.040	1.050
Mo	0.190	0.193	0.068	0.054
Ni	2.000	2.072	0.590	0.610
P	0.014	0.0144	0.041	0.0417
V	0.011	0.011	0.040	0.040
C	0.383	0.386	0.160	0.162/0.161
S	0.014	N/A	0.036	0.0354
Si	0.222	0.208	0.390	0.383

Material ID: Low Alloy Steel: NBS Certified Reference Standards

	NBS 363		NBS 364	
	Certified	Measured (a)	Certified	Measured (a)
Metals	Concentration in Weight Percent			
Fe *	94.40	(matrix)	96.70	(matrix)
Co	0.048	0.051	0.150	0.149
Cu	0.100	0.102	0.249	0.252
Cr	1.310	1.315	0.063	0.058
Ni	0.300	0.314	0.144	0.139
Mn	1.500	1.539	0.255	0.250
Mo	0.028	0.025	0.490	0.491
P	0.029	0.0285	0.010	0.0096
V	0.310	-----	0.105	0.100
C	0.620	-----	0.870	N/A
S	0.0068	-----	0.0250	0.0247
Si	0.740	0.710	0.065	N/A

* Matrix element calculated as difference for material balance.
N/A - Not analyzed

(a) Method of analysis -- Inductively Coupled Plasma Spectrometry (ICPS) for all elements except C, S and Si.

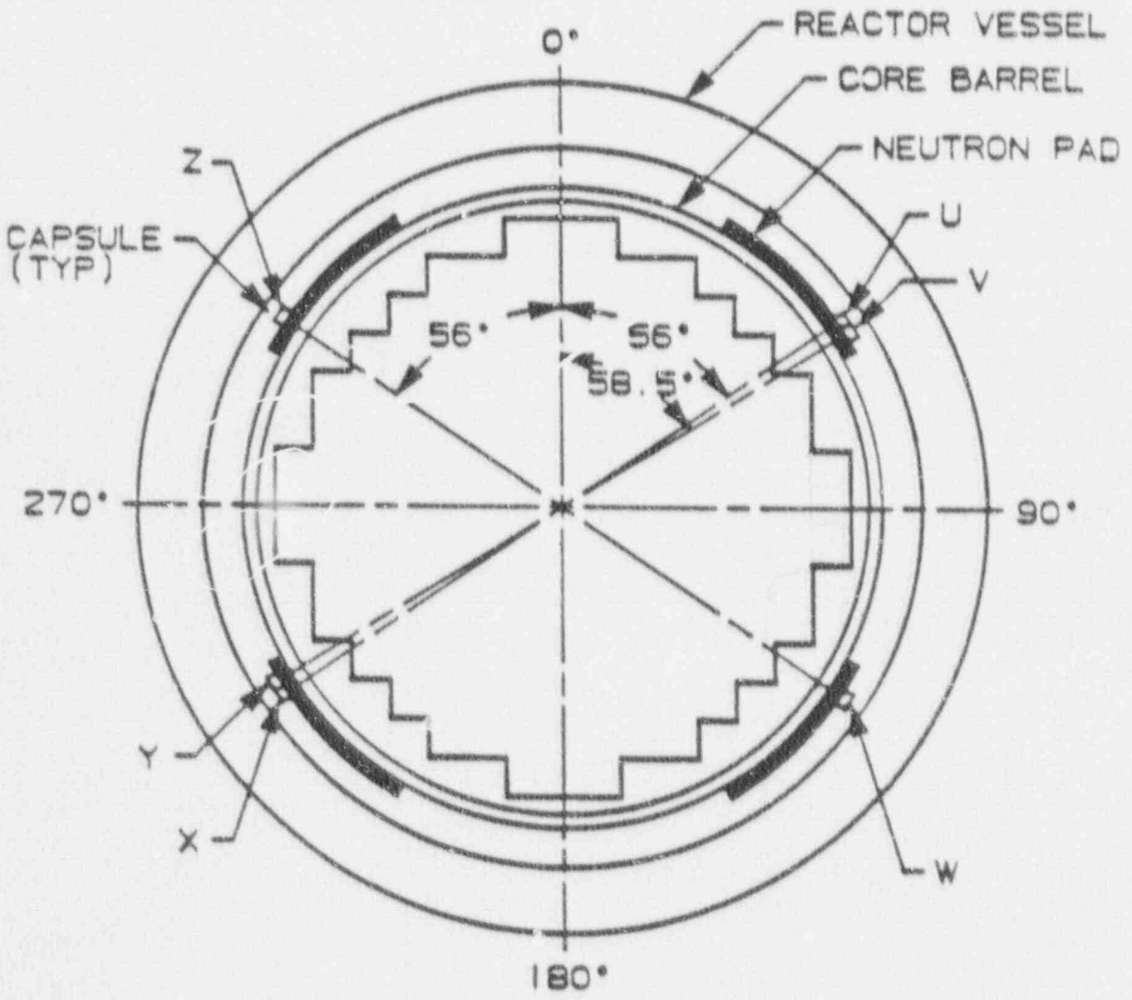

Figure 4-1. Arrangement of Surveillance Capsules in the Diablo Canyon Unit 2 Reactor Vessel

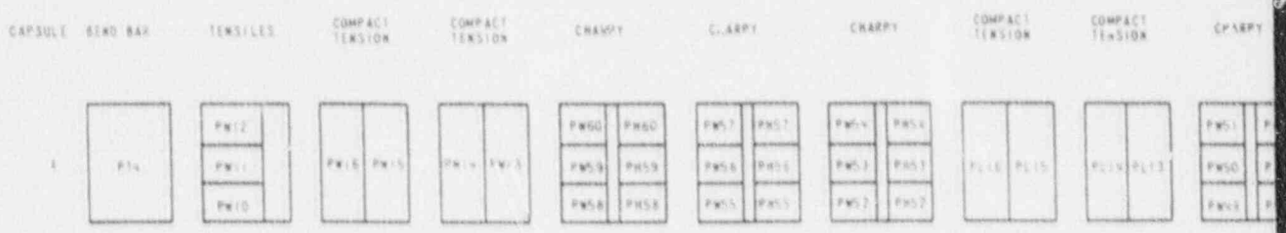

LEGEND: PH - HAZ
PL - PLATE B5454-1 LONGITUDINAL
PT - PLATE B5454-1 TRANSVERSE
PW - WELD METAL

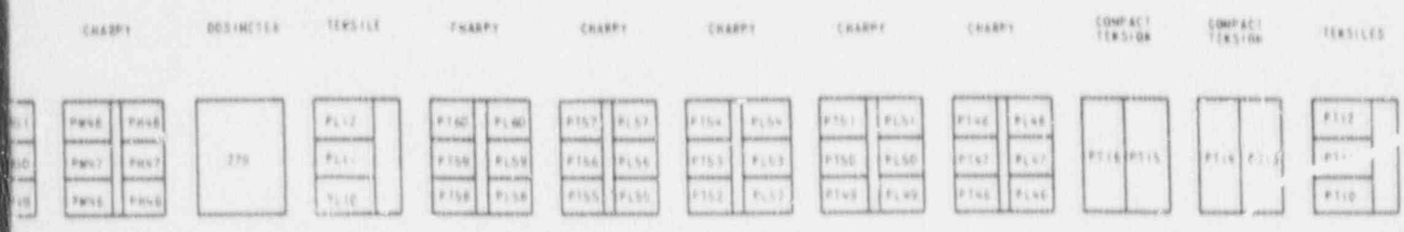

Figure 4-2 Capsule X Diagram Showing Location of Specimens, Thermal Monitors and Dosimeters

SECTION 5.0
TESTING OF SPECIMENS FROM CAPSULE X

5.1 Overview

The post-irradiation mechanical testing of the Charpy V-notch and tensile specimens was performed at the Westinghouse Science and Technology Center with consultation by Westinghouse Power Systems personnel. Testing was performed in accordance with 10CFR50, Appendices G and H[4], ASTM Specification E185-82[8], and Westinghouse Procedure MHL 8402, Revision 1 as modified by RMF Procedures 8102, Revision 1 and 8103, Revision 1.

Upon receipt of the capsule at the laboratory, the specimens and spacer blocks were carefully removed, inspected for identification number, and checked against the master list in WCAP-8783[1]. No discrepancies were found.

Examination of the two low-melting point 304°C (579°F) and 310°C (590°F) eutectic alloys indicated no melting of either type of thermal monitor. Based on this examination, the maximum temperature to which the test specimens were exposed was less than 304°C (579°F).

The Charpy impact tests were performed per ASTM Specification E23-88[9] and RMF Procedure 8103, Revision 1 on a Tinius-Olsen Model 74, 358J machine. The tup (striker) of the Charpy machine is instrumented with an Effects Technology Model 500 instrumentation system. With this system, load-time and energy-time signals can be recorded in addition to the standard measurement of Charpy energy (E_D). From the load-time curve, the load of general yielding (P_{GY}), the time to general yielding (t_{GY}), the maximum load (P_M), and the time to maximum load (t_M) can be determined. Under some test conditions, a sharp drop in load indicative of fast fracture was observed. The load at which fast fracture was initiated is identified as the fast fracture load (P_F), and the load at which fast fracture terminated is identified as the arrest load (P_A).

The energy at maximum load (E_M) was determined by comparing the energy-time record and the load-time record. The energy at maximum load is approximately equivalent to the energy required to initiate a crack in the specimen. Therefore, the propagation energy for the crack ( ) is the difference between the total energy to fracture (E_D) and the energy at maximum load.

The yield stress (σ_Y) was calculated from the three-point bend formula having the following expression:

$$\sigma_Y = P_{GY} * [L / (B * (W-a)^2 * C)] \quad (1)$$

where the constant C is dependent on the notch flank angle (ϕ), notch root radius (ρ), and the type of loading (i.e., pure bending or three-point bending). In three-point bending a Charpy specimen in which $\phi = 45°$ and $\rho = 0.010"$, Equation 1 is valid with with C = 1.21. Therefore (for L = 4W),

$$\sigma_Y = P_{GY} * [L / (B (W-a)^2 * 1.21)] = [3.3P_{GY}W]/[B(W-a)^2] \quad (2)$$

For the Charpy specimens, B = 0.394 in., W = 0.394 in., and a = 0.079 in. Equation 2 then reduces to:

$$\sigma_Y = 33.3 \times P_{GY} \quad (3)$$

where σ_Y is in units of psi and P_{gy} is in units of lbs. The flow stress was calculated from the average of the yield and maximum loads, also using the three-point bend formula.

Percent shear was determined from post-fracture photographs using the ratio-of-areas methods in compliance with ASTM Specification A370-89[10]. The lateral expansion was measured using a dial gage rig similar to that shown in the same specification.

Tension tests were performed on a 20,000-pound Instron, split-console test machine (Model 1115) per ASTM Specification E8-89b[11] and E21-79(1988)[12], and RMF Procedure 8102, Revision 1. All pull rods, grips, and pins were made of Inconel 718 hardened to HRC45. The upper pull rod was connected through a universal joint to improve axiality of loading. The tests were conducted at a constant crosshead speed of 0.05 inches per minute throughout the test.

Extension measurements were made with a linear variable displacement transducer (LVDT) extensometer. The extensometer knife edges were spring-loaded to the specimen and operated through specimen failure. The extensometer gage length is 1.00 inch. The extensometer is rated as Class B-2 per ASTM E83-85[13].

Elevated test temperatures were obtained with a three-zone electric resistance split-tube furnace with a 9-inch hot zone. All tests were conducted in air.

Because of the difficulty in remotely attaching a thermocouple directly to the specimen, the following procedure was used to monitor specimen temperature. Chromel-alumel thermocouples were inserted in shallow holes in the center and each end of the gage section of a dummy specimen and in each grip. In the test configuration, with a slight load on the specimen, a plot of specimen temperature versus upper and lower grip and controller temperatures was developed over the range of room temperature to 550°F (288°C). The upper grip was used to control the furnace temperature. During the actual testing the grip temperatures were used to obtained desired specimen temperatures. Experiments indicated that this method is accurate to $\pm$2°F.

The yield load, ultimate load, fracture load, total elongation, and uniform elongation were determined directly from the load-extension curve. The yield strength, ultimate strength, and fracture strength were calculated using the original cross-sectional area. The final diameter and final gage length were determined from post-fracture photographs. The fracture area used to calculate the fracture stress (true stress at fracture) and percent reduction in area was computed using the final diameter measurement.

5.2 Charpy V-Notch Impact Test Results

The results of Charpy V-notch impact tests performed on the various materials contained in Capsule X irradiated to 8.87 x 10^{18} n/cm^2 (E > 1.0 MeV) are presented in Tables 5-1 through 5-4 and are compared with unirradiated results[1] as shown in Figures 5-1 through 5-4. The transition temperature increases and upper shelf energy decreases for the Capsule X surveillance materials are summarized in Table 5-5.

Irradiation of the reactor vessel intermediate shell plate B5454-1 Charpy specimens to 8.87 x 10^{18} n/cm^2 (E > 1.0 MeV) at 550F (Figure 5-1) resulted in a 30 ft-lb transition temperature increase of 101 °F and a 50 ft-lb transition temperature increase of 121 °F for specimens oriented with the longitudinal axis parallel to the major working direction of the plate (longitudinal orientation). This resulted in a 30 ft-lb transition temperature of 105.7 °F and a 50 ft-lb transition temperature of 154.6 °F for specimens oriented with the longitudinal axis parallel to the major working direction of the plate (longitudinal orientation).

The average upper shelf energy (USE) of the intermediate shell plate B5454-1 Charpy specimens (longitudinal orientation) resulted in a average upper shelf energy decrease of 30 ft-lbs after irradiation to 8.87 x 10^{18} n/cm^2 (E > 1.0 MeV) at 550°F. This results in a average USE of 115 ft-lb (Figure 5-1).

Irradiation of the reactor vessel intermediate shell plate B5454-1 Charpy specimens to 8.87 x 10^{18} n/cm^2 (E > 1.0 MeV) at 550°F (Figure 5-2) resulted in a 30 ft-lb transition temperature increase of 99 ° and 50 ft-lb transition temperature increase of 99 °F for specimens oriented with the longitudinal axis perpendicular to the major working direction of the plate (transverse orientation). This resulted in a 30 ft-lb transition temperature of 126 °F and a 50 ft-lb transition temperature of 173 °F for specimens oriented with the longitudinal axis perpendicular to the major working direction of the plate (transverse orientation).

The average upper shelf energy (USE) of the intermediate shell plate B5454-1 Charpy specimens (Transverse Orientation) resulted in a average upper shelf energy decrease of 10 ft-lbs after irradiation to 8.87 x 10^{18} n/cm^2 (E > 1.0 MeV) at 550°F. This results in an average USE of 85 ft-lb (Figure 5-2).

Irradiation of the reactor vessel core region weld metal Charpy specimens to 8.87 x 10^{18} n/cm^2 (E > 1.0 MeV) at 550°F (Figure 5-3) resulted in a 30 ft-lb transition temperature increase of 204 °F and 50 ft-lb transition temperature increase of 214 °F. This resulted in a 30 ft-lb transition temperature of 191 °F and a 50 ft-lb transition temperature of 229 °F.

The average upper shelf energy (USE) of the reactor vessel core region weld metal resulted in a average upper shelf energy decrease of 47 ft-lbs after irradiation to 8.87 x 10^{18} n/cm^2 (E > 1.0 MeV) at 550°F. This results in an average USE of 74 ft-lb (Figure 5-3).

Irradiation of the reactor vessel weld metal Heat-Affected-Zone (HAZ) specimens to 8.87 x 10^{18} n/cm^2 (E > 1.0 MeV) at 550°F (Figure 5-4) resulted in a 30 ft-lb trarsition temperature increase of 252 °F and a 50 ft-lb transition temperature increase of 247 °F. This results in a 30 ft-lb transition temperature of 26 °F and a 50 ft-lb transition temperature of 96 °F.

The average upper shelf energy (USE) of the reactor vessel weld HAZ metal resulted in a average upper shelf energy decrease of 46 ft-lbs after irradiation to 8.87 x 10^{18} n/cm^2 (E > 1.0 MeV) at 550°F. This results in an average USE of 101 ft-lb (Figure 5-4).

The fracture appearance of each irradiated Charpy specimen from the various materials is shown in Figures 5-5 through 5-8 and show an increasingly ductile or tougher appearance with increasing test temperature.

A comparison of the 30 ft-lb transition temperature increases and the % decrease in USE for the various Diablo Canyon Unit 2 surveillance materials with predicted values using the methods of NRC Regulatory Guide 1.99, Revision 2[5] is presented in Table 5-6. This comparison indicates that the actual transition temperature increases and USE decreases resulting from irradiation to 8.87 x 10^{18} n/cm^2 (E > 1.0 MeV) at 550 °F are in close agreement with the NRC Regulatory Guide 1.99, Revision 2 predictions.

5.3 Tension Test Results

The results of tension tests performed on the intermediate shell plate B5454-1 (longitudinal and transverse Orientation) and the weld metal irradiated to 8.87 x 10^{18} n/cm^2 (E > 1.0 MeV) are shown in Table 5-7 and are compared with unirradiated results[1] in Figures 5-9, 5-10 and 5-11.

Irradiation of the reactor vessel intermediate shell plate B5454-1 tensile specimens to 8.87 x 10^{18} n/cm^2 (E > 1.0 MeV) at 550°F (Figure 5-9) resulted in an increase of 13 to 25 ksi in 0.2 percent offset yield strength and an increase of 13 to 14 ksi in ultimate tensile strength for specimens oriented with the longitudinal axis parallel to the major working direction of the plate (longitudinal orientation)

Irradiation of the reactor vessel intermediate shell plate B5454-1 tensile specimens to 8.87 x 10^{18} n/cm^2 (E > 1.0 MeV) at 550°F (Figure 5-10) resulted in an increase of 13 to 18 ksi for the 0.2 percent offset yield strength and an increase of 12 to 15 ksi for the ultimate tensile strength for specimens oriented with the longitudinal axis perpendicular to the major working direction of the plate (transverse orientation).

Irradiation of the reactor vessel weld metal tensile specimens to 8.87 x 10^{18} n/cm^2 (E > 1.0 MeV) at 550°F (Figure 5-11) resulted in an increase of 20 to 25 ksi for the 0.2 percent offset yield strength and an increase of 8 to 28 ksi for the ultimate tensile strength.

The fractured tension specimens for the plate material are shown in Figures 5-12 and 5-13, while the fractured specimens for the weld metal are shown in Figure 5-14.

Engineering stress-strain curves for the tension specimens are shown in Figures 5-15 through 5-19.

True stress-strain curves for the tension specimens to the point of necking are shown in Figures 5-20 through 5-24.

5.4 Compact Tension Tests

Per the surveillance capsule testing program with the Pacific Gas and Electric Company, 1/2 T-compact tension fracture mechanics specimens will not be tested and will be stored at the Westinghouse Science and Technology Center Hot Cell.

TABLE 5-1

CHARPY V-NOTCH IMPACT DATA FOR THE DIABLO CANYON UNIT 2

PLATE B5454-1 IRRADIATED AT 550°F,

FLUENCE 8.87 x 10^{18} n/cm^2 (E > 1.0 MeV)

Sample No.	Temperature (°F)	(°C)	Impact Energy (ft-lb)	(J)	Lateral Expansion (mils)	(mm)	Shear (%)
			Longitudinal Orientation				
PL54	25	(- 4)	7.0	(9.5)	9.0	(0.23)	5
PL47	80	(27)	21.0	(28.5)	19.0	(0.48)	15
PL57	80	(27)	29.0	(39.5)	28.0	(0.71)	20
PL60	105	(41)	17.0	(23.0)	16.0	(0.41)	15
PL58	105	(41)	29.0	(39.5)	23.0	(0.58)	25
PL51	115	(46)	34.0	(46.0)	26.0	(0.66)	30
PL49	115	(46)	40.0	(54.0)	31.0	(0.79)	35
PL59	125	(52)	45.0	(61.0)	36.0	(0.91)	40
PL48	140	(60)	42.0	(57.0)	38.0	(0.97)	40
PL53	140	(60)	43.0	(58.5)	34.0	(0.86)	45
PL55	225	(107)	73.0	(99.0)	62.0	(1.57)	95
PL50	280	(138)	111.0	(150.5)	85.0	(2.16)	100
PL46	300	(149)	100.0	(135.5)	79.0	(2.01)	100
PL56	350	(177)	104.0	(141.0)	83.0	(2.11)	100
PL52	375	(191)	112.0	(152.0)	85.0	(2.16)	100
			Transverse Orientation				
PT56	25	(- 4)	8.0	(11.0)	6.0	(0.15)	5
PT48	80	(27)	21.0	(28.5)	20.0	(0.51)	15
PT59	80	(27)	17.0	(23.0)	18.0	(0.46)	15
PT54	120	(49)	27.0	(36.5)	23.0	(0.58)	20
PT52	125	(52)	26.0	(35.5)	25.0	(0.64)	25
PT46	135	(57)	38.0	(51.5)	31.0	(0.79)	35
PT60	140	(60)	34.0	(46.0)	30.0	(0.76)	30
PT53	180	(82)	47.0	(63.5)	42.0	(1.07)	45
PT51	200	(93)	55.0	(74.5)	47.0	(1.19)	50
PT58	225	(107)	82.0	(111.0)	68.0	(1.73)	100
PT49	250	(121)	76.0	(103.0)	64.0	(1.63)	100
PT55	280	(138)	76.0	(103.0)	70.0	(1.78)	100
PT47	320	(160)	85.0	(115.0)	68.0	(1.73)	100
PT57	330	(166)	79.0	(107.0)	68.0	(1.73)	100
PT50	350	(177)	82.0	(111.0)	69.0	(1.75)	100

TABLE 5-2

CHARPY V-NOTCH IMPACT DATA FOR THE DIABLO CANYON UNIT 2 REACTOR VESSEL WELD METAL AND HAZ METAL IRRADIATED AT 550°F, FLUENCE 8.87 x 10^{18} n/cm^2 (E > 1.0 MeV)

Sample No.	Temperature (°F)	(°C)	Impact Energy (ft-lb)	(J)	Lateral Expansion (mils)	(mm)	Shear (%)
			Weld Metal				
PW38	100	(38)	15.0	(20.5)	14.0	(0.35)	10
PW57	150	(66)	16.0	(21.5)	15.0	(0.38)	15
PW55	185	(85)	19.0	(26.0)	17.0	(0.43)	35
PW60	185	(85)	25.0	(34.0)	25.0	(0.64)	25
PW49	195	(91)	32.0	(43.5)	32.0	(0.81)	60
PW50	195	(91)	33.0	(44.5)	28.0	(0.71)	60
PW59	210	(99)	37.0	(50.0)	30.0	(0.76)	60
PW47	210	(99)	50.0	(68.0)	41.0	(1.04)	95
PW56	250	(121)	53.0	(72.0)	45.0	(1.14)	95
PW46	250	(121)	63.0	(85.5)	56.0	(1.42)	95
PW53	300	(149)	74.0	(100.5)	62.0	(1.57)	100
PW51	350	(177)	71.0	(96.5)	62.0	(1.57)	100
PW52	375	(191)	76.0	(103.0)	67.0	(1.70)	100
PW48	400	(204)	72.0	(97.5)	62.0	(1.57)	100
PW54	420	(216)	73.0	(99.0)	85.0	(2.16)	100
			HAZ Metal				
PH59	0	(-18)	18.0	(24.5)	15.0	(0.38)	15
PH51	50	(10)	36.0	(49.0)	34.0	(0.86)	35
PH53	50	(10)	29.0	(39.5)	26.0	(0.66)	25
PH55	75	(24)	24.0	(32.5)	23.0	(0.58)	25
PH54	75	(24)	75.0	(101.5)	52.0	(1.32)	65
PH46	125	(52)	94.0	(127.5)	73.0	(1.85)	90
PH52	125	(52)	57.0	(77.5)	44.0	(1.12)	60
PH58	175	(79)	58.0	(78.5)	47.0	(1.19)	65
PH57	175	(79)	48.0	(65.0)	45.0	(1.14)	70
PH60	200	(93)	58.0	(78.5)	55.0	(1.40)	90
PH49	275	(135)	113.0	(153.0)	84.0	(2.13)	100
PH47	275	(135)	97.0	(131.5)	80.0	(2.03)	100
PH48	300	(149)	123.0	(167.0)	81.0	(2.06)	100
PH56	300	(149)	71.0	(96.5)	67.0	(1.70)	100
PH50	325	(163)	102.0	(138.5)	76.0	(1.93)	100

TABLE 5-3

INSTRUMENTED CHARPY IMPACT TEST RESULTS FOR THE DIABLO CANYON UNIT 2 SHELL PLATE

B5454-1 IRRADIATED AT 550°F, FLUENCE 8.87 x 10^{18} n/cm^2 (E > 1.0 MeV)

Sample Number	Test Temp (°F)	Charpy Energy (ft-lb)	Normalized Energies Charpy Ed/A (ft-lb/in²)	Maximum Em/A (ft-lb/in²)	Prop Ep/A (ft-lb/in²)	Yield Load (kips)	Time to Yield (μsec)	Maximum Load (kips)	Time to Maximum (μsec)	Fracture Load (kips)	Arrest Load (kips)	Yield Stress (ksi)	Flow Stress (ksi)
Longitudinal Orientation													
PL54	25	7.0	56	37	19	2.00	75	3.45	145	3.45	0.15	88	90
PL47	80	21.0	169	101	68	2.90	115	3.75	300	3.70	0.10	97	110
PL57	80	29.0	234	184	49	3.35	175	4.35	455	4.25	0.10	111	127
PL60	105	17.0	137	69	68	3.15	115	3.45	225	3.40	0.60	104	109
PL58	105	29.0	234	187	47	3.25	140	4.30	475	4.3	0.25	107	125
PL51	115	34.0	274	197	78	3.45	115	4.50	455	4.40	0.50	113	132
PL49	115	40.0	322	215	108	2.80	95	4.15	520	4.10	0.65	92	115
PL59	125	45.0	362	214	148	3.20	145	4.10	550	4.00	0.75	108	121
PL48	140	42.0	338	262	76	3.2	115	4.40	605	4.35	0.25	105	125
PL53	140	43.0	346	228	118	3.35	115	4.50	530	4.50	0.85	107	128
PL55	225	73.0	588	242	346	2.75	115	3.95	800	3.90	3.30	91	111
PL50	280	111.0	894	224	670	2.65	95	4.30	535	-*	-*	87	115
PL46	300	100.0	805	283	523	2.65	140	4.10	720	-*	-*	87	111
PL56	350	104.0	837	224	613	2.30	115	3.60	630	-*	-*	75	98
PL52	375	113.0	902	271	630	2.70	125	3.90	695	-*	-*	89	109
Transverse Orientation													
PT56	25	8.0	64	40	24	2.75	105	3.35	180	3.35	0.10	92	101
PT59	80	17.0	137	90	47	3.10	105	3.80	255	3.75	0.45	102	114
PT48	80	21.0	169	105	64	3.2	125	3.70	310	3.50	0.10	105	113
PT54	120	27.0	217	137	80	3.15	115	3.90	370	3.85	0.70	104	116
PT52	125	26.0	209	122	87	2.80	115	3.65	355	3.65	0.75	93	107
PT46	135	38.0	306	231	75	3.35	115	4.35	535	4.35	0.95	110	127
PT60	140	34.0	274	204	70	2.85	105	4.10	500	4.10	0.80	95	116
PT53	180	47.0	378	218	160	3.25	115	4.30	510	4.30	1.95	107	125
PT51	200	55.0	443	200	242	2.85	115	3.90	525	3.85	1.55	94	112
PT58	225	82.0	661	COMPUTER MALFUNCTION		–	–	–	–	–	–	–	–
PT49	250	76.0	612	204	408	2.60	105	3.90	530	-*	-*	86	107
PT55	280	76.0	612	185	427	2.85	115	3.95	485	-*	-*	94	112
PT47	320	85.0	684	198	488	2.80	125	3.85	530	-*	-*	93	110
PT57	330	79.0	636	195	442	2.40	95	3.75	530	-*	-*	80	102
PT50	350	82.0	660	197	463	2.50	105	3.80	530	-*	-*	82	104

*Fully ductile fracture; no arrest load

TABLE 5-4

INSTRUMENTED CHARPY IMPACT TEST RESULTS FOR THE DIABLO CANYON UNIT 2

WELD METAL AND HAZ METAL IRRADIATED AT 550°F, FLUENCE 8.87 x 10^{18} n/cm^2 (E > 1.0 MeV)

Sample Number	Test Temp (°F)	Charpy Energy (ft-lb)	Normalized Energies (ft-lb/in^2) Charpy Ed/A	Maximum Em/A	Prop Ep/A	Yield Load (kips)	Time to Yield (μsec)	Maximum Load (kips)	Time to Maximum (μsec)	Fracture Load (kips)	Arrest Load (kips)	Yield Stress (ksi)	Flow Stress (ksi)
							Weld Metal						
PW58	100	15.0	121	89	32	3.30	125	3.60	270	3.60	0.10	109	114
PW57	150	16.0	129	65	64	3.55	145	3.80	220	3.75	0.85	117	121
PW55	185	19.0	153	38	115	2.95	125	3.30	170	3.15	1.25	97	103
PW60	185	25.0	201	150	52	3.55	125	4.25	375	4.25	1.05	117	129
PW49	195	32.0	258	136	121	3.25	125	3.90	370	3.90	1.85	107	118
PW50	195	33.0	266	198	68	3.45	115	4.30	460	4.3	1.00	115	129
PW59	210	37.0	298	207	91	3.00	125	3.80	535	3.80	1.30	99	113
PW47	210	50.0	403	198	304	3.40	135	4.35	480	4.30	3.20	112	128
PW56	250	53.0	427	186	241	3.15	145	4.05	485	4.00	3.60	104	119
PW46	250	63.0	507	203	304	2.90	125	3.86	535	3.85	3.20	98	112
PW53	300	74.0	596	218	378	3.70	220	4.20	535	–*	–*	122	131
PW51	350	71.0	572	225	347	3.55	210	4.25	545	–*	–*	118	129
PW52	375	76.0	612	224	388	3.20	190	4.20	550	–*	–*	106	123
PW54	420	73.0	588	205	383	2.90	145	3.95	535	–*	–*	96	113
PW13	300	63.0	507	205	302	2.45	140	3.30	605	–*	–*	81	95
							HAZ Metal						
PH59	0	18.0	145	124	21	4.00	135	4.45	310	4.45	0.10	132	140
PH53	50	29.0	234	174	60	3.60	125	4.15	425	4.15	0.85	118	128
PH4	50	38.0	290	247	43	3.75	175	4.75	545	4.75	1.20	125	141
PH55	75	24.0	194	COMPUTER MALFUNCTION		–	–	–	–	–	–	–	–
PH54	75	75.0	604	259	345	3.40	125	4.25	605	3.70	1.55	112	128
PH52	125	57.0	459	231	228	3.55	140	4.40	550	4.05	1.85	117	131
PH48	125	94.0	757	214	543	2.70	105	4.10	530	2.60	1.50	90	113
PH57	175	48.0	387	224	163	2.30	125	4.30	535	4.20	2.9	109	125
PH58	175	58.0	467	205	262	2.95	125	4.00	535	3.30	1.50	97	114
PH60	200	58.0	467	220	247	3.2	150	4.25	555	3.75	2.05	105	123
PH47	275	97.0	781	219	562	2.95	130	4.20	555	–*	–*	98	118
PH49	275	113.0	910	298	612	2.85	125	4.30	705	–*	–*	94	118
PH56	300	71.0	572	213	359	2.80	115	4.15	530	–*	–*	92	115
PH48	300	123.0	990	282	708	2.95	135	4.00	715	–*	–*	98	112
PH50	325	102.0	821	291	531	2.75	115	4.20	695	–*	–*	90	115

*Fully ductile fracture; no arrest load

TABLE 5-5

EFFECT OF 550°F IRRADIATION TO 8.87×10^{18} n/cm^2 (E > 1.0 MeV)

ON NOTCH TOUGHNESS PROPERTIES OF DIABLO CANYON UNIT 2 REACTOR VESSEL SURVEILLANCE MATERIALS

Material	Average 30 ft-lb Temperature (°F)			Average 35 mil Lateral Expansion Temperature (°F)			Average 50 ft-lb Temperature (°F)			Average Energy Absorption at Full Shear (ft-lb)		
	Unirradiated	Irradiated	ΔT	Unirradiated	Irradiated	ΔT	Unirradiated	Irradiated	ΔT	Unirradiated	Irradiated	Δ(ft-lb)
Plate B5454-1 (longitudinal)	4.6	105.7	101.1	18.4	135.6	117.2	33.3	154.6	121.4	144.7	114.9	29.8
Plate B5454-1 (transverse)	26.6	125.5	98.9	54.4	149.1	94.7	74.6	173.1	98.5	94.9	85	9.9
Weld Metal	-13.6	190.6	204.2	-0.7	212.3	213.0	14.9	228.7	213.8	120.9	74.4	46.5
HAZ Metal	-226.0	26.1	252.1	-169.9	69.9	239.8	-151.2	96.2	247.4	147.6	101.2	46.4

TABLE 5-6

COMPARISON OF DIABLO CANYON UNIT 2 SURVEILLANCE MATERIAL 30 FT-LB TRANSITION TEMPERATURE SHIFTS AND UPPER SHELF ENERGY DECREASES WITH REGULATORY GUIDE 1.99 REVISION 2 PREDICTIONS

			30 ft-lb Transition Temp. Shift			Upper Shelf Energy Decrease	
			R.G. 1.99 Rev. 2 (Predicted) (°F)			R.G. 1.99 Rev. 2 (Predicted)	Measured
Material	Capsule	Fluence 10^{18} n/cm^2	NOTE 1	NOTE 2	Measured (°F)	(%)	(%)
Plate B5454-1 (longitudinal)	U	3.51	72.1	71.7	65.0	18	14.3
	X	8.87	98.4	98.0	101.1	24	20.6
Plate B5454-1 (transverse)	U	3.51	72.1	71.7	73.0	18	0.9
	X	8.87	98.4	98.0	98.9	24	10.4
Weld Metal	U	3.51	149.3	158.0	174.0	28	29.7
	X	8.87	204.0	215.9	204.2	38	38.8
HAZ Metal	U	3.51	---	---	232.7	--	40.4
	X	8.87	---	---	252.1	--	31.4

NOTES:

1. ΔRT_{NDT} calculated with a CF = 101.5 (plate) and CF = 210.3 (weld). These CF's are based on the mean wt. % values of Cu and Ni from the unirradiated data[1] and capsules U[2] and X analyses.
2. ΔRT_{NDT} calculated with a CF = 101.0 (plate) and CF = 222.6 (weld). These CF's are based on the measured shifts from surveillance capsules U[2] and X per Regulatory Guide 1.99 Revision 2 using longitudinal and transverse data.

TABLE 5-7

TENSILE PROPERTIES FOR DIABLO CANYON UNIT 2 REACTOR VESSEL SURVEILLANCE MATERIAL

IRRADIATED AT 550°F TO 8.87×10^{18} n/cm^2 (E > 1.0 MeV)

Material	Sample Number	Test Temp. (°F)	0.2% Yield Strength (ksi)	Ultimate Strength (ksi)	Fracture Load (kip)	Fracture Stress (ksi)	Fracture Strength (ksi)	Uniform Elongation (%)	Total Elongation (%)	Reduction in Area (%)
Plate B5454-1 (Longitudinal)	PL10	74	77.9	93.8	3.20	169.6	65.2	13.5	26.1	62
	PL11	300	71.3	90.7	3.10	208.8	63.2	11.1	22.2	70
	PL12	550	81.0	93.7	3.90	200.2	79.5	9.0	16.2	60
Plate B5454-1 (Tranverse)	PT10	74	79.5	100.7	3.70	196.1	75.4	12.0	22.1	62
	PT11	300	71.8	90.7	3.30	159.1	67.2	10.5	19.5	58
	PT12	550	66.2	91.7	3.50	188.8	71.3	10.5	19.1	58
Weld	PW10	74	90.7	105.9	3.70	196.1	75.4	13.5	24.3	62
	PW11	300	81.5	96.8	3.60	197.1	73.3	10.5	21.3	63
	PW12	550	77.4	85.6	3.75	151.5	76.4	10.2	18.0	50

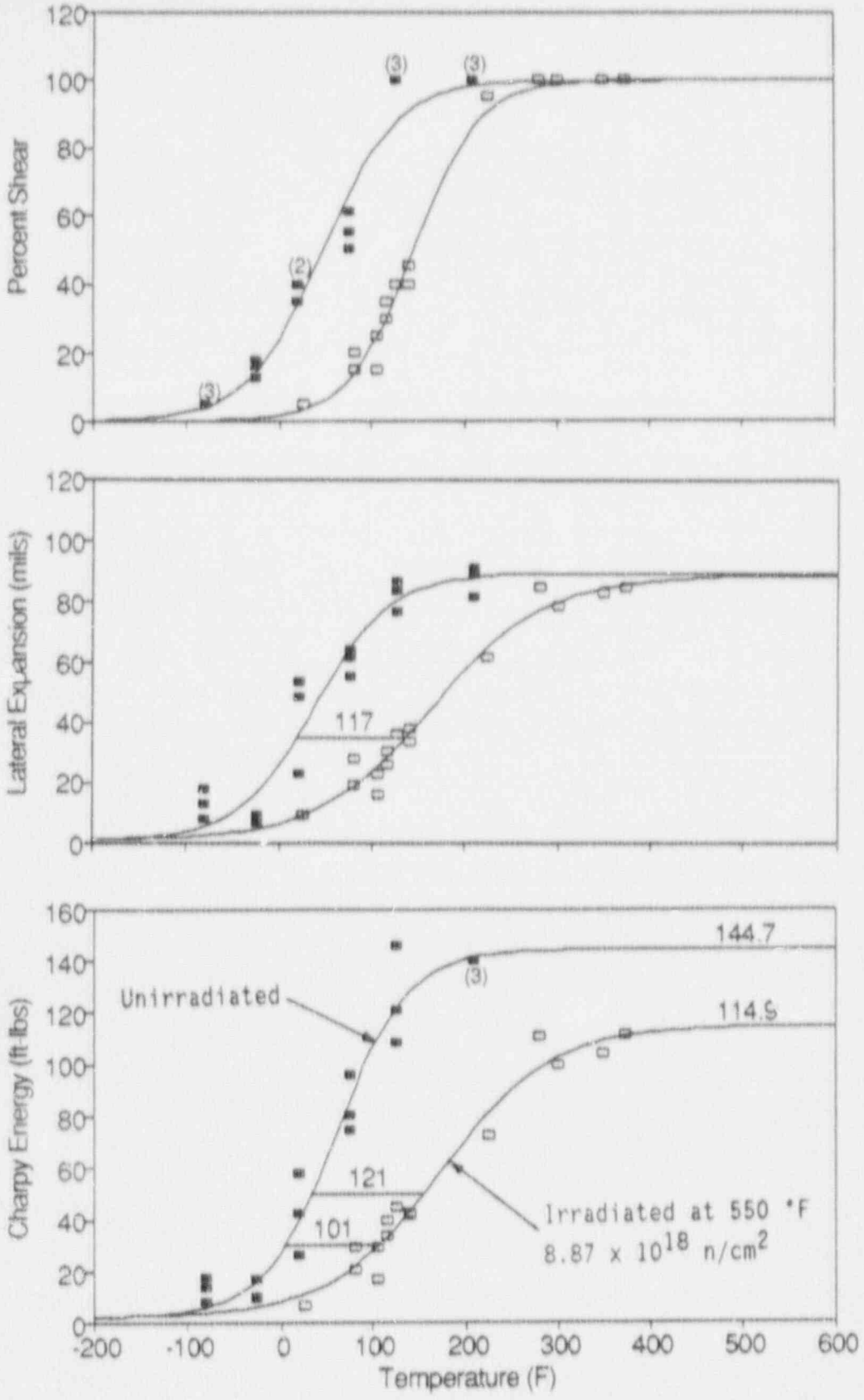

Figure 5-1. Charpy V-Notch Impact Properties for Diablo Canyon Unit 2 Reactor Vessel Intermediate Shell Plate B5454-1 (Longitudinal Orientation)

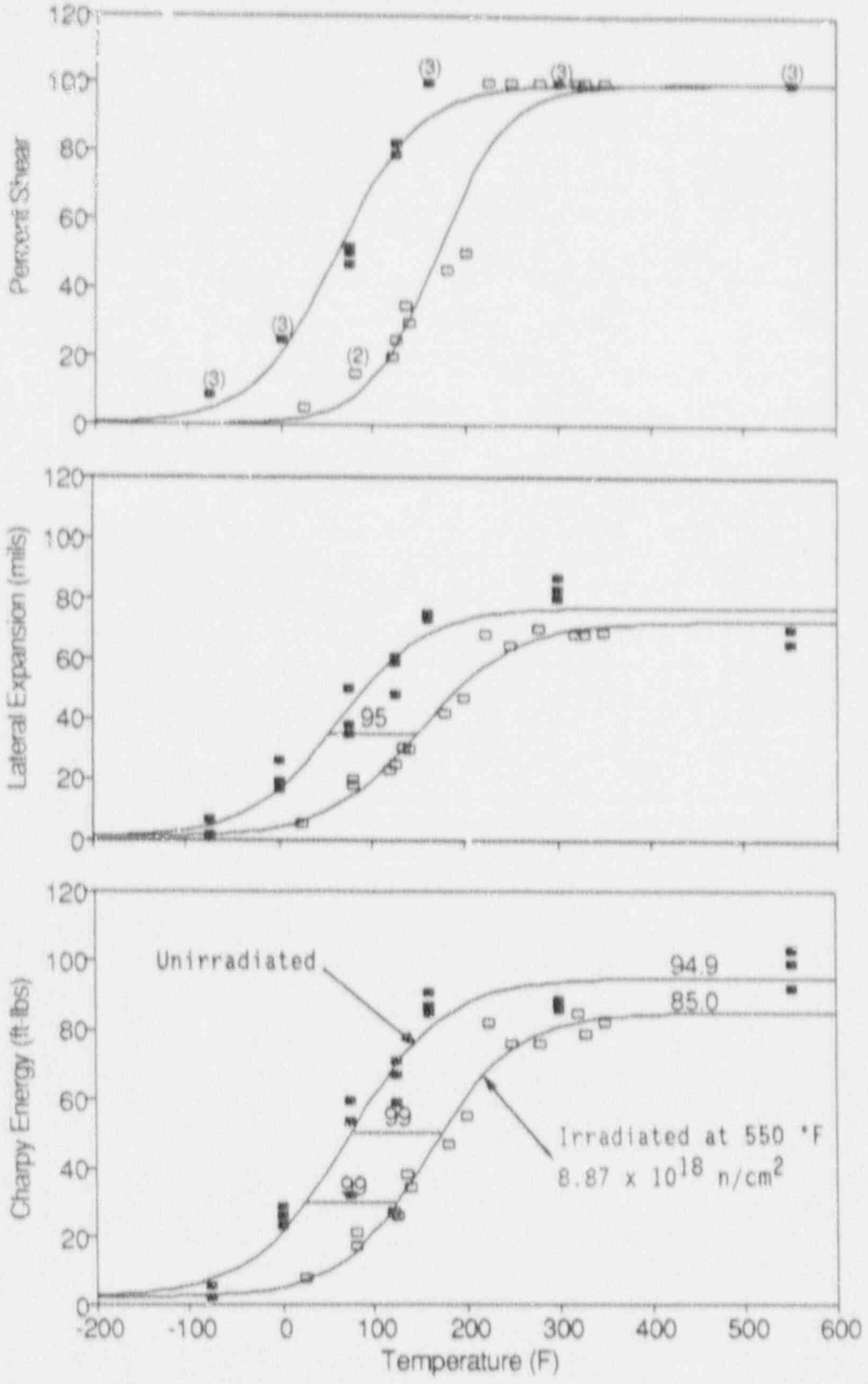

Figure 5-2. Charpy V-Notch Impact Properties for Diablo Canyon Unit 2 Reactor Vessel Intermediate Shell Plate B5454-1 (Transverse Orientation)

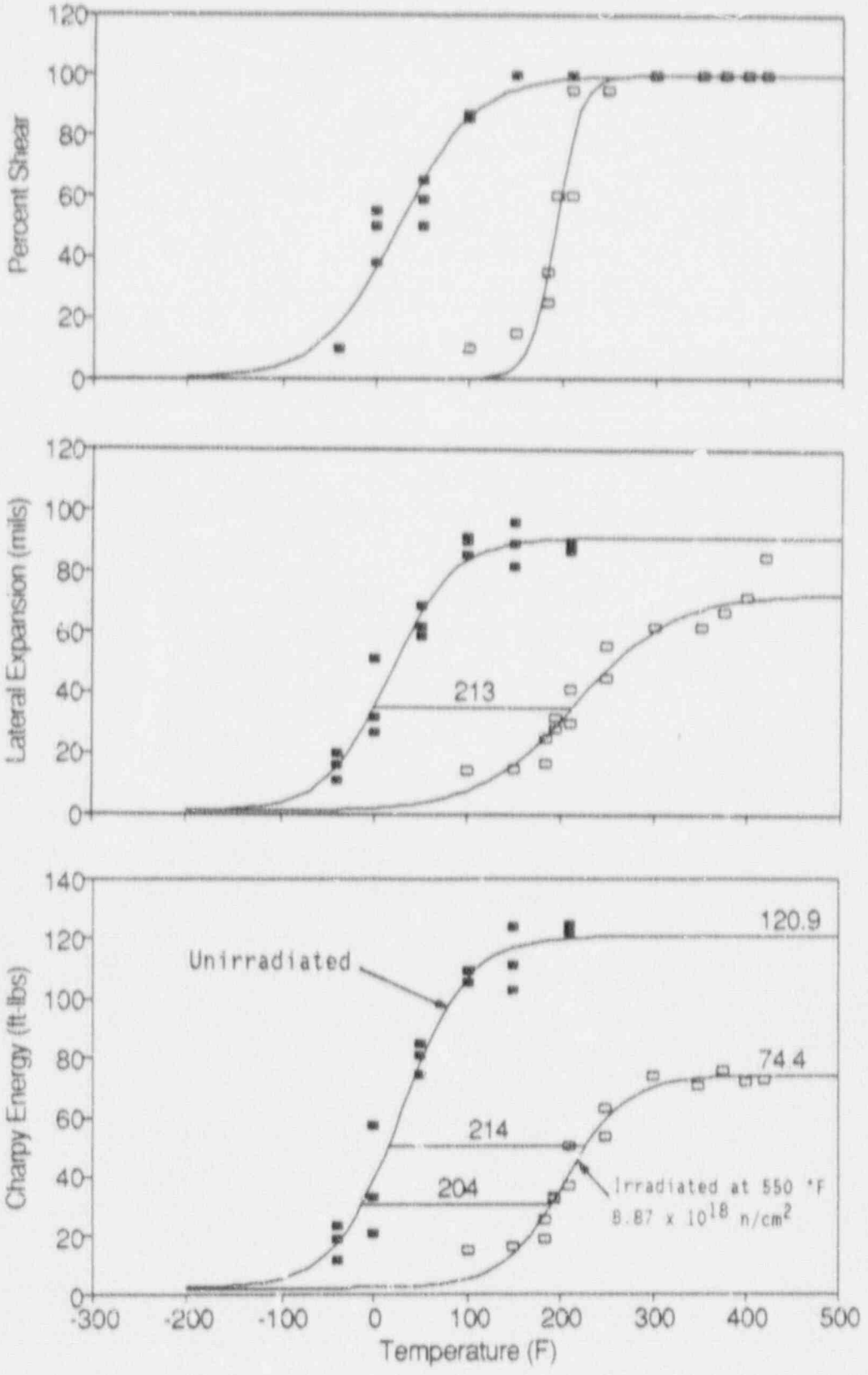

Figure 5-3. Charpy V-Notch Impact Properties for Diablo Canyon Unit 2 Reactor Vessel Weld Metal

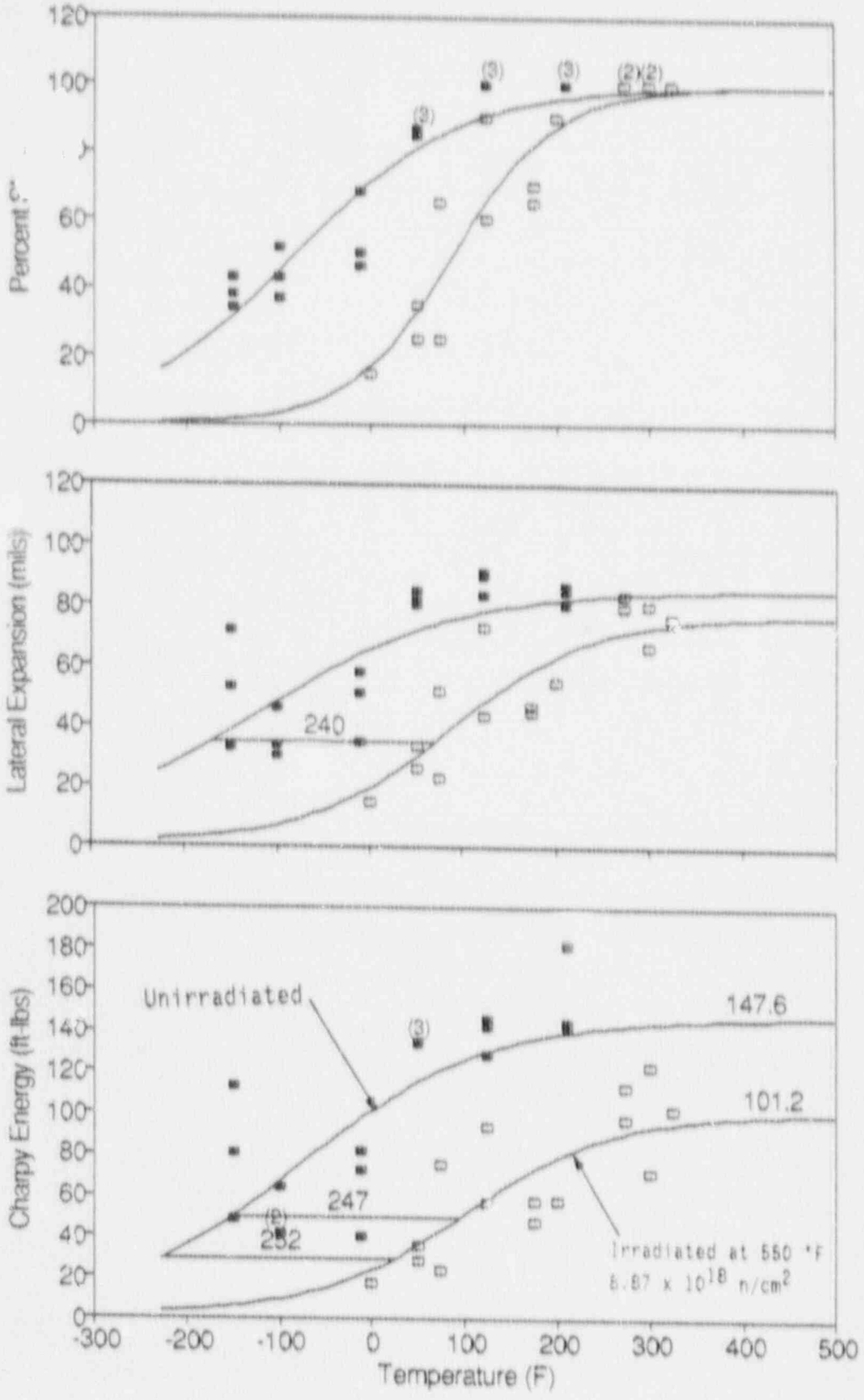

Figure 5-4. Charpy V-Notch Impact Properties for Diablo Canyon Unit 2 Reactor Weld Heat Affected Zone Metal

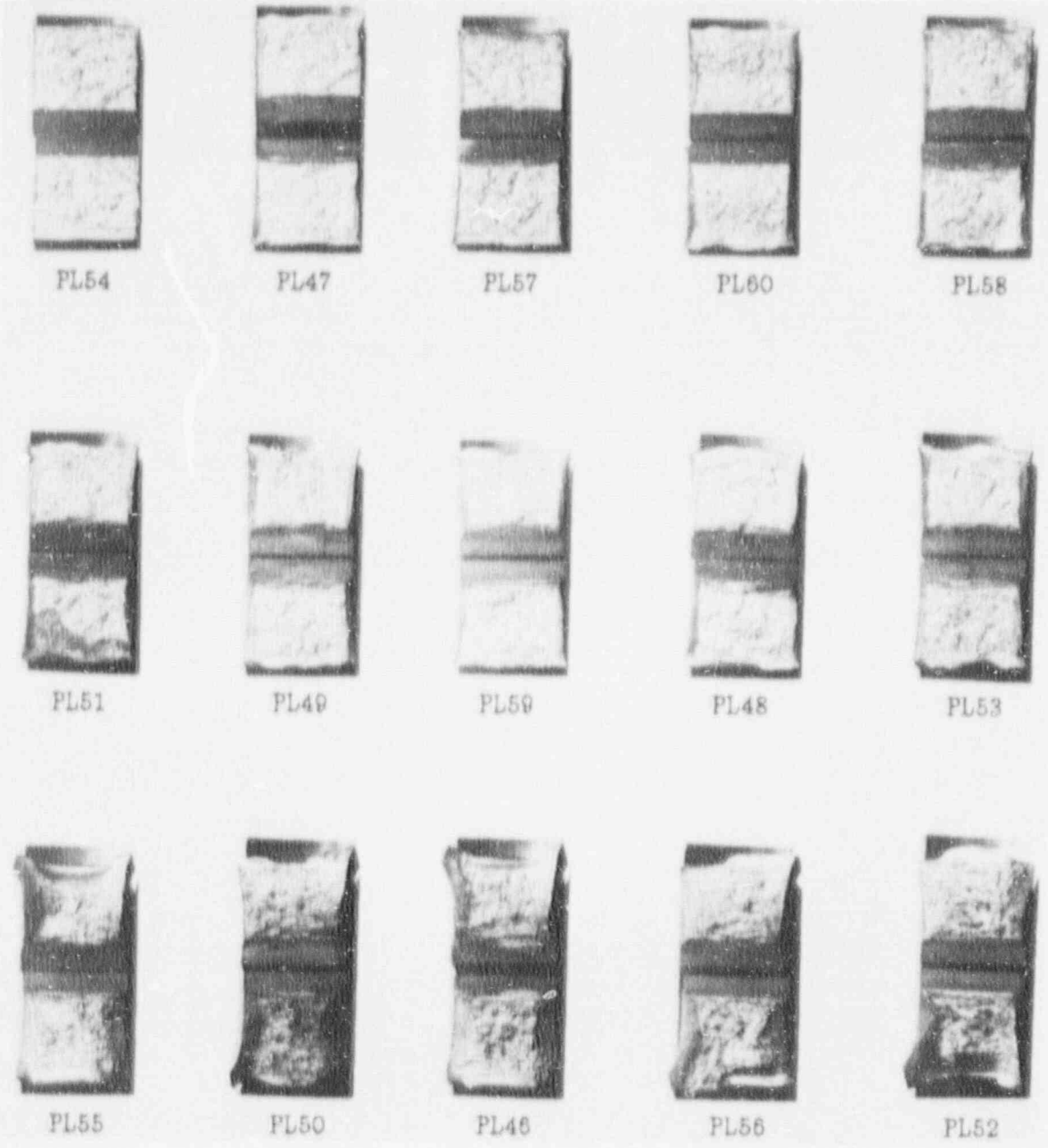

Figure 5-5. Charpy Impact Specimen Fracture Surfaces for Diablo Canyon Unit 2 Reactor Vessel Intermediate Shell Plate B5454-1 (Longitudinal Orientation)

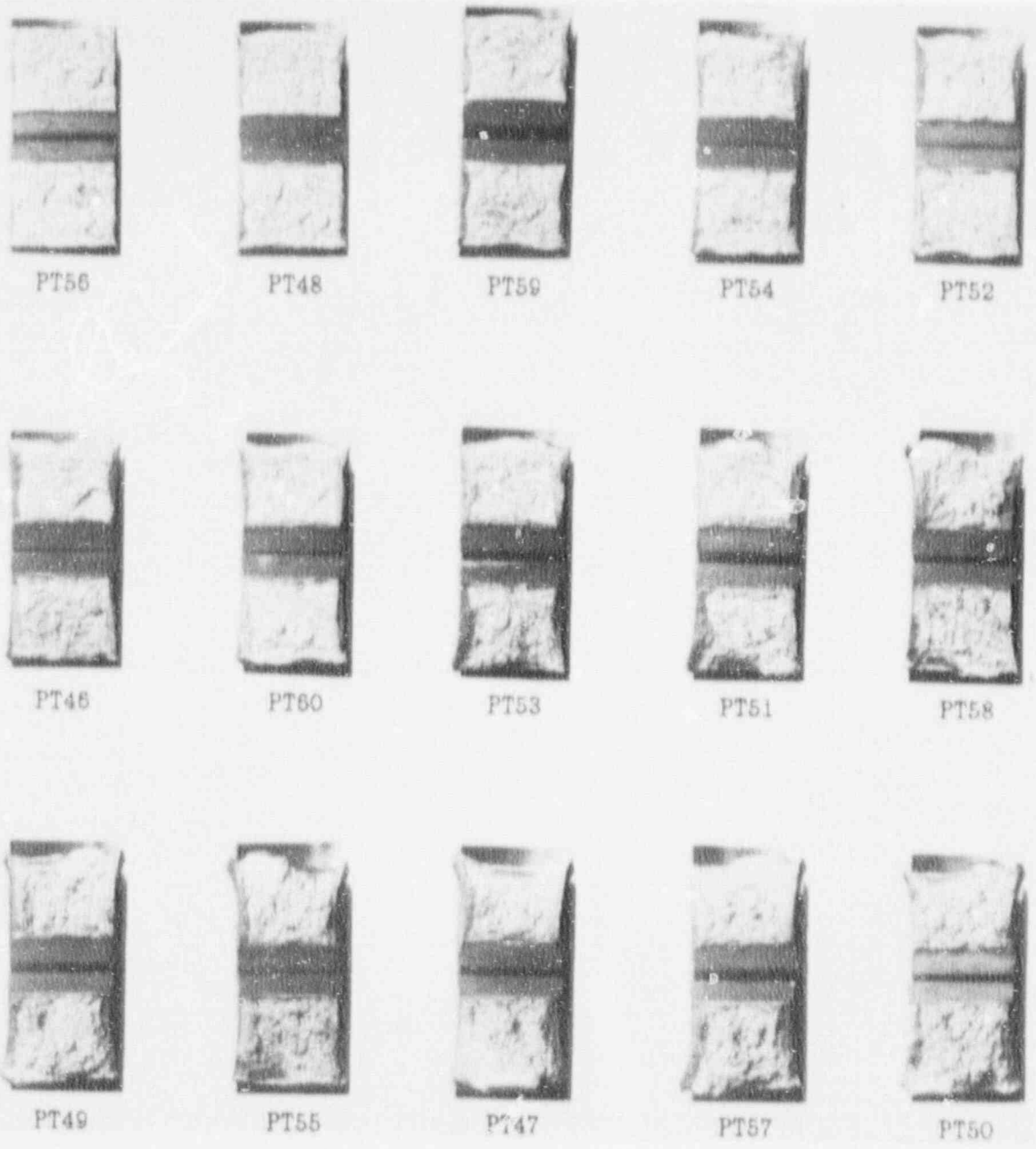

Figure 5-6. Charpy Impact Specimen Fracture Surfaces for Diablo Canyon Unit 2 Reactor Vessel Intermediate Shell Plate B5454-1 (Transverse Orientation)

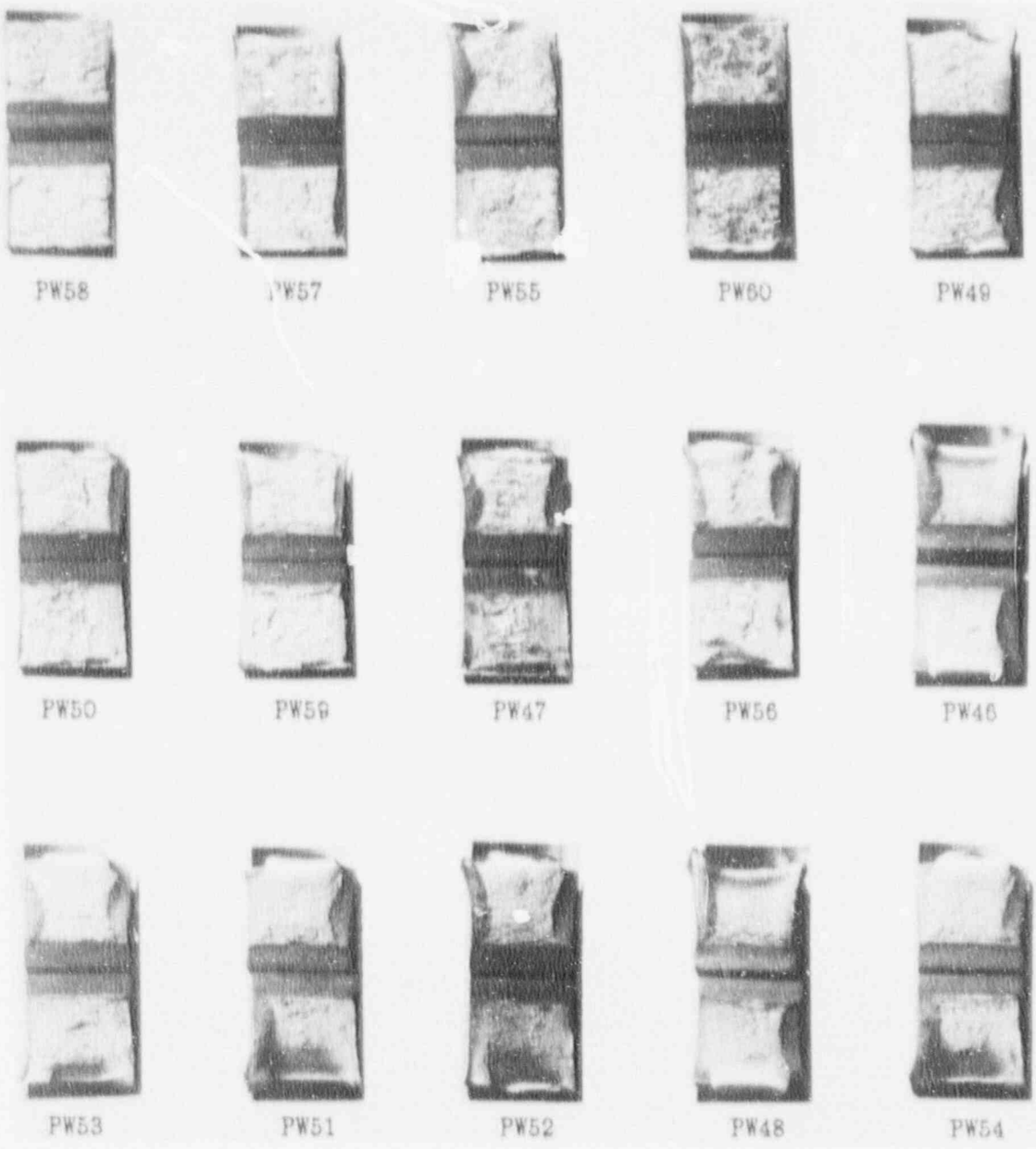

Figure 5-7. Charpy Impact Specimen Fracture Surfaces for Diablo Canyon Unit 2 Reactor Vessel Weld Metal

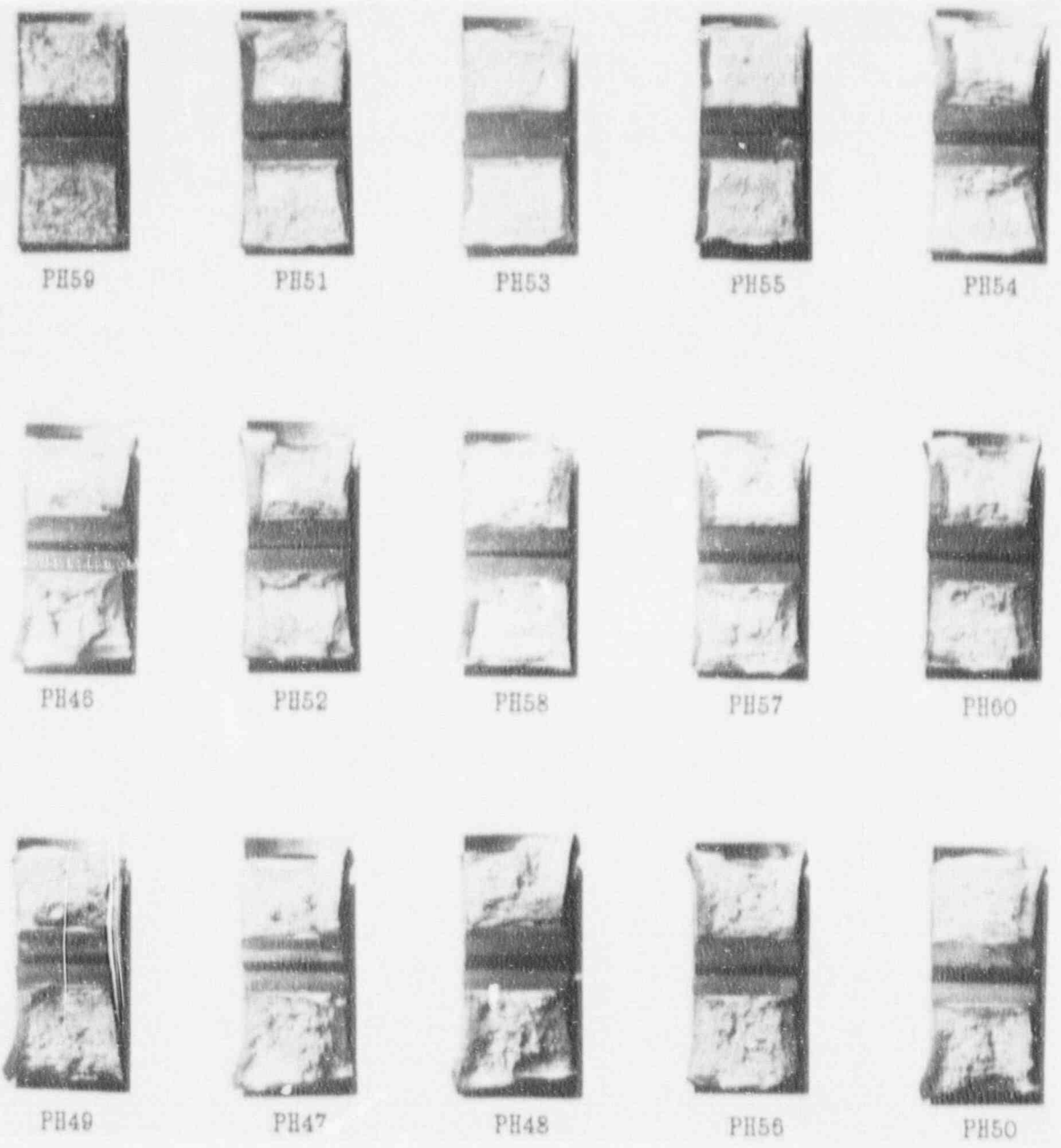

Figure 5-8. Charpy Impact Specimen Fracture Surfaces for Diablo Canyon Unit 2 Reactor Vessel Weld Heat Affected Zone (HAZ) Metal

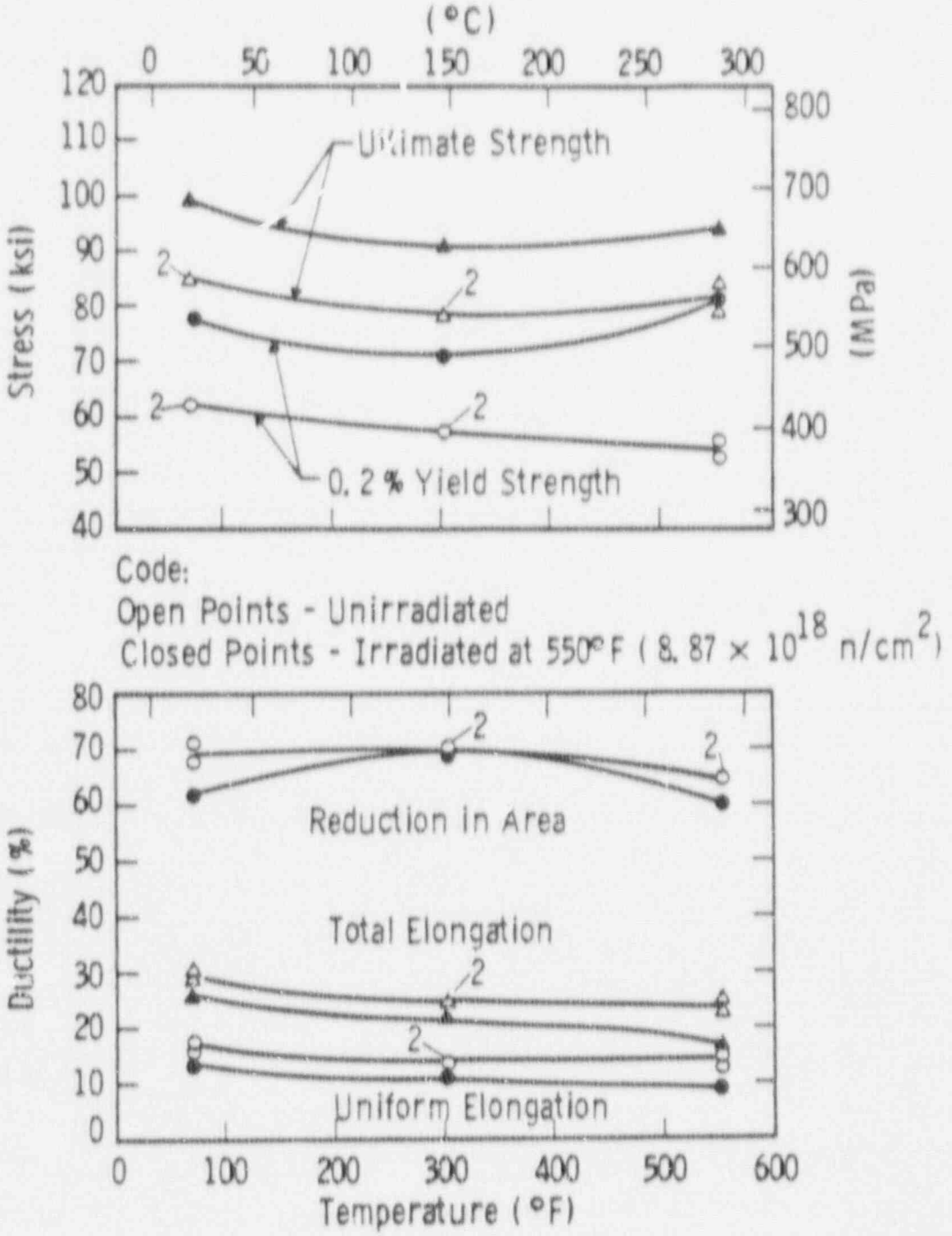

Figure 5-9. Tensile Properties for Diablo Canyon Unit 2 Reactor Vessel Intermediate Shell Plate B5454-1 (Longitudinal Orientation)

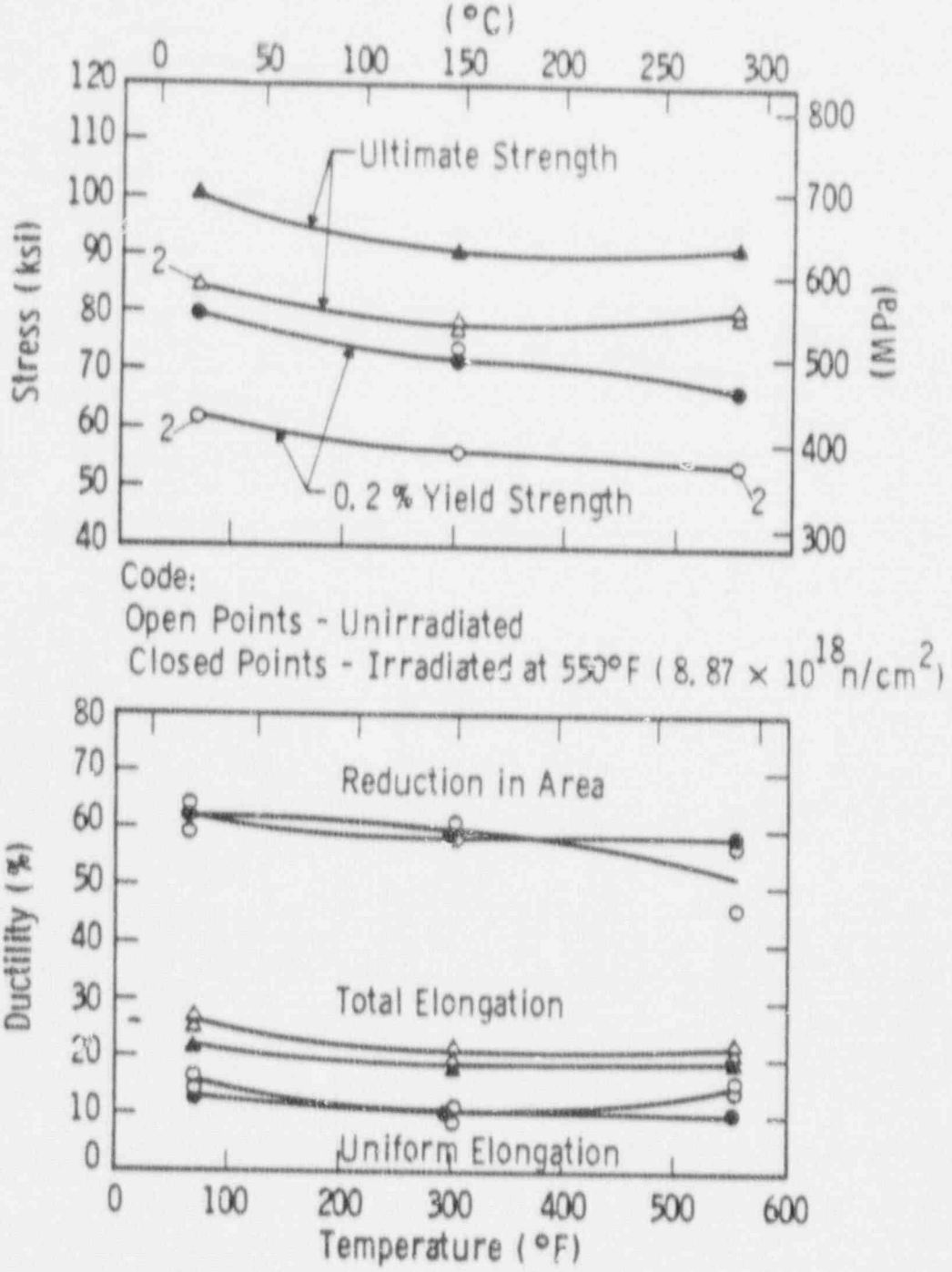

Figure 5-10. Tensile Properties for Diablo Canyon Unit 2 Reactor Vessel Intermediate Shell Plate B5454-1 (Transverse Orientation)

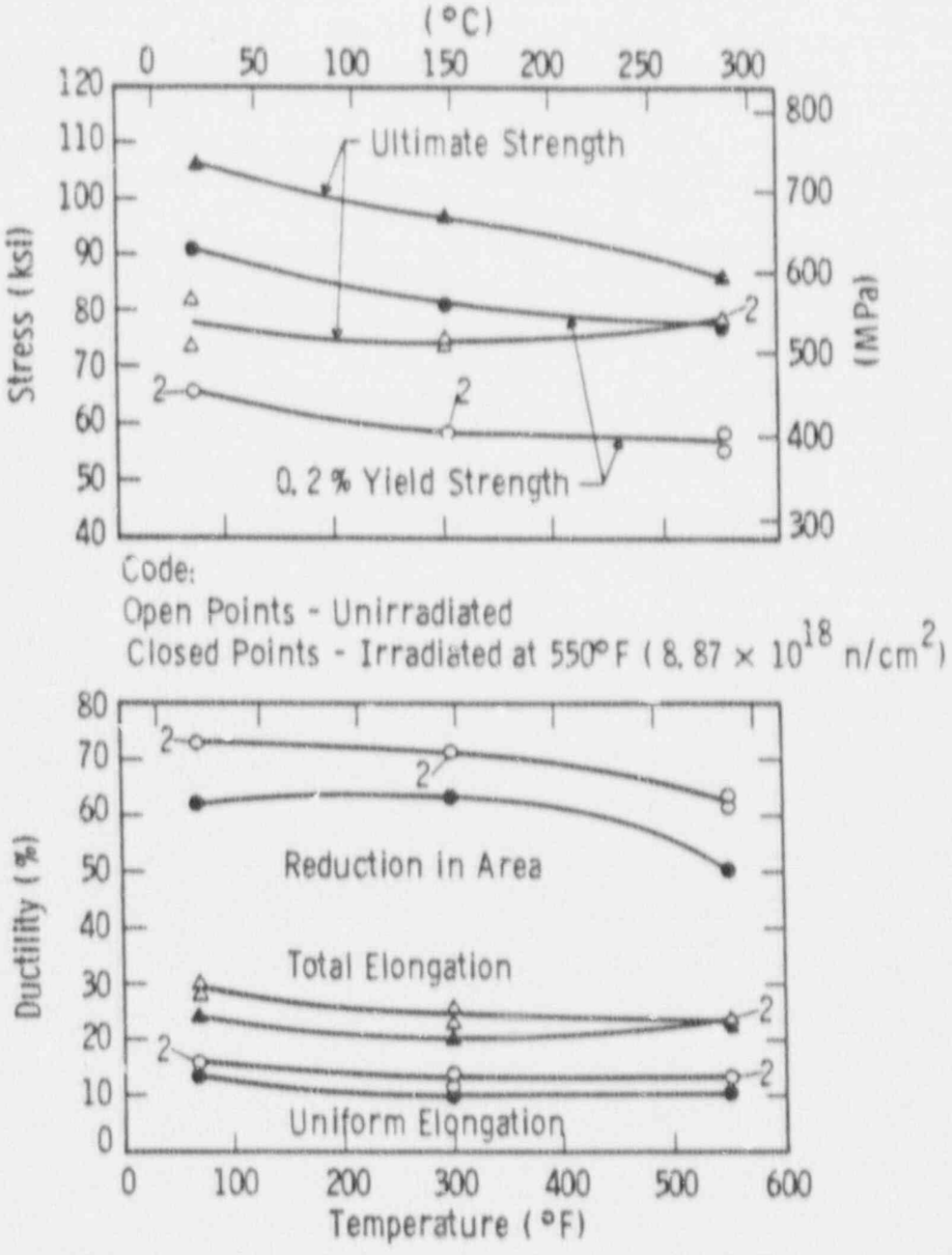

Figure 5-11. Tensile Properties for Diablo Canyon Unit 2 Reactor Vessel Weld Metal

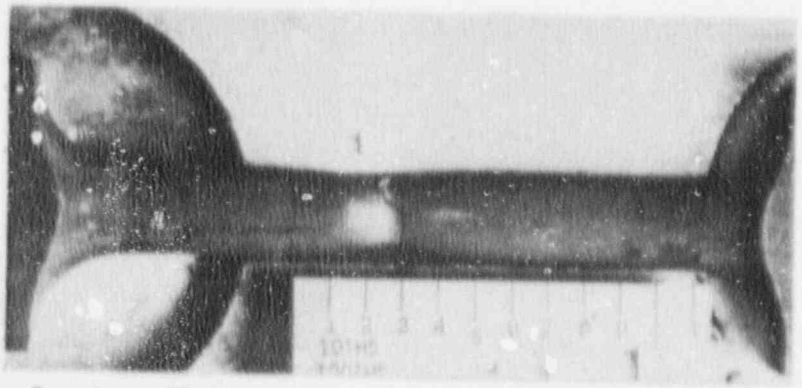

Specimen PL10 74°F

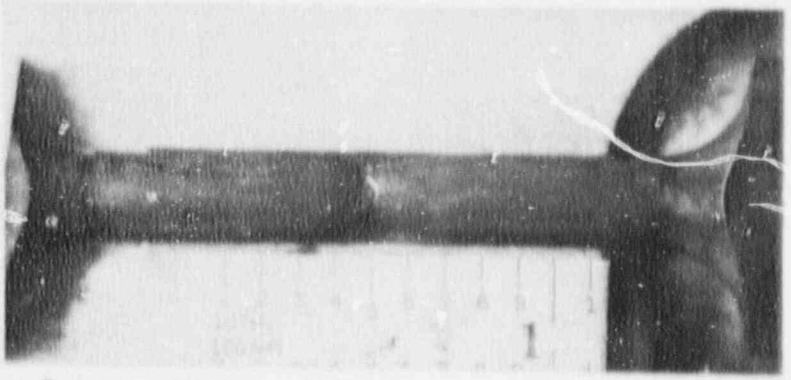

Specimen PL11 300°F

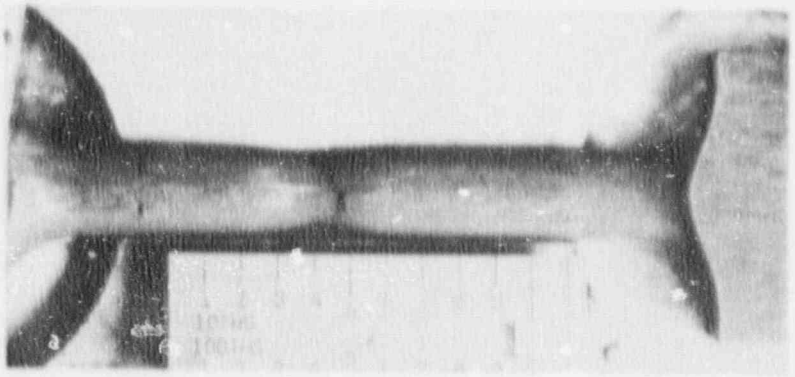

Specimen PL12 550°F

Figure 5-12. Fractured Tensile Specimens from Diablo Canyon Unit 2 Reactor Vessel Intermediate Shell Plate B5454-1 (Longitudinal Orientation)

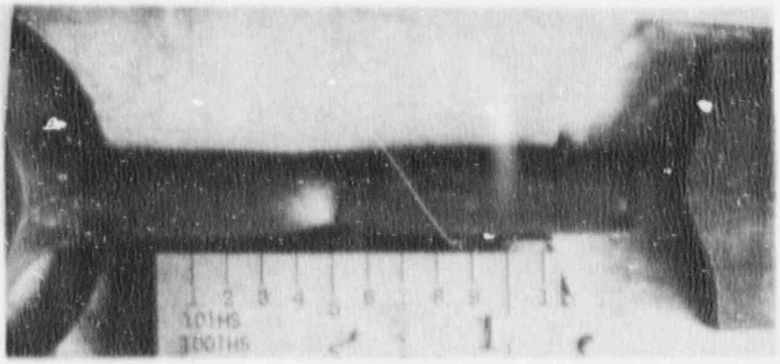

Specimen PT10 74°F

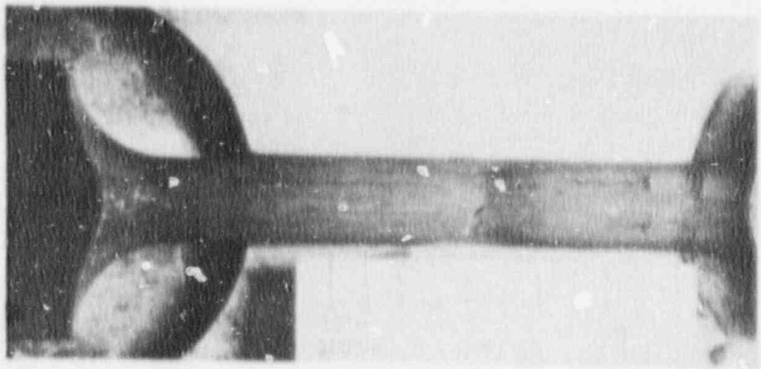

Specimen PT11 300°F

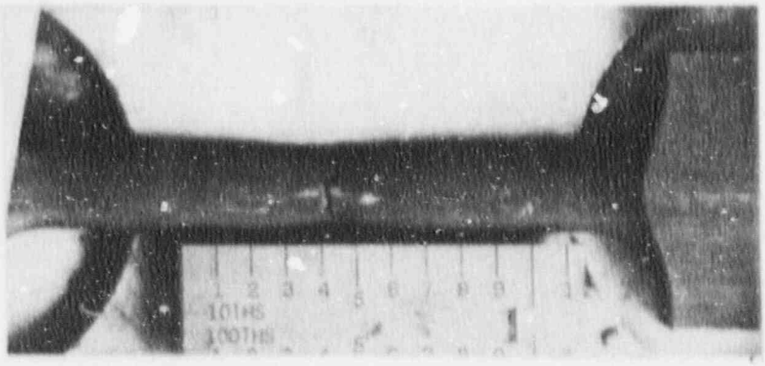

Specimen PT12 550°F

Figure 5-13. Fractured Tensile Specimens from Diablo Canyon Unit 2 Reactor Vessel Intermediate Shell Plate B5454-1 (Transverse Orientation)

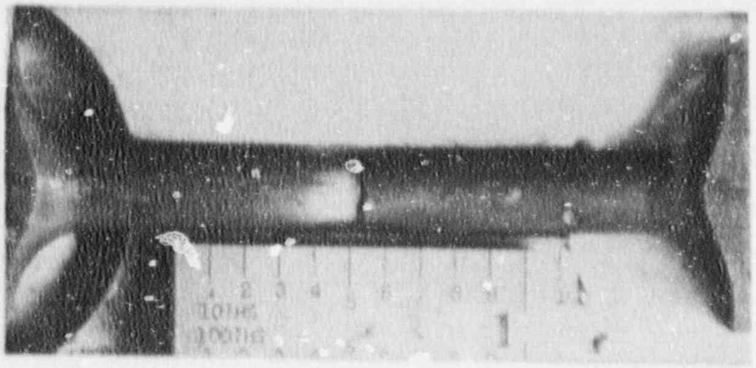

Specimen PW10 74°F

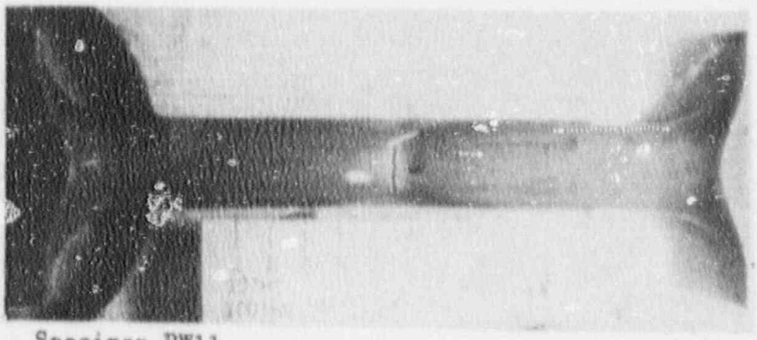

Specimen PW11 300°F

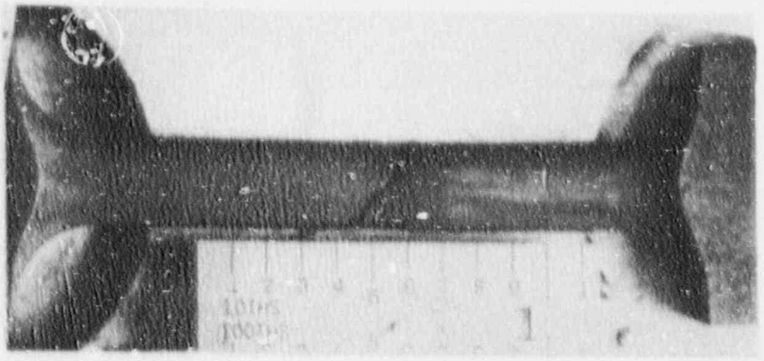

Specimen PW12 550°F

Figure 5-14. Fractured Tensile Specimens from Diablo Canyon Unit 2 Reactor Vessel Weld Metal

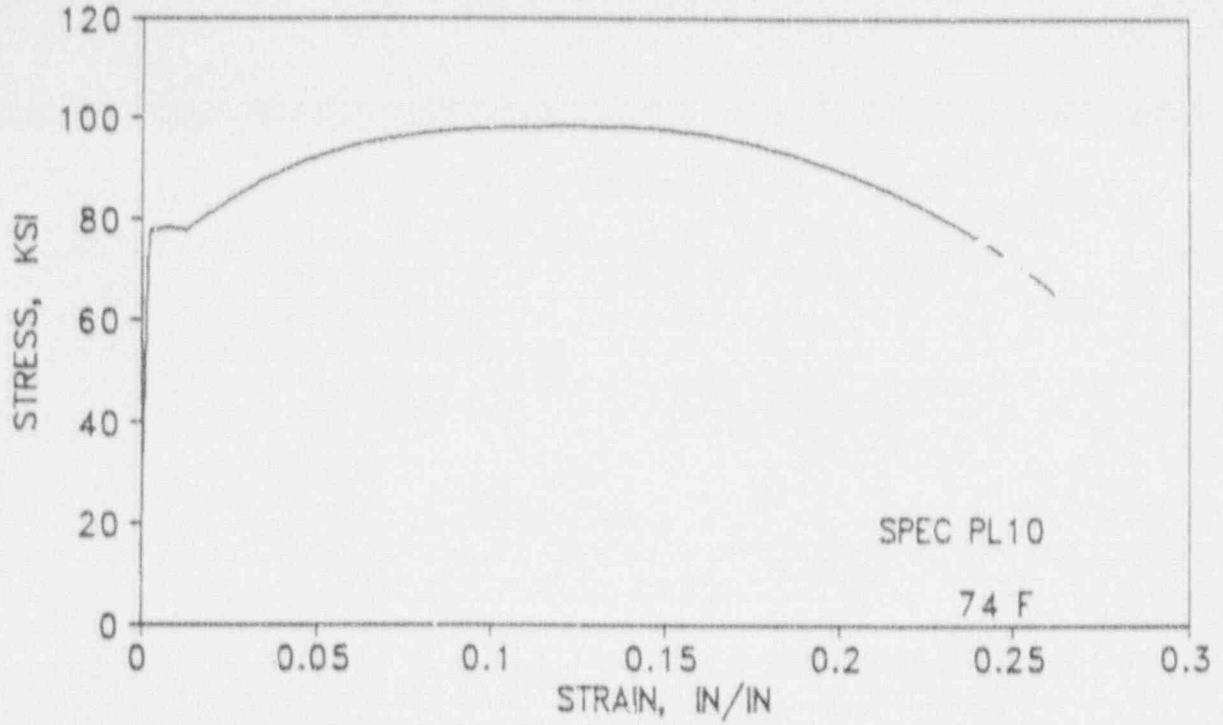

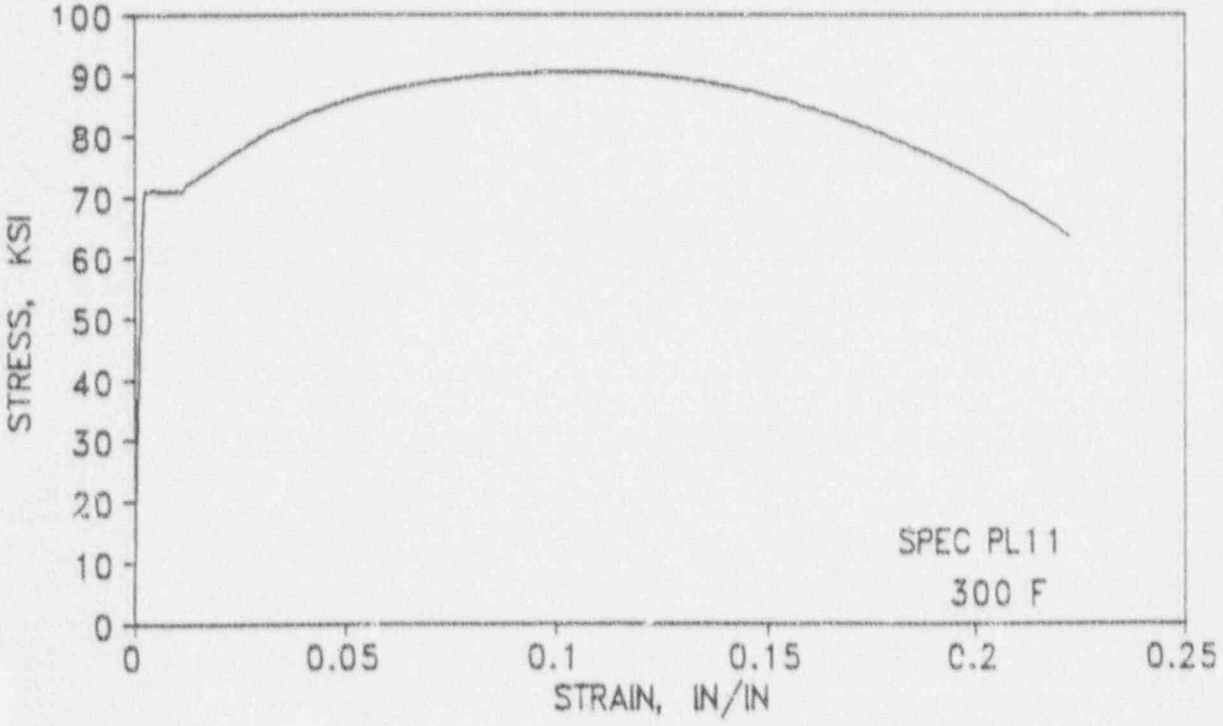

Figure 5-15. Engineering Stress-Strain Curves for Diablc Canyon Unit 2 Reactor Vessel Intermediate Shell Plate B5454-1 Tension Specimens PL10 and PL11

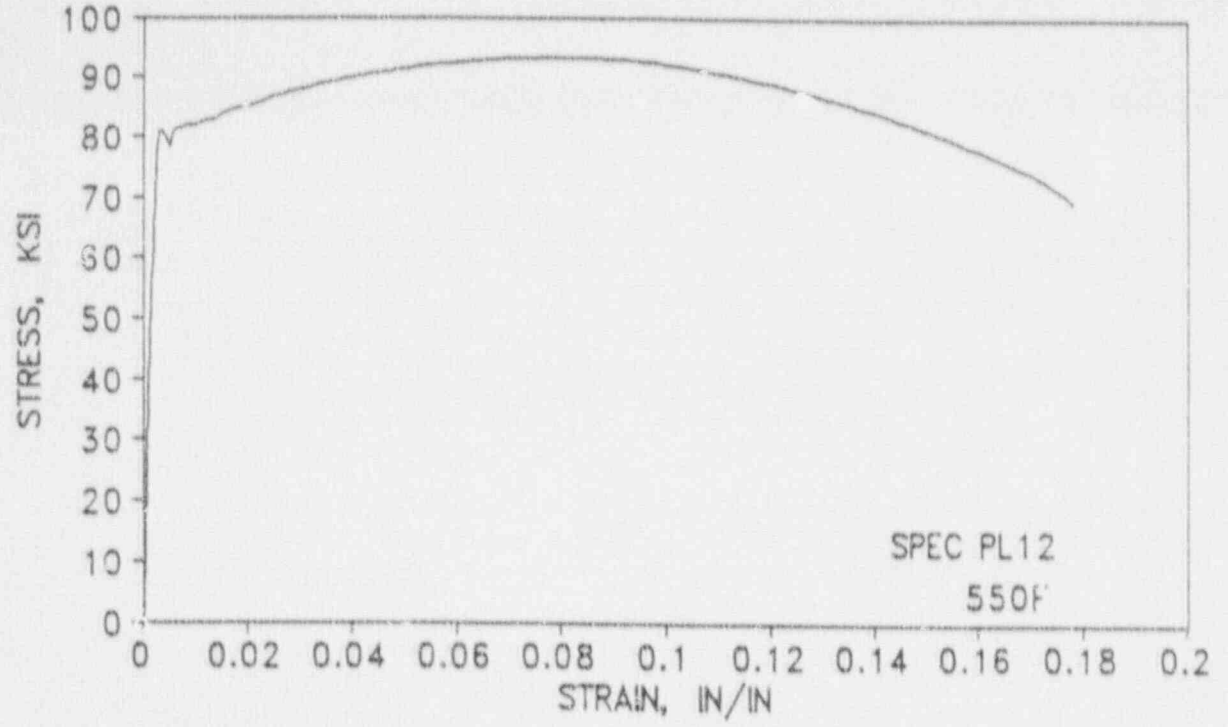

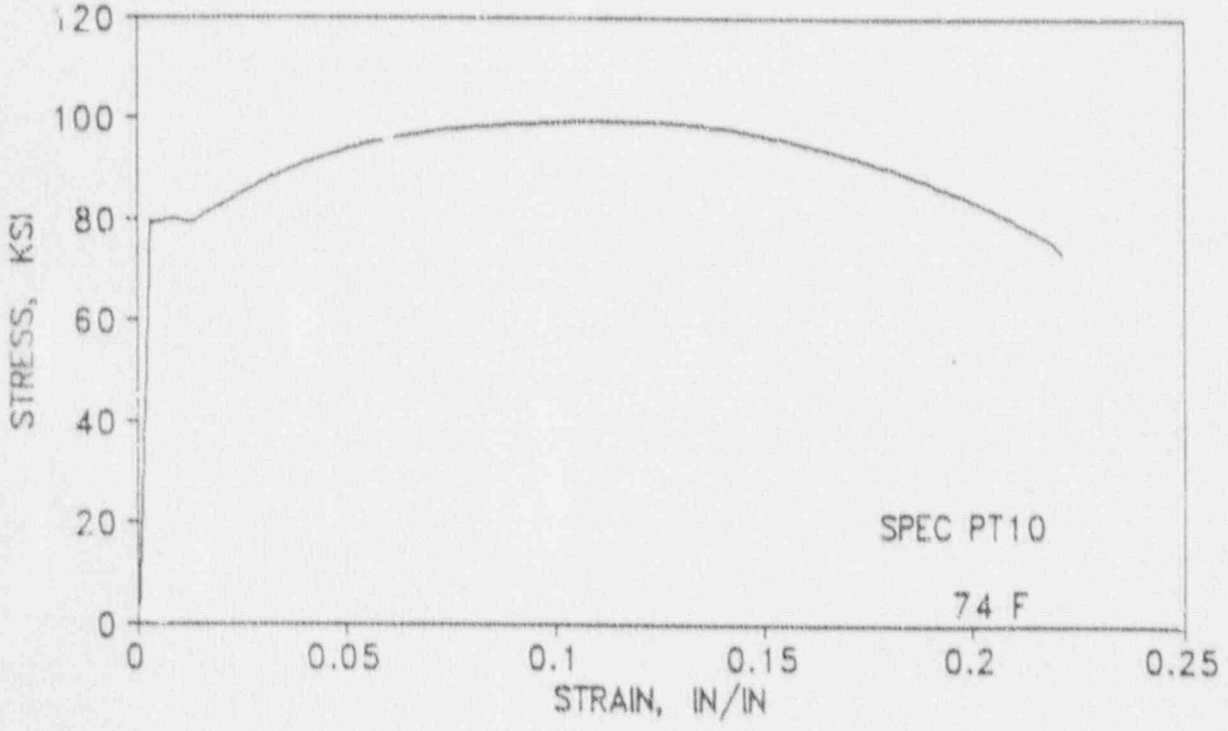

Figure 5-16. Engineering Stress-Strain Curves for Diablo Canyon Unit 2 Reactor Vessel Intermediate Shell Plate B5451-1 Tension Specimens PL12 and PT10

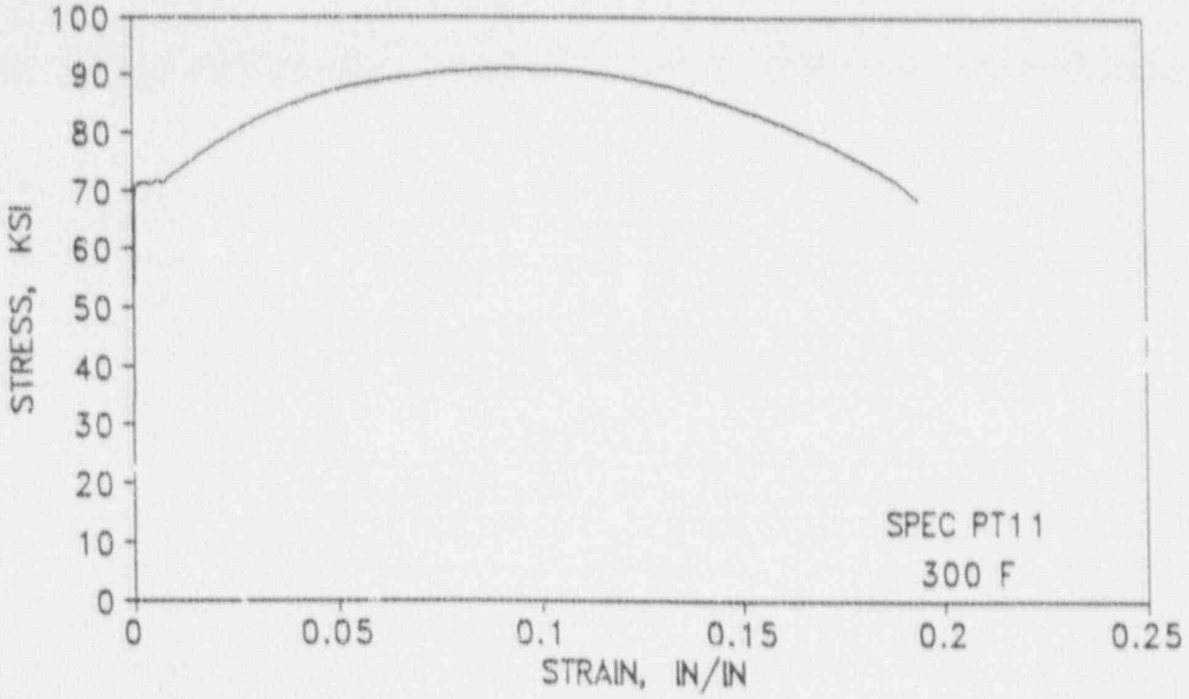

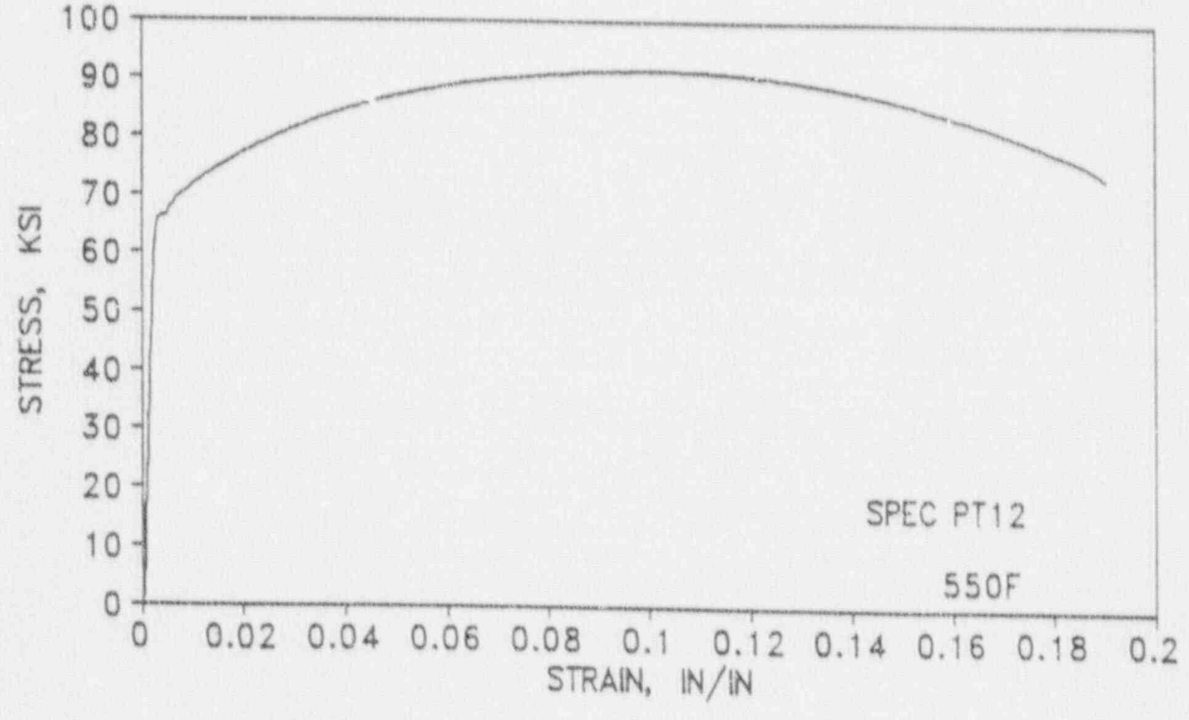

Figure 5-17. Engineering Stress-Strain Curves for Diablo Canyon Unit 2 Reactor Vessel Intermediate Shell Plate B5454-1 Tension Specimens PT11 and PT12

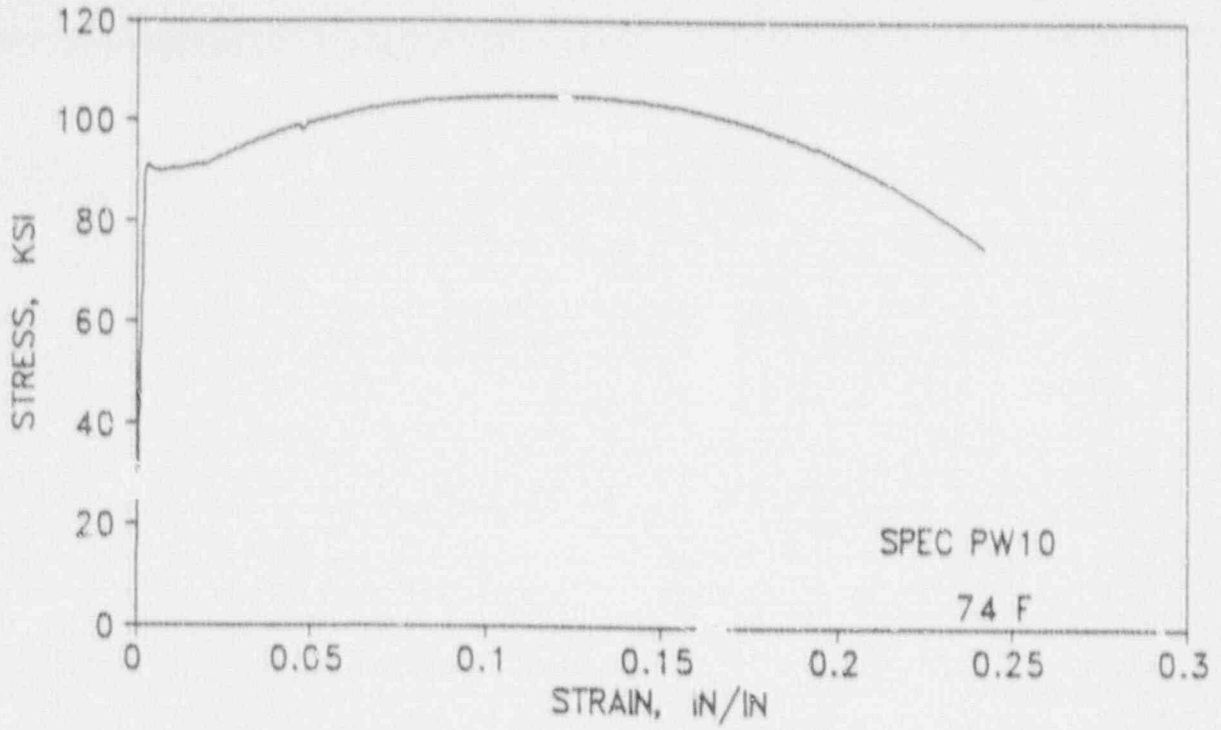

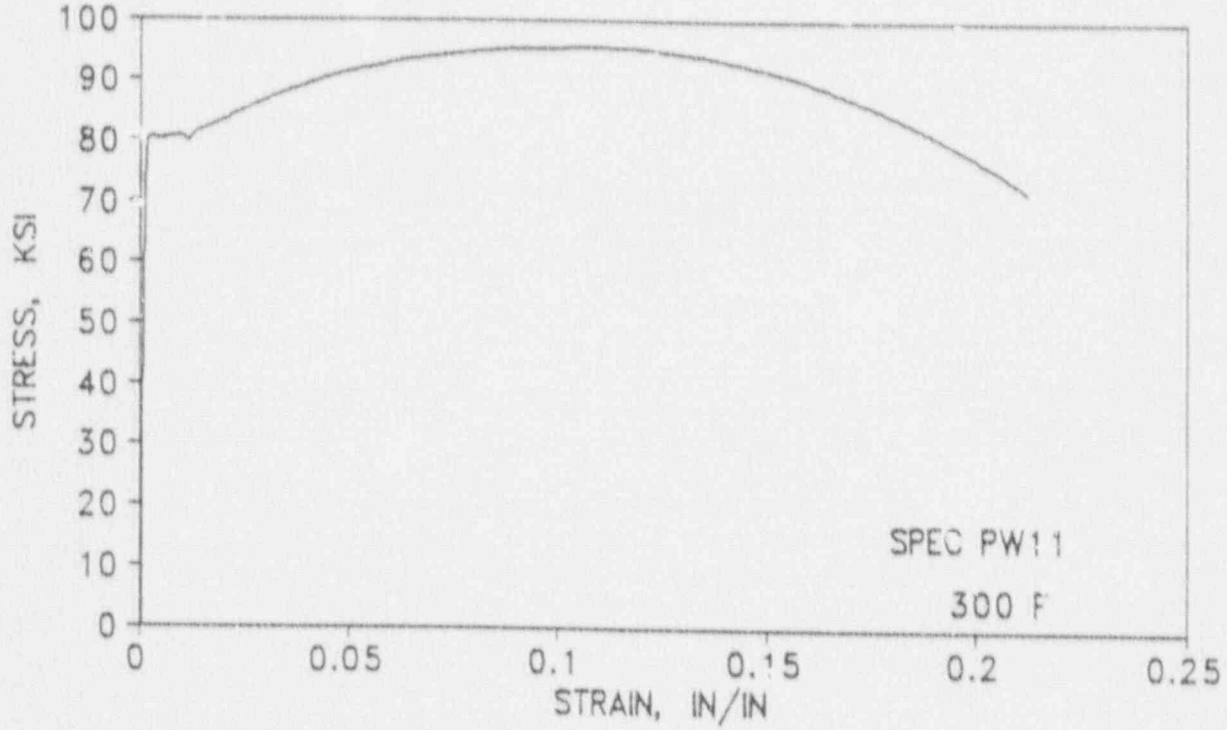

Figure 5-18. Engineering Stress-Strain Curves for Diablo Canyon Unit 2 Reactor Vessel Weld Metal Tension Specimens PW10 and PW11

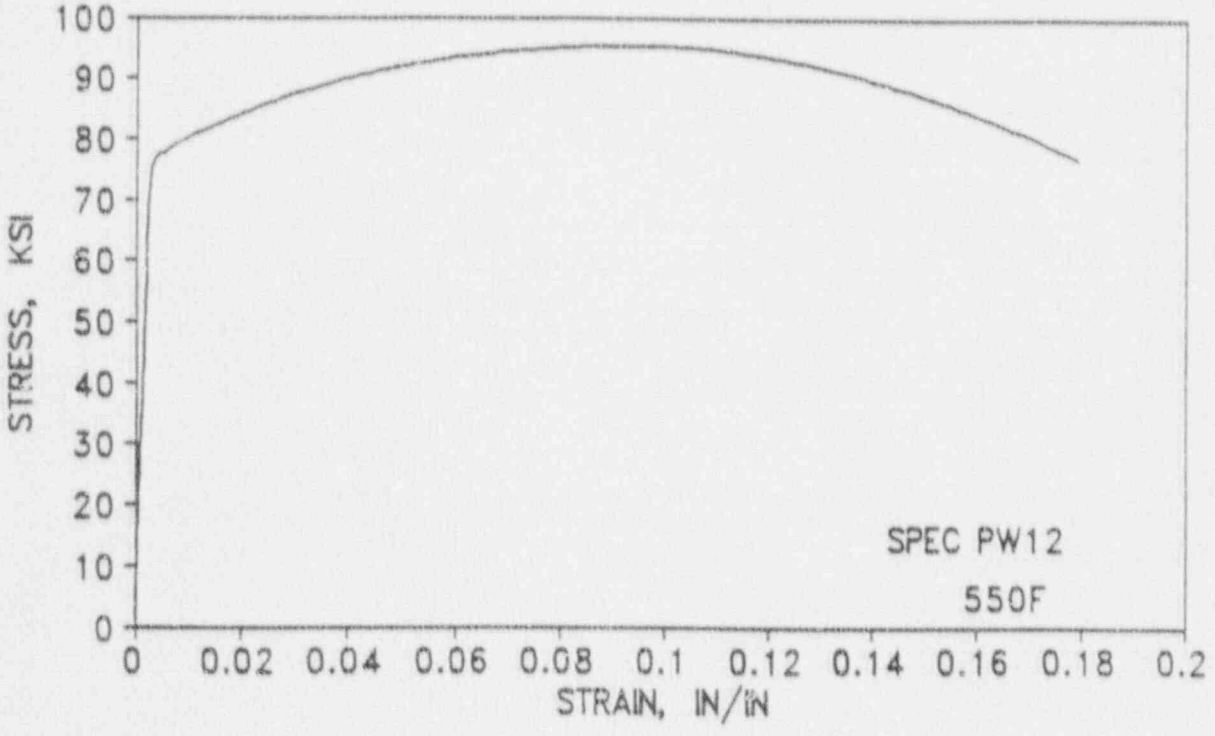

Figure 5-19. Engineering Stress-Strain Curves for Diablo Canyon Unit 2 Reactor Vessel Weld Metal Tension Specimen PW12

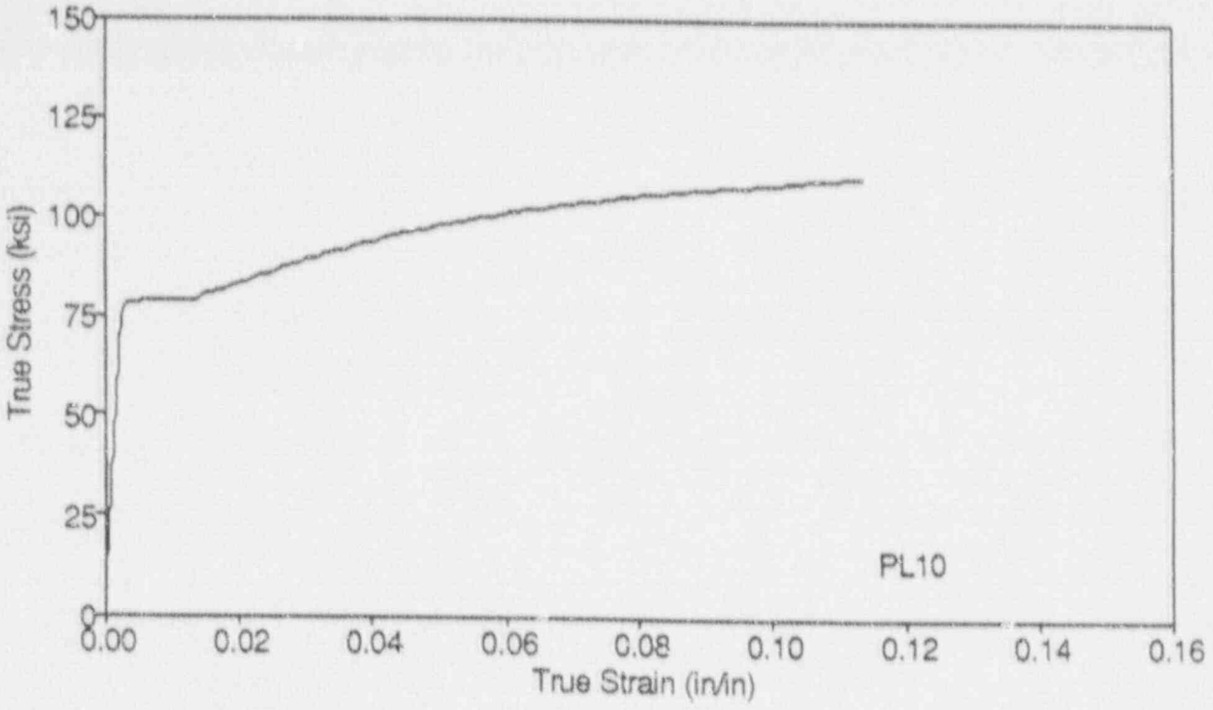

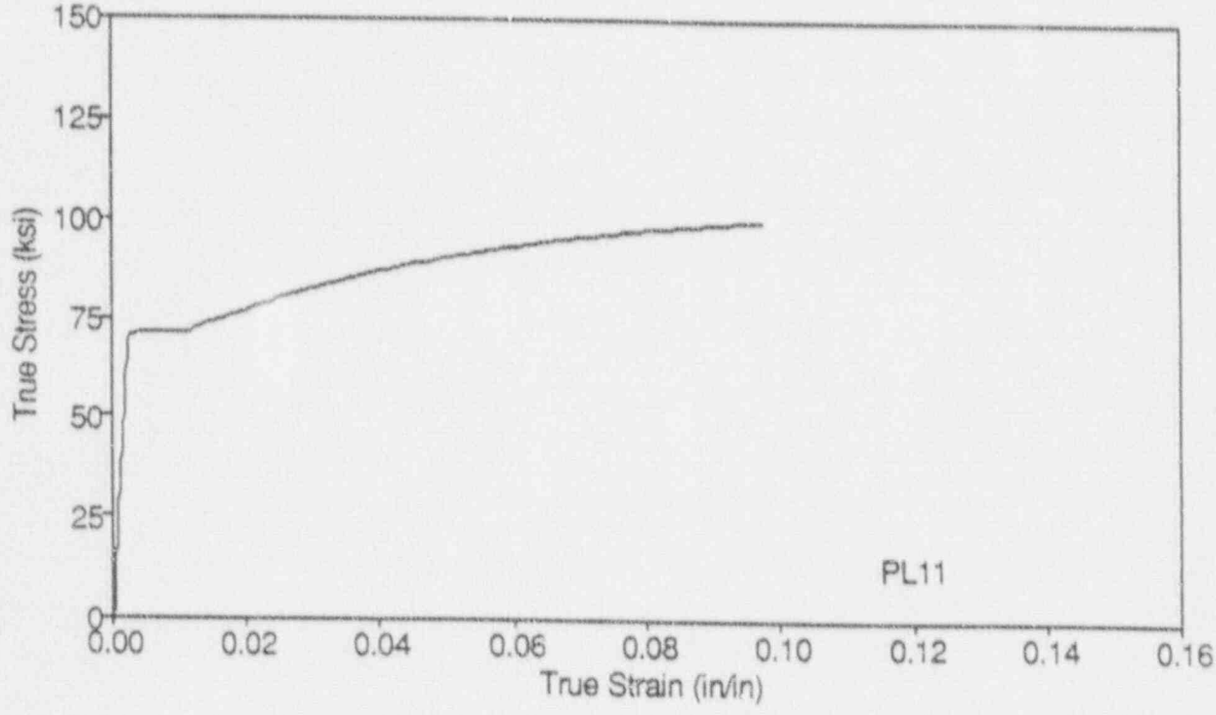

Figure 5-20. True Stress-Strain Curves for Diablo Canyon Unit 2 Reactor Vessel Intermediate Shell Plate B5454-1 Tension Specimens PL10 and PL11

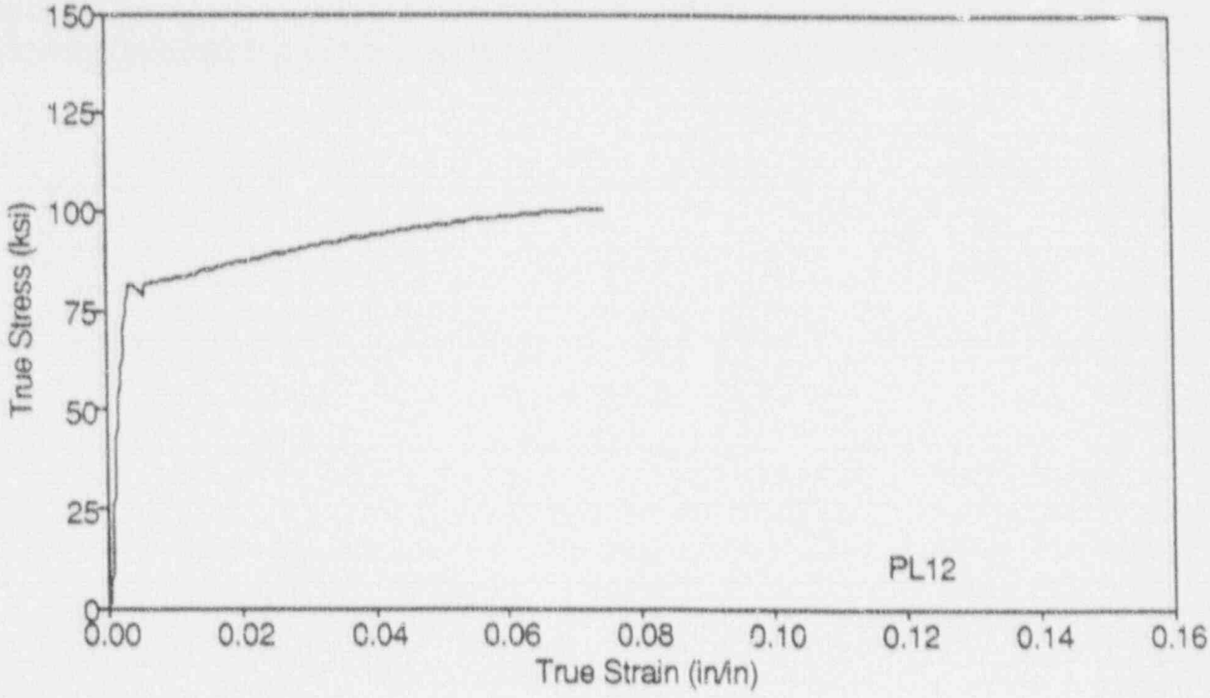

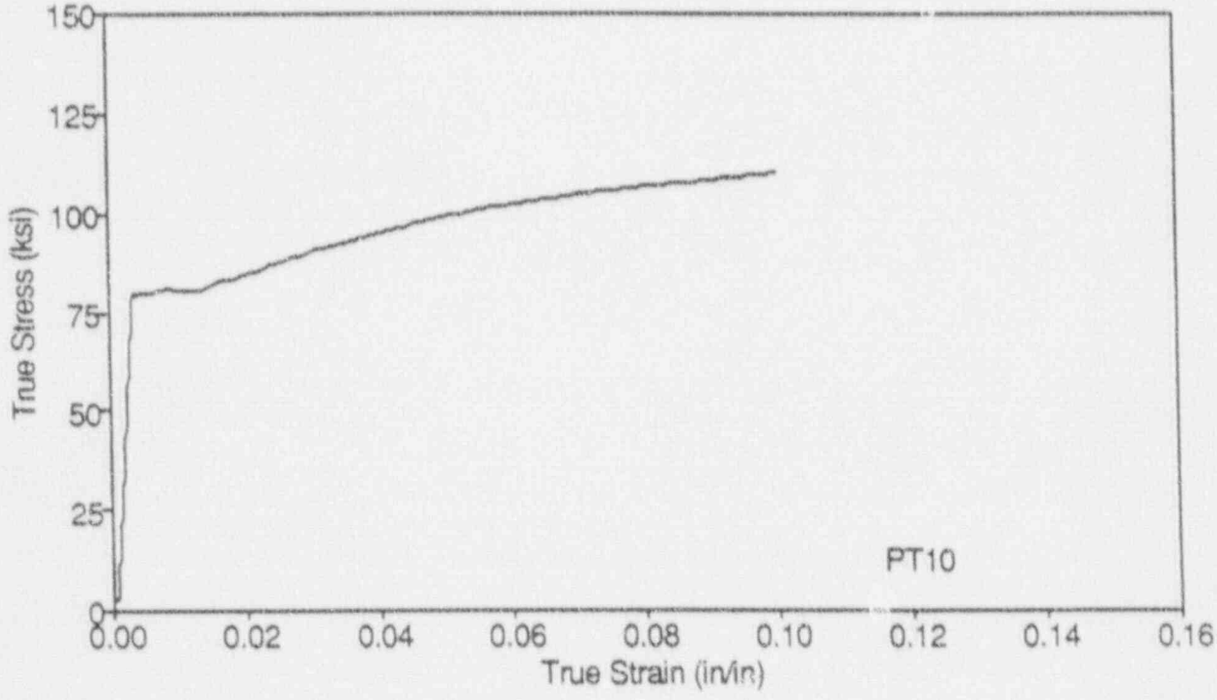

Figure 5-21. True Stress-Strain Curves for Diablo Canyon Unit 2 Reactor Vessel Intermediate Shell Plate B5454-1 Tension Specimens PL12 and PT10

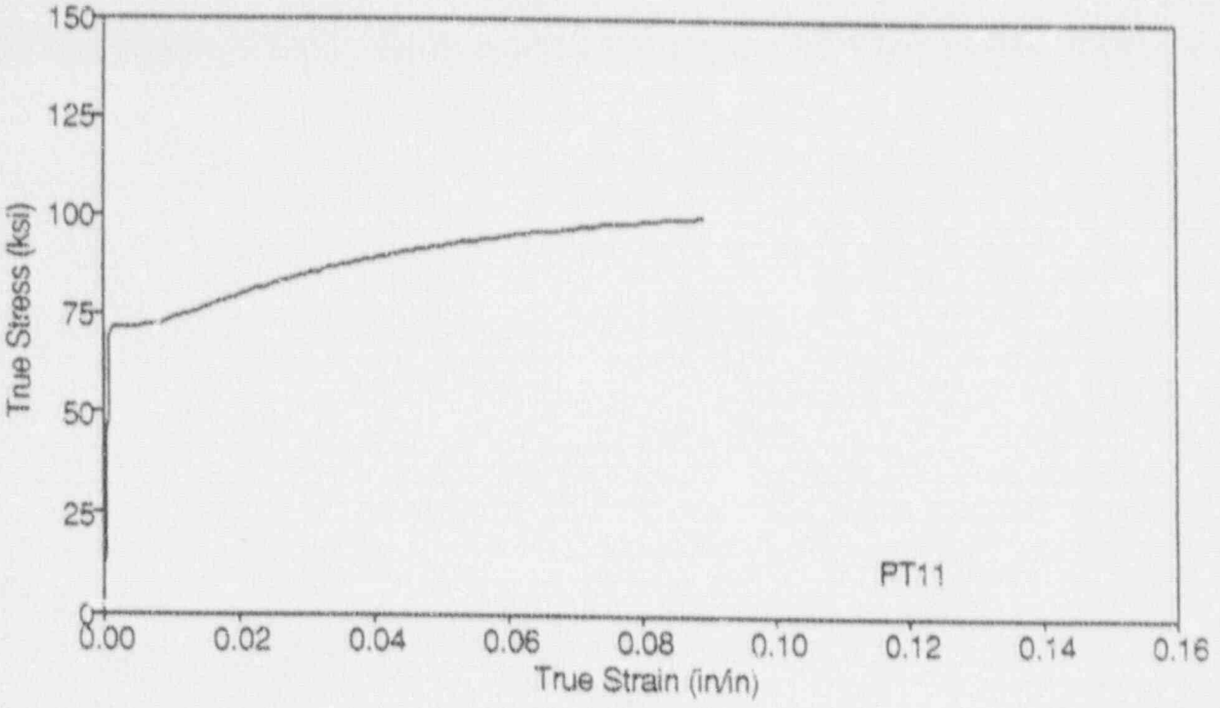

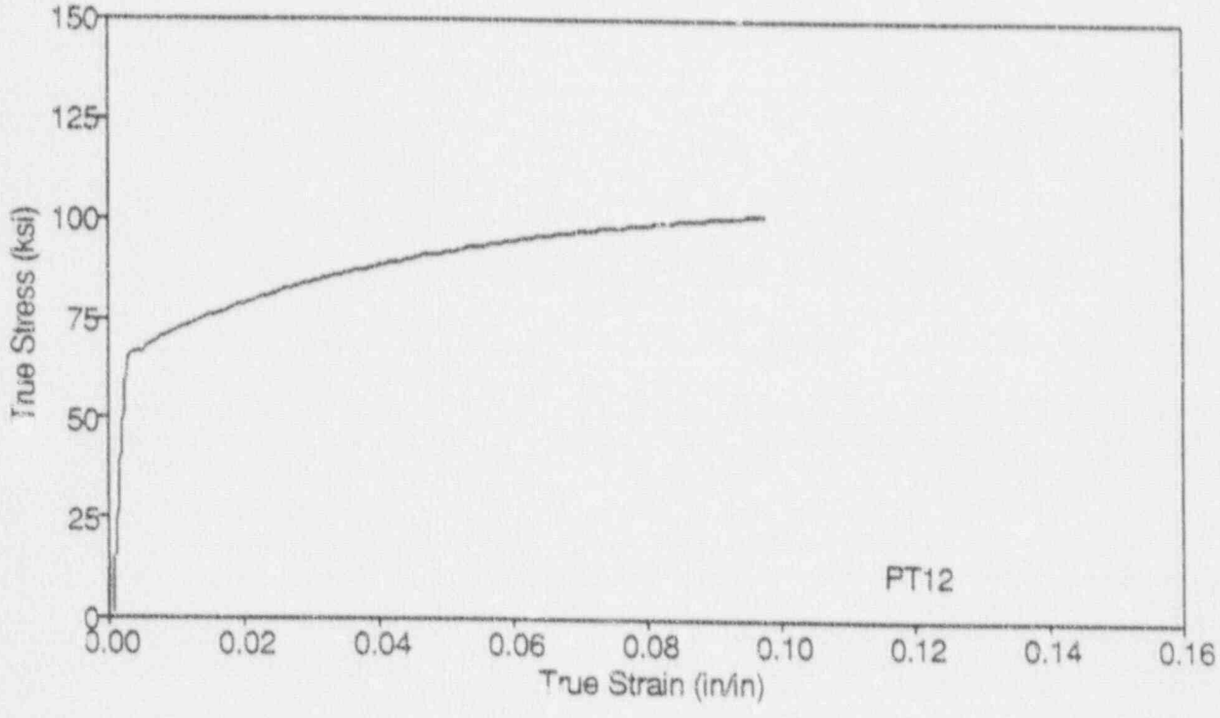

Figure 5-22. True Stress-Strain Curves for Diablo Canyon Unit 2 Reactor Vessel Intermediate Shell Plate B5454-1 Tension Specimens PT11 and PT12

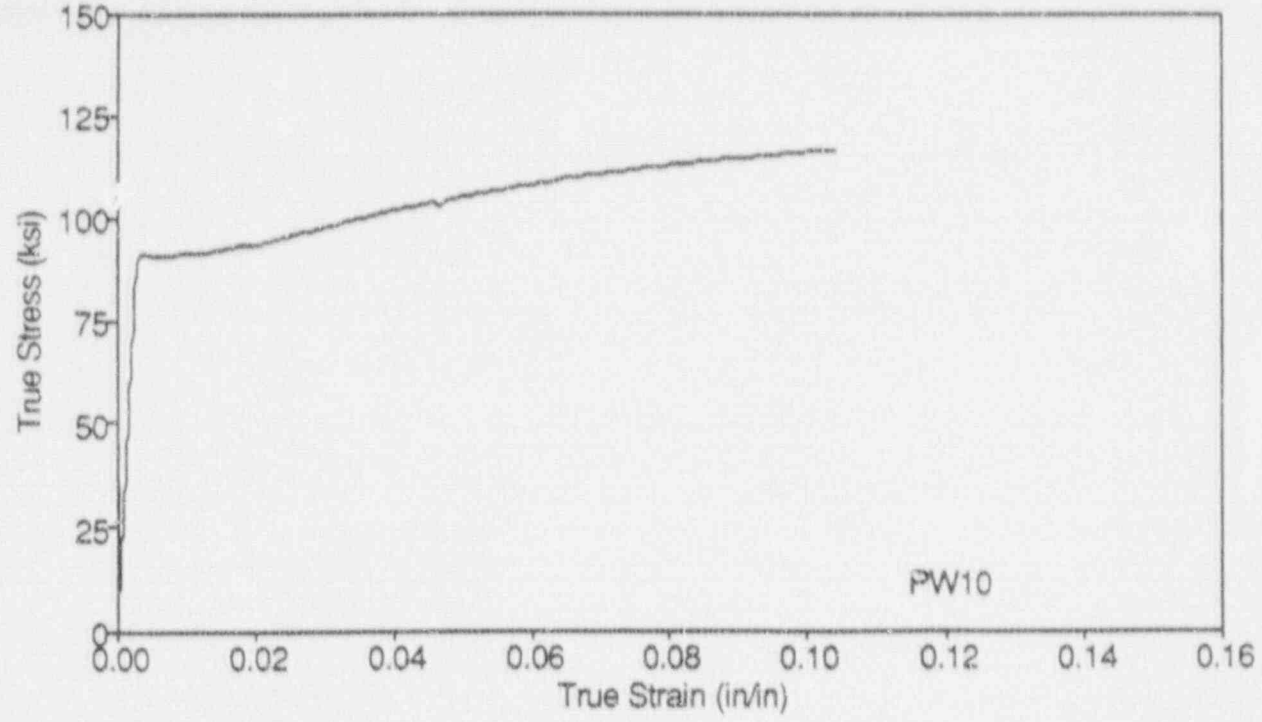

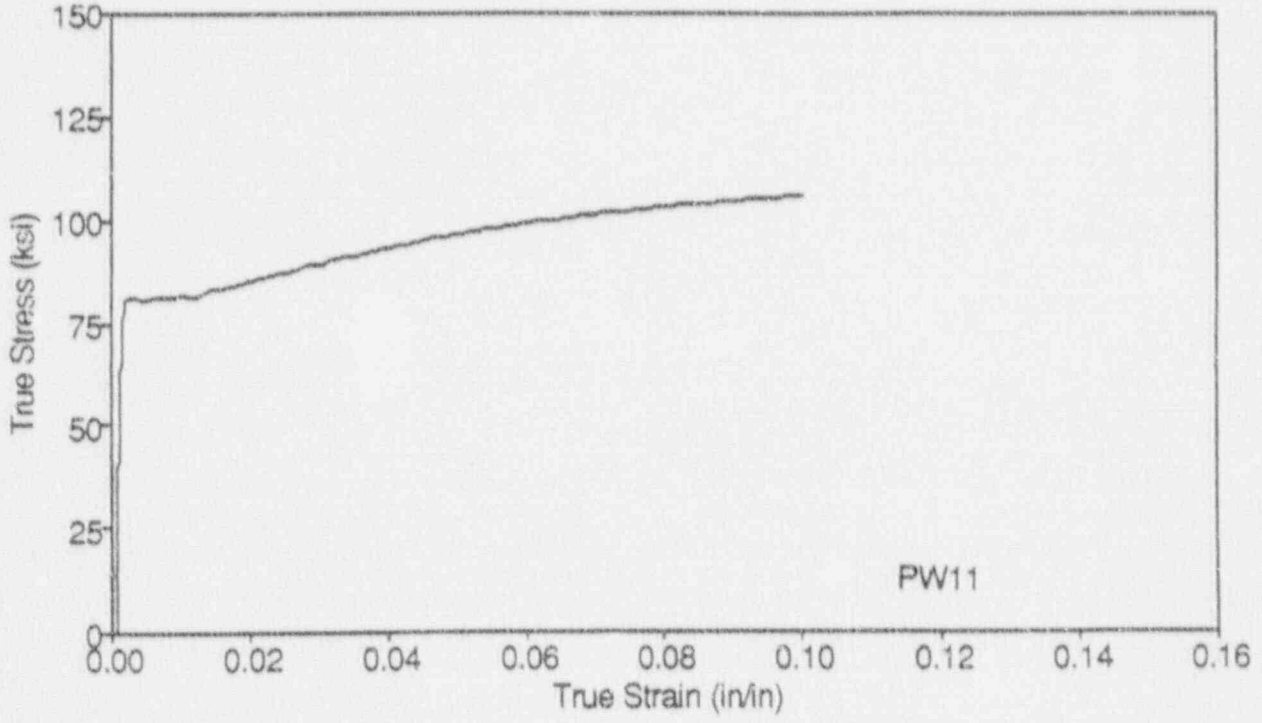

Figure 5-23. True Stress-Strain Curves for Diablo Canyon Unit 2 Reactor Vessel Weld Metal Tension Specimens PW10 and PW11

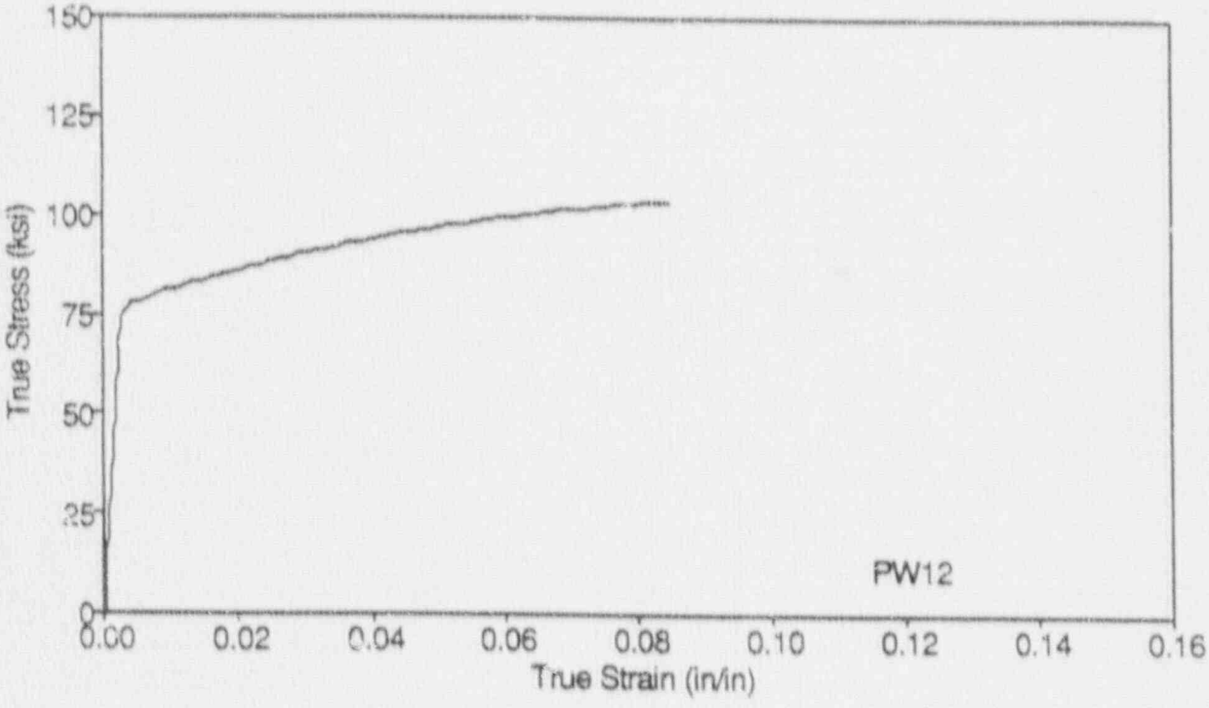

Figure 5-24. True Stress-Strain Curves for Diablo Canyon Unit 2 Reactor Vessel Weld Metal Tension Specimen PW12

SECTION 6.0
RADIATION ANALYSIS AND NEUTRON DOSIMETRY

6.1 Introduction

Knowledge of the neutron environment within the reactor pressure vessel and surveillance capsule geometry is required as an integral part of LWR reactor pressure vessel surveillance programs for two reasons. First, in order to interpret the neutron radiation-induced material property changes observed in the test specimens, the neutron environment (energy spectrum, flux, fluence) to which the test specimens were exposed must be known. Second, in order to relate the changes observed in the test specimens to the present and future condition of the reactor vessel, a relationship must be established between the neutron environment at various positions within the reactor vessel and that experienced by the test specimens. The former requirement is normally met by employing a combination of rigorous analytical techniques and measurements obtained with passive neutron flux monitors contained in each of the surveillance capsules. The latter information is derived solely from analysis.

The use of fast neutron fluence (E > 1.0 MeV) to correlate measured materials properties changes to the neutron exposure of the material for light water reactor applications has traditionally been accepted for development of damage trend curves as well as for the implementation of trend curve data to assess vessel condition. In recent years, however, it has been suggested that an exposure model that accounts for differences in neutron energy spectra between surveillance capsule locations and positions within the vessel wall could lead to an improvement in the uncertainties associated with damage trend curves as well as to a more accurate evaluation of damage gradients through the pressure vessel wall.

Because of this potential shift away from a threshold fluence toward an energy dependent damage function for data correlation, ASTM Standard Practice E853, "Analysis and Interpretation of Light Water Reactor Surveillance Results," recommends reporting displacements per iron atom (dpa) along with fluence

(E > 1.0 MeV) to provide a data base for future reference. The energy dependent dpa function to be used for this evaluation is specified in ASTM Standard Practice E693, "Characterizing Neutron Exposures in Ferritic Steels in Terms of Displacements per Atom." The application of the dpa parameter to the assessment of embrittlement gradients through the thickness of the pressure vessel wall has already been promulgated in Revision 2 to the Regulatory Guide 1.99, "Radiation Damage to Reactor Vessel Materials."

This section provides the results of the neutron dosimetry evaluations performed in conjunction with the analysis of test specimens contained in surveillance capsule X. Fast neutron exposure parameters in terms of fast neutron fluence (E > 1.0 MeV), fast neutron fluence (E > 0.1 MeV), and iron atom displacements (dpa) are established for the capsule irradiation history. The analytical formalism relating the measured capsule exposure to the exposure of the vessel wall is described and used to project the integrated exposure of the vessel itself. Also uncertainties associated with the derived exposure parameters at the surveillance capsule and with the projected exposure of the pressure vessel are provided.

6.2 Discrete Ordinates Analysis

A plan view of the reactor geometry at the core midplane is shown in Figure 4-1. Six irradiation capsules attached to the neutron pads are included in the reactor design to constitute the reactor vessel surveillance program. The capsules are located at azimuthal angles of 56.0°, 58.5°, 124.0°, 236.0°, 238.5°, and 304.0° relative to the core cardinal axis as shown in Figure 4-1.

A plan view of a dual surveillance capsule holder attached to the neutron pad is shown in Figure 6-1. The stainless steel specimen containers are 1.182 by 1-inch and approximately 56 inches in height. The containers are positioned axially such that the specimens are centered on the core midplane, thus spanning the central 5 feet of the 12-foot high reactor core.

From a neutron transport standpoint, the surveillance capsule structures are significant. They have a marked effect on both the distribution of neutron flux and the neutron energy spectrum in the water annulus between the neutron pad and the reactor vessel. In order to properly determine the neutron environment at the test specimen locations, the capsules themselves must be included in the analytical model.

In performing the fast neutron exposure evaluations for the surveillance capsules and reactor vessel, two distinct sets of transport calculations were carried out. The first, a single computation in the conventional forward mode, was used primarily to obtain relative neutron energy distributions throughout the reactor geometry as well as to establish relative radial distributions of exposure parameters [$\phi(E > 1.0$ MeV), $\phi(E > 0.1$ MeV), and dpa] through the vessel wall. The neutron spectral information was required for the interpretation of neutron dosimetry withdrawn from the surveillance capsule as well as for the determination of exposure parameter ratios; i.e., dpa/$\phi(E >$ 1.0 MeV), within the pressure vessel geometry. The relative radial gradient information was required to permit the projection of measured exposure parameters to locations interior to the pressure vessel wall; i.e., the 1/4T, 1/2T, and 3/4T locations.

The second set of calculations consisted of a series of adjoint analyses relating the fast neutron flux ($E > 1.0$ MeV) at surveillance capsule positions, and several azimuthal locations on the pressure vessel inner radius to neutron source distributions within the reactor core. The importance functions generated from these adjoint analyses provided the basis for all absolute exposure projections and comparison with measurement. These importance functions, when combined with cycle specific neutron source distributions, yielded absolute predictions of neutron exposure at the locations of interest for the first 3 cycles of irradiation; and established the means to perform similar predictions and dosimetry evaluations for all subsequent fuel cycles. It is important to note that the cycle specific neutron source distributions utilized in these analyses included not only spatial variations of fission rates within the reactor core; but, also accounted for the effects

of varying neutron yield per fission and fission spectrum introduced by the build-up of plutonium as the burnup of individual fuel assemblies increased.

The absolute cycle specific data from the adjoint evaluations together with relative neutron energy spectra and radial distribution information from the forward calculation provided the means to:

1. Evaluate neutron dosimetry obtained from surveillance capsule locations.

2. Extrapolate dosimetry results to key locations at the inner radius and through the thickness of the pressure vessel wall.

3. Enable a direct comparison of analytical prediction with measurement.

4. Establish a mechanism for projection of pressure vessel exposure as the design of each new fuel cycle evolves.

The forward transport calculation for the reactor model summarized in Figures 4-1 and 6-1 was carried out in R, θ geometry using the DOT two-dimensional discrete ordinates code[14] and the SAILOR cross-section library[15]. The SAILOR library is a 47 group ENDFB-IV based data set produced specifically for light water reactor applications. In these analyses anisotopic scattering was treated with a P_3 expansion of the cross-sections and the angular discretization was modeled with an S_8 order of angular quadrature.

The reference core power distribution utilized in the forward analysis was derived from statistical studies of long-term operation of Westinghouse 4-loop plants. Inherent in the development of this reference core power distribution is the use of an out-in fuel management strategy; i.e., fresh fuel on the core periphery. Furthermore, for the peripheral fuel assemblies, a 2σ uncertainty derived from the statistical evaluation of plant to plant and cycle to cycle variations in peripheral power was used. Since it is unlikely that a single reactor would have a power distribution at the nominal $+2\sigma$

level for a large number of fuel cycles, the use of this reference distribution is expected to yield somewhat conservative results.

All adjoint analyses were also carried out using an S_8 order of angular quadrature and the P_3 cross-section approximation from the SAILOR library. Adjoint source locations were chosen at several azimuthal locations along the pressure vessel inner radius as well as the geometric center of each surveillance capsule. Again, these calculations were run in R, θ geometry to provide neutron source distribution importance functions for the exposure parameter of interest; in this case, ϕ (E > 1.0 MeV). Having the importance functions and appropriate core source distributions, the response of interest could be calculated as:

$$R(r, \theta) = \int_r \int_\theta \int_E I(r, \theta, E)\, S(r, \theta, E)\, r\, dr\, d\theta\, dE$$

where: $R(r, \theta)$ = ϕ (E > 1.0 MeV) at radius r and azimuthal angle θ

$I(r, \theta, E)$ = Adjoint importance function at radius, r, azimuthal angle θ, and neutron source energy E.

$S(r, \theta, E)$ = Neutron source strength at core location r, θ and energy E.

Although the adjoint importance functions used in the Diablo Canyon Unit 2 analysis were based on a response function defined by the threshold neutron flux (E > 1.0 MeV), prior calculations have shown that, while the implementation of low leakage loading patterns significantly impact the magnitude and the spatial distribution of the neutron field, changes in the relative neutron energy spectrum are of second order. Thus, for a given location the ratio of dpa/ϕ (E > 1.0 MeV) is insensitive to changing core source distributions. In the application of these adjoint important functions to the Diablo Canyon Unit 2 reactor, therefore, calculation of the iron displacement rates (dpa) and the neutron flux (E > 0.1 MeV) were computed on a cycle specific basis by using dpa/ϕ (E > 1.0 MeV) and ϕ (E > 0.1 MeV)/ϕ (E > 1.0 MeV) ratios from the forward analysis in conjunction with the cycle specific ϕ (E > 1.0 MeV) solutions from the individual adjoint evaluations.

The reactor core power distributions, used in the plant specific adjoint calculations, were taken from the fuel cycle design report for the first three operating cycles of Diablo Canyon Unit 2 [16 through 18]. The relative power levels in fuel assemblies that are significant contributors to the neutron exposure of the pressure vessel and surveillance capsules are summarized in Figure 6-2. For comparison purposes, the core power distribution (design basis) used in the reference forward calculation is also illustrated in Figure 6-2.

Selected results from the neutron transport analyses performed for the Diablo Canyon Unit 2 reactor are provided in Tables 6-1 through 6-5. The data listed in these tables establish the means for absolute comparisons of analysis and measurement for the capsule irradiation period and provide the means to correlate dosimetry results with the corresponding neutron exposure of the pressure vessel wall.

In Table 6-1, the calculated exposure parameters [ϕ (E > 1.0 MeV), ϕ(E > 0.1 MeV), and dpa] are given at the geometric center of the two surveillance capsule positions for both the design basis and the plant specific core power distributions. The plant specific data, based on the adjoint transport analysis, are meant to establish the absolute comparison of measurement with analysis. The design basis data derived from the forward calculation are provided as a point of reference against which plant specific fluence evaluations can be compared. Similar data is given in Table 6-2 for the pressure vessel inner radius. Again, the three pertinent exposure parameters are listed for both the design basis and the cycles 1 through 3 plant specific power distributions. It is important to note that the data for the vessel inner radius were taken at the clad/base metal interface; and, thus, represent the maximum exposure levels of the vessel wall itself.

Radial gradient information for neutron flux (E > 1.0 MeV), neutron flux (E > 0.1 MeV), and iron atom displacement rate is given in Tables 6-3, 6-4, and 6-5, respectively. The data, obtained from the forward neutron transport calculation, are presented on a relative basis for each exposure parameter at

several azimuthal locations. Exposure parameter distributions within the wall may be obtained by normalizing the calculated or projected exposure at the vessel inner radius to the gradient data given in Tables 6-3 through 6-5.

For example, the neutron flux (E > 1.0 MeV) at the 1/4T position on the 45° azimuth is given by:

$$\phi_{1/4T}(45°) = \phi(220.27, 45°)\ F\ (225.75, 45°)$$

where: $\phi_{1/4T}(45°)$ = Projected neutron flux at the 1/4T position on the 45° azimuth

$\phi\ (220.27,45°)$ = Projected or calculated neutron flux at the vessel inner radius on the 45° azimuth.

$F\ (225.75, 45°)$ = Relative radial distribution function from Table 6-3.

Similar expressions apply for exposure parameters in terms of ϕ (E > 0.1 MeV) and dpa/sec.

6.3 Neutron Dosimetry

The passive neutron sensors included in the Diablo Canyon Unit 2 surveillance program are listed in Table 6-6. Also given in Table 6-6 are the primary nuclear reactions and associated nuclear constants that were used in the evaluation of the neutron energy spectrum within the capsule and the subsequent determination of the various exposure parameters of interest [ϕ (E > 1.0 MeV), ϕ (E > 0.1 MeV), dpa].

The relative locations of the neutron sensors within the capsules are shown in Figure 4-2. The iron, nickel, copper, and cobalt-aluminum monitors, in wire form, were placed in holes drilled in spacers at several axial levels within the capsules. The cadmium-shielded neptunium and uranium fission monitors were accommodated within the dosimeter block located near the center of the capsule.

The use of passive monitors such as those listed in Table 6-6 does not yield a direct measure of the energy dependent flux level at the point of interest. Rather, the activation or fission process is a measure of the integrated effect that the time- and energy-dependent neutron flux has on the target material over the course of the irradiation period. An accurate assessment of the average neutron flux level incident on the various monitors may be derived from the activation measurements only if the irradiation parameters are well known. In particular, the following variables are of interest:

- The specific activity of each monitor.
- The operating history of the reactor.
- The energy response of the monitor.
- The neutron energy spectrum at the monitor location.
- The physical characteristics of the monitor.

The specific activity of each of the neutron monitors was determined using established ASTM procedures [19 through 32]. Following sample preparation and weighing, the activity of each monitor was determined by means of a lithium-drifted germanium, Ge(Li), gamma spectrometer. The irradiation history of the Diablo Canyon Unit 2 reactor during cycles 1 through 3 was obtained from NUREG-0020, "Licensed Operating Reactors Status Summary Report" for the applicable period.

The irradiation history applicable to capsule X is given in Table 6-7. Measured and saturated reaction product specific activities as well as measured full power reaction rates are listed in Table 6-8. Reaction rate values were derived using the pertinent data from Tables 6-6 and 6-7.

Values of key fast neutron exposure parameters were derived from the measured reaction rates using the FERRET least squares adjustment code [33]. The FERRET approach used the measured reaction rate data and the calculated neutron energy spectrum at the center of the surveillance capsule as input and

proceeded to adjust a priori (calculated) group fluxes to produce a best fit (in a least squares sense) to the reaction rate data. The exposure parameters along with associated uncertainties where then obtained from the adjusted spectra.

In the FERRET evaluations, a log normal least-squares algorithm weights both the a priori values and the measured data in accordance with the assigned uncertainties and correlations. In general, the measured values f are linearly related to the flux ϕ by some response matrix A:

$$f^{(s,\alpha)} = \sum_g A_{ig}^{(s)} \phi_g^{(\alpha)}$$

where i indexes the measured values belonging to a single data set s, g designates the energy group and α delineates spectra that may be simultaneously adjusted. For example,

$$R_i = \sum_g \sigma_{ig} \phi_g$$

relates a set of measured reaction rates R_i to a single spectrum ϕ_g by the multigroup cross section σ_{ig}. (In this case, FERRET also adjusts the cross-sections.) The lognormal approach automatically accounts for the physical constraint of positive fluxes, even with the large assigned uncertainties.

In the FERRET analysis of the dosimetry data, the continuous quantities (i.e., fluxes and cross-sections) were approximated in 53 groups. The calculated fluxes from the discrete ordinates analysis were expanded into the FERRET group structure using the SAND-II code [34]. This procedure was carried out by first expanding the a priori spectrum into the SAND-II 620 group structure

using a SPLINE interpolation procedure for interpolation in regions where group boundaries do not coincide. The 620-point spectrum was then easily collapsed to the group scheme used in FERRET.

The cross-sections were also collapsed into the 53 energy-group structure using SAND II with calculated spectra (as expanded to 620 groups) as weighting functions. The cross sections were taken from the ENDF/B-V dosimetry file. Uncertainty estimates and 53 x 53 covariance matrices were constructed for each cross section. Correlations between cross sections were neglected due to data and code limitations, but are expected to be unimportant.

For each set of data or a priori values, the inverse of the corresponding relative covariance matrix M is used as a statistical weight. In some cases, as for the cross sections, a multigroup covariance matrix is used. More often, a simple parameterized form is used:

$$M_{gg'} = R_N^2 + R_g R_{g'} P_{gg'}$$

where R_N specifies an overall fractional normalization uncertainty (i.e., complete correlation) for the corresponding set of values. The fractional uncertainties R_g specify additional random uncertainties for group g that are correlated with a correlation matrix:

$$P_{gg'} = (1 - \theta)\, \delta_{gg'} + \theta \exp\left[\frac{-(g-g')^2}{2\gamma^2}\right]$$

The first term specifies purely random uncertainties while the second term describes short-range correlations over a range γ (θ specifies the strength of the latter term).

For the a priori calculated fluxes, a short-range correlation of $\gamma = 6$ groups was used. This choice implies that neighboring groups are strongly correlated when θ is close to 1. Strong long-range correlations (or anticorrelations) were justified based on information presented by R.E. Maerker[35]. Maerker's results are closely duplicated when $\gamma = 6$. For the integral reaction rate covariances, simple normalization and random uncertainties were combined as deduced from experimental uncertainties.

Results of the FERRET evaluation of the capsule X dosimetry are given in Table 6-9. The data summarized in Table 6-9 indicated that the capsule received an integrated exposure of 8.87×10^{18} n/cm^2 (E > 1.0 MeV) with an associated uncertainty of ± 8%. Also reported are capsule exposures in terms of fluence (E > 0.1 MeV) and iron atom displacements (dpa). Summaries of the fit of the adjusted spectrum are provided in Table 6-10. In general, excellent results were achieved in the fits of the adjusted spectrum to the individual experimental reaction rates. The adjusted spectrum itself is tabulated in Table 6-11 for the FERRET 53 energy group structure.

A summary of the measured and calculated neutron exposure of capsule X is presented in Table 6-12. The agreement between calculation and measurement falls within ± 6-10% for all fast neutron exposure parameters listed.

Neutron exposure projections at key locations on the pressure vessel inner radius are given in Table 6-13. Along with the current (3.11 EFPY) exposure derived from the capsule X measurements, projections are also provided for exposure periods of 8 EFPY, 16 EFPY and to end of vessel design life (32 EFPY). The time averaged exposure rates for the first 3.11 EFPY of operation were used to perform projections beyond the end of the Cycle 1 through 3 exposure period.

$$[\text{e.g. } \Phi_{8\ \text{EFPY}} = 8\ \text{EFPY}\ (\Phi_{3.11\ \text{EFPY}} / 3.11\ \text{EFPY})]$$

In the calculation of exposure gradients for use in the development of heatup and cooldown curves for the Diablo Canyon Unit 2 reactor coolant system, exposure projections to 16 EFPY and 32 EFPY were employed. Data based on both a fluence (E > 1.0 MeV) slope and a plant specific dpa slope through the vessel

wall are provided in Table 6-14. In order to access RT_{NDT} vs. fluence trend curves, dpa equivalent fast neutron fluence levels for the 1/4T and 3/4T positions were defined by the relations

$$\Phi' \text{ (1/4T)} = \Phi \text{ (Surface)} \left[\frac{\text{dpa (1/4T)}}{\text{dpa (Surface)}}\right]$$

$$\Phi' \text{ (3/4T)} = \Phi \text{ (Surface)} \left[\frac{\text{dpa (3/4T)}}{\text{dpa (Surface)}}\right]$$

Using this approach results in the dpa equivalent fluence values listed in Table 6-14.

In Table 6-15 updated lead factors are listed for each of the Diablo Canyon Unit 2 surveillance capsules. These data may be used as a guide in establishing future withdrawal schedules for the remaining capsules.

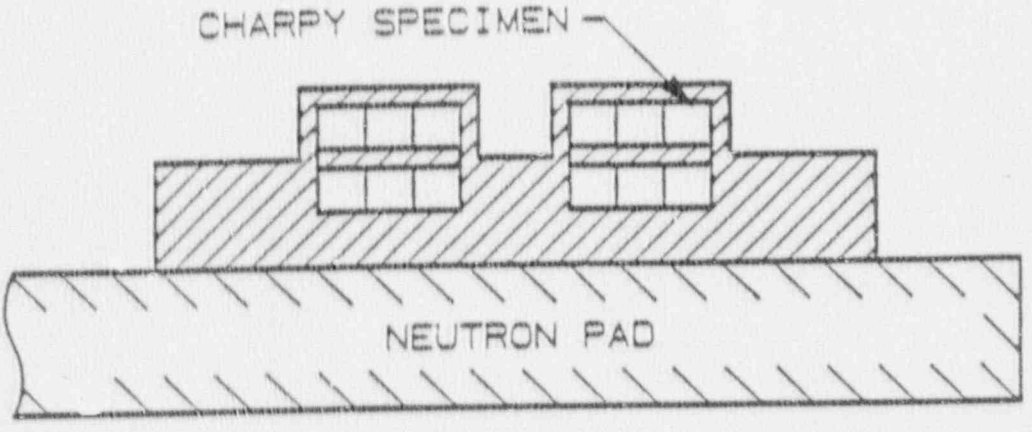

Figure 6-1. Plan View of a Dual Reactor Vessel Surveillance Capsule

1.01	1.04	0.96	0.77	DESIGN BASIS	
0.73	0.77	0.68	0.56	CYCLE 1	
0.59	0.50	0.54	0.36	CYCLE 2	
0.51	0.53	0.43	0.33	CYCLE 3	
1.02	1.10	1.00	1.05	1.10	0.71
0.99	1.04	0.96	0.98	0.89	0.51
0.94	1.19	0.94	1.10	0.88	0.40
1.19	1.18	1.14	1.05	0.83	0.33
1.05	0.87	0.87	1.07	1.00	1.05
1.13	1.10	1.11	1.06	0.99	0.97
1.10	0.99	1.30	1.13	1.09	1.01
1.11	1.17	1.17	1.15	1.18	0.74
1.09	1.06	0.88	1.10	1.04	
1.14	1.17	1.13	1.12	1.18	
1.12	1.29	1.04	1.30	1.10	
1.13	1.30	1.00	1.30	1.10	
0.90	1.04	1.12	0.92		
1.18	1.15	1.18	1.14		
1.27	1.03	1.26	1.04		
1.30	1.11	1.30	1.14		

Figure 6-2. Core Power Distributions Used in Transport Calculations for Diablo Canyon Unit 2

TABLE 6-1

CALCULATED FAST NEUTRON EXPOSURE PARAMETERS
AT THE SURVEILLANCE CAPSULE CENTER

CYCLE	IRRADIATION TIME (EFPS)	ϕ (E > 1.0 MeV) [n/cm^2-sec]		ϕ (E > 0.1 MeV) [n/cm^2-sec]		dpa/sec	
		31.5°	34.0°	31.5°	34.0°	31.5°	34.0°
DESIGN BASIS		1.11×10^{11}	1.29×10^{11}	4.88×10^{11}	5.93×10^{11}	2.21×10^{-10}	2.62×10^{-10}
CYCLE 1	3.13×10^{7}	8.35×10^{10}	9.52×10^{10}	3.67×10^{11}	4.37×10^{11}	1.66×10^{-10}	1.93×10^{-10}
CYCLE 2	3.15×10^{7}	7.00×10^{10}	8.01×10^{10}	3.08×10^{11}	3.68×10^{11}	1.40×10^{-10}	1.62×10^{-10}
CYCLE 3	3.52×10^{7}	6.70×10^{10}	7.61×10^{10}	2.95×10^{11}	3.49×10^{11}	1.34×10^{-10}	1.54×10^{-10}

TABLE 6-2

CALCULATED FAST NEUTRON EXPOSURE PARAMETERS AT
THE PRESSURE VESSEL CLAD/BASE METAL INTERFACE

	ϕ(E > 1.0 MeV) [n/cm^2-sec]			
	0°	15°	30°	45°
DESIGN BASIS	1.45×10^{10}	2.21×10^{10}	1.69×10^{10}	2.44×10^{10}
Cycle 1	1.08×10^{10}	1.62×10^{10}	1.27×10^{10}	1.81×10^{10}
Cycle 2	7.99×10^{9}	1.20×10^{10}	1.02×10^{10}	1.49×10^{10}
Cycle 3	8.19×10^{9}	1.20×10^{10}	9.84×10^{9}	1.37×10^{10}

	ϕ(E > 0.1 MeV) [n/cm^2-sec]			
	0°	15°	30°	45°
DESIGN BASIS	3.02×10^{10}	4.66×10^{10}	4.25×10^{10}	6.11×10^{10}
Cycle 1	2.25×10^{10}	3.41×10^{10}	3.20×10^{10}	4.53×10^{10}
Cycle 2	1.67×10^{10}	2.53×10^{10}	2.57×10^{10}	3.73×10^{10}
Cycle 3	1.71×10^{10}	2.53×10^{10}	2.48×10^{10}	3.43×10^{10}

	dpa/sec			
	0°	15°	30°	45°
DESIGN BASIS	2.25×10^{-11}	3.41×10^{-11}	2.73×10^{-11}	3.88×10^{-11}
Cycle 1	1.68×10^{-11}	2.50×10^{-11}	2.05×10^{-11}	2.88×10^{-11}
Cycle 2	1.24×10^{-11}	1.85×10^{-11}	1.65×10^{-11}	2.37×10^{-11}
Cycle 3	1.24×10^{-11}	1.85×10^{-11}	1.59×10^{-11}	2.18×10^{-11}

TABLE 6-3

RELATIVE RADIAL DISTRIBUTIONS OF NEUTRON FLUX (E > 1.0 MeV)
WITHIN THE PRESSURE VESSEL WALL

Radius (cm)	0°	15°	30°	45°
220.27(1)	1.00	1.00	1.00	1.00
220.64	0.979	0.979	0.980	0.979
221.66	0.891	0.891	0.893	0.889
222.99	0.771	0.769	0.773	0.763
224.31	0.655	0.652	0.658	0.648
225.63	0.552	0.549	0.555	0.543
226.95	0.463	0.459	0.467	0.452
228.28	0.387	0.383	0.390	0.376
229.60	0.322	0.318	0.326	0.311
230.92	0.268	0.263	0.271	0.257
232.25	0.222	0.218	0.225	0.211
233.57	0.183	0.180	0.187	0.174
234.89	0.151	0.148	0.155	0.142
236.22	0.125	0.121	0.128	0.116
237.54	0.102	0.0992	0.105	0.0945
238.86	0.0831	0.0807	0.0862	0.0762
240.19	0.0673	0.0650	0.0703	0.0608
241.51	0.0539	0.0512	0.0567	0.0472
242.17(2)	0.0508	0.0477	0.0536	0.0438

NOTES: 1) Base Metal Inner Radius
2) Base Metal Outer Radius

TABLE 6-4

RELATIVE RADIAL DISTRIBUTIONS OF NEUTRON FLUX (E > 0.1 MeV)
WITHIN THE PRESSURE VESSEL WALL

Radius (cm)	0°	15°	30°	45°
220.27(1)	1.00	1.00	1.00	1.00
220.64	1.00	1.00	1.00	1.00
221.66	1.00	1.00	1.00	0.995
222.99	0.974	0.966	0.982	0.956
224.31	0.928	0.915	0.938	0.902
225.63	0.875	0.859	0.886	0.843
226.95	0.819	0.802	0.832	0.782
228.28	0.762	0.743	0.777	0.722
229.60	0.705	0.686	0.721	0.663
230.92	0.649	0.629	0.665	0.605
232.25	0.594	0.575	0.611	0.549
233.57	0.540	0.522	0.558	0.495
234.89	0.488	0.470	0.506	0.443
236.22	0.436	0.421	0.455	0.392
237.54	0.386	0.373	0.406	0.343
238.86	0.337	0.326	0.358	0.296
240.19	0.290	0.280	0.310	0.248
241.51	0.244	0.232	0.261	0.201
242.17(2)	0.233	0.219	0.249	0.188

NOTES: 1) Base Metal Inner Radius
2) Base Metal Outer Radius

TABLE 6-5

RELATIVE RADIAL DISTRIBUTIONS OF IRON DISPLACEMENT RATE (dpa)
WITHIN THE PRESSURE VESSEL WALL

Radius (cm)	0°	15°	30°	45°
220.27(1)	1.00	1.00	1.00	1.00
220.64	0.982	0.982	0.986	0.984
221.66	0.911	0.910	0.923	0.915
222.99	0.813	0.812	0.837	0.821
224.31	0.721	0.718	0.751	0.730
225.63	0.637	0.633	0.673	0.646
226.95	0.562	0.558	0.602	0.572
228.28	0.496	0.491	0.539	0.505
229.60	0.438	0.433	0.481	0.447
230.92	0.387	0.381	0.430	0.394
232.25	0.341	0.335	0.383	0.347
233.57	0.300	0.295	0.341	0.305
234.89	0.263	0.258	0.302	0.266
236.22	0.230	0.225	0.267	0.231
237.54	0.199	0.195	0.234	0.199
238.86	0.171	0.168	0.203	0.169
240.19	0.145	0.142	0.174	0.140
241.51	0.121	0.117	0.146	0.113
242.17(2)	0.116	0.110	0.140	0.106

NOTES: 1) Base Metal Inner Radius
2) Base Metal Outer Radius

TABLE 6-6

NUCLEAR PARAMETERS FOR NEUTRON FLUX MONITORS

Monitor Material	Reaction of Interest	Target Weight Fraction	Response Range	Product Half-Life	Fission Yield (%)
Copper	$Cu^{63}(n,\alpha)Co^{60}$	0.6917	E > 4.7 MeV	5.272 yrs	
Iron	$Fe^{54}(n,p)Mn^{54}$	0.0582	E > 1.0 MeV	312.2 days	
Nickel	$Ni^{58}(n,p)Co^{58}$	0.6830	E > 1.0 MeV	70.90 days	
Uranium-238*	$U^{238}(n,f)Cs^{137}$	1.0	E > 0.[illegible] MeV	30.12 yrs	5.99
Neptunium-237*	$Np^{237}(n,f)Cs^{137}$	1.0	E > 0.08 MeV	30.12 yrs	6.50
Cobalt-Aluminum*	$Co^{59}(n,\gamma)Co^{60}$	0.0015	0.4ev>E> 0.015 MeV	5.272 yrs	
Cobalt-Aluminum*	$Co^{59}(n,\gamma)Co^{60}$	0.0015	E > 0.015 MeV	5.272 yrs	

*Denotes that monitor is cadmium shielded.

TABLE 6-7

IRRADIATION HISTORY OF NEUTRON SENSORS
CONTAINED IN CAPSULE X

Irradiation Period	P_J (MW)	P_J/P_{Max}	Irradiation Time (days)	Decay Time (days)
10/85	734	.215	13	1750
11/85	1272	.373	30	1720
12/85	1305	.383	31	1689
1/86	750	.220	31	1658
2/86	341	.100	28	1630
3/86	1845	.541	31	1599
4/86	2859	.838	30	1569
5/86	3088	.905	31	1538
6/86	2789	.8[illegible]	30	1508
7/86	2396	.702	31	1477
8/86	32[illegible]	.951	31	1446
9/86	2779	.815	30	1416
10/86	3206	.940	31	1385
11/86	3279	.961	30	1355
12/86	3128	.917	31	1324
1/87	3103	.910	31	1293
2/87	2647	.776	28	1265
3/87	2029	.595	31	1234
4/87	254	.075	30	1204
5/87	0	.000	31	1173
6/87	0	.000	30	1143
7/87	980	.287	31	1112

NOTE: Reference Power = 3411 MW_t

TABLE 6-7 (Cont'd)

IRRADIATION HISTORY OF NEUTRON SENSORS
CONTAINED IN CAPSULE X

Irradiation Period	P_J (MW)	P_J/P_{Max}	Irradiation Time (days)	Decay Time (days)
8/87	3116	.914	31	1081
9/87	3405	.998	30	1051
10/87	3317	.973	31	1020
11/87	2587	.758	30	990
12/87	3190	.935	31	959
1/88	3330	.976	31	928
2/88	2336	.685	29	899
3/88	3034	.890	31	868
4/88	3336	.978	30	838
5/88	3402	.997	31	807
6/88	3274	.960	30	777
7/88	1619	.475	31	746
8/88	2281	.669	31	715
9/88	1541	.452	30	685
10/88	0	.000	31	654
11/88	0	.000	30	624
12/88	1954	.573	31	593
1/89	3400	.997	31	562
2/89	3379	.991	28	534
3/89	3403	.998	31	503
4/89	2017	.591	30	473
5/89	3309	.970	31	442

TABLE 6-7 (Cont'd)

IRRADIATION HISTORY OF NEUTRON SENSORS
CONTAINED IN CAPSULE X

Irradiation Period	P_J (MW)	P_J/P_{Max}	Irradiation Time (days)	Decay Time (days)
6/89	3401	.997	30	412
7/89	2662	.781	31	381
8/89	3052	.895	31	350
9/89	3337	.978	30	320
10/89	2782	.816	31	289
11/89	2767	.811	30	259
12/89	3300	.967	31	228
1/90	3405	.998	31	197
2/90	3365	.987	28	169
3/90	2487	.729	4	165

TABLE 6-8

MEASURED SENSOR ACTIVITIES AND REACTION RATES

Monitor and Axial Location	Measured Activity (dis/sec-gm)	Saturated Activity (dis/sec-gm)	Reaction Rate (RPS/NUCLEUS)
Cu-63 (n,α) Co-60			
Top	8.85×10^{4}	3.00×10^{5}	
Bottom	9.23×10^{4}	3.13×10^{5}	
Average	9.04×10^{4}	3.06×10^{5}	4.67×10^{-17}
Fe-54(n,p) Mn-54			
Top	1.41×10^{6}	2.79×10^{6}	
Middle	1.49×10^{6}	2.95×10^{6}	
Bottom	1.48×10^{6}	2.93×10^{6}	
Average	1.46×10^{6}	2.89×10^{6}	4.61×10^{-15}
Ni-58 (n,p) Co-58			
Top	7.23×10^{6}	4.32×10^{7}	
Middle	7.64×10^{6}	4.57×10^{7}	
Bottom	7.57×10^{6}	4.53×10^{7}	
Average	7.48×10^{6}	4.47×10^{7}	6.38×10^{-15}
U-238 (n,f) Cs-137 (Cd)			
Middle	2.99×10^{5}	4.44×10^{6}	2.93×10^{-14}

TABLE 6-8 (Cont'd)
MEASURED SENSOR ACTIVITIES AND REACTION RATES

Monitor and Axial Location	Measured Activity (dis/sec-gm)	Saturated Activity (dis/sec-gm)	Reaction Rate (RPS/NUCLEUS)
Np-237(n,f) Cs-137 (Cd)			
Middle	3.13×10^{6}	4.65×10^{7}	2.82×10^{-13}
Co-59 (n,γ) Co-60			
Top	2.17×10^{7}	7.35×10^{7}	
Middle	1.95×10^{7}	6.59×10^{7}	
Bottom	2.12×10^{7}	7.17×10^{7}	
Average	2.08×10^{7}	7.04×10^{7}	4.59×10^{-12}
Co-59 (n,γ) Co-60 (Cd)			
Top	1.21×10^{7}	4.10×10^{7}	
Middle	1.12×10^{7}	3.80×10^{7}	
Bottom	1.20×10^{7}	4.07×10^{7}	
Average	1.18×10^{7}	3.99×10^{7}	2.60×10^{-12}

TABLE 6-9

SUMMARY OF NEUTRON DOSIMETRY RESULTS

	TIME AVERAGED EXPOSURE RATES	
ϕ (E > 1.0 MeV) [n/cm^2-sec]	9.05×10^{10}	± 8%
ϕ (E > 0.1 MeV) [n/cm^2-sec]	4.24×10^{11}	± 15%
dpa/sec	1.80×10^{-10}	± 11%
ϕ (E < 0.414 eV) [n/cm^2-sec]	8.17×10^{11}	± 22%
	INTEGRATED CAPSULE EXPOSURE	
Φ (E > 1.0 MeV) [n/cm^2]	8.87×10^{18}	± 8%
Φ (E > 0.1 MeV) [n/cm^2]	4.16×10^{19}	± 15%
dpa	1.77×10^{-2}	± 11%
Φ (E < 0.414 eV) [n/cm^2]	8.02×10^{18}	± 22%

NOTE: Total Irradiation Time = 3.11 EFPY

TABLE 6-10

COMPARISON OF MEASURED AND FERRET CALCULATED
REACTION RATES AT THE SURVEILLANCE CAPSULE CENTER

Reaction	Measured	Adjusted Calculation	C/M
Cu-63 (n,α) Co-60	4.67×10^{-17}	4.66×10^{-17}	1.00
Fe-54 (n,p) Mn-54	4.61×10^{-15}	4.67×10^{-15}	1.01
Ni-58 (n,p) Co-58	6.38×10^{-15}	6.40×10^{-15}	1.00
U-238 (n,f) Cs-137 (Cd)	2.93×10^{-14}	2.74×10^{-14}	0.94
Np-237 (n,f) Cs-137 (Cd)	2.82×10^{-13}	2.90×10^{-13}	1.03
Co-59 (n,γ) Co-60 (Cd)	2.60×10^{-12}	2.61×10^{-12}	0.99
Co-59 (n,γ) Co-60	4.59×10^{-12}	4.55×10^{-12}	1.00

TABLE 6-11

ADJUSTED NEUTRON ENERGY SPECTRUM AT

THE SURVEILLANCE CAPSULE CENTER

Group	Energy (Mev)	Adjusted Flux (n/cm^2-sec)	Group	Energy (Mev)	Adjusted Flux (n/cm^2-sec)
1	1.73×10^{1}	3.97×10^{6}	28	9.12×10^{-3}	1.98×10^{10}
2	1.49×10^{1}	9.69×10^{6}	29	5.53×10^{-3}	2.57×10^{10}
3	1.35×10^{1}	4.45×10^{7}	30	3.36×10^{-3}	8.06×10^{9}
4	1.16×10^{1}	1.13×10^{8}	31	2.84×10^{-3}	7.74×10^{9}
5	1.00×10^{1}	2.71×10^{8}	32	2.40×10^{-3}	7.48×10^{9}
6	8.61×10^{0}	4.86×10^{8}	33	2.04×10^{-3}	2.11×10^{10}
7	7.41×10^{0}	1.15×10^{9}	34	1.23×10^{-3}	1.93×10^{10}
8	6.07×10^{0}	1.67×10^{9}	35	7.49×10^{-4}	1.78×10^{10}
9	4.97×10^{0}	3.52×10^{9}	36	4.54×10^{-4}	1.69×10^{10}
10	3.68×10^{0}	4.68×10^{9}	37	2.75×10^{-4}	1.82×10^{10}
11	2.87×10^{0}	9.79×10^{9}	38	1.67×10^{-4}	1.96×10^{10}
12	2.23×10^{0}	1.36×10^{10}	39	1.01×10^{-4}	1.96×10^{10}
13	1.74×10^{0}	1.93×10^{10}	40	6.14×10^{-5}	1.95×10^{10}
14	1.35×10^{0}	2.19×10^{10}	41	3.73×10^{-5}	1.89×10^{10}
15	1.11×10^{0}	4.10×10^{10}	42	2.26×10^{-5}	1.83×10^{10}
16	8.21×10^{-1}	4.77×10^{10}	43	1.37×10^{-5}	1.77×10^{10}
17	6.39×10^{-1}	5.04×10^{10}	44	8.32×10^{-6}	1.68×10^{10}
18	4.98×10^{-1}	3.70×10^{10}	45	5.04×10^{-6}	1.53×10^{10}
19	3.88×10^{-1}	5.37×10^{10}	46	3.06×10^{-6}	1.42×10^{10}
20	3.02×10^{-1}	5.38×10^{10}	47	1.86×10^{-6}	1.29×10^{10}
21	1.83×10^{-1}	5.42×10^{10}	48	1.13×10^{-6}	9.72×10^{9}
22	1.11×10^{-1}	4.35×10^{10}	49	6.83×10^{-7}	1.19×10^{10}
23	6.74×10^{-2}	3.00×10^{10}	50	4.14×10^{-7}	1.48×10^{10}
24	4.09×10^{-2}	1.69×10^{10}	51	2.51×10^{-7}	1.45×10^{10}
25	2.55×10^{-2}	2.30×10^{10}	52	1.52×10^{-7}	1.35×10^{10}
26	1.99×10^{-2}	1.09×10^{10}	53	9.24×10^{-8}	3.88×10^{10}
27	1.50×10^{-2}	1.36×10^{10}			

NOTE: Tabulated energy levels represent the upper energy of each group.

TABLE 6-12

COMPARISON OF CALCULATED AND MEASURED
EXPOSURE LEVELS FOR CAPSULE X

	Calculated	Measured	C/M
$\Phi(E > 1.0\ MeV)\ [n/cm^2]$	8.18×10^{18}	8.87×10^{18}	0.92
$\Phi(E > 0.1\ MeV)\ [n/cm^2]$	3.76×10^{19}	4.16×10^{19}	0.90
dpa	1.66×10^{-2}	1.77×10^{-2}	0.94
$\Phi(E < 0.414\ eV)\ [n/cm^2]$	3.22×10^{18}	8.02×10^{18}	0.40

TABLE 6-13

NEUTRON EXPOSURE PROJECTIONS AT KEY LOCATIONS
ON THE PRESSURE VESSEL CLAD/BASE METAL INTERFACE

	AZIMUTHAL ANGLE			
	0°	15°	30°	45°
3.11 EFPY				
Φ(E>1.0 MeV) (n/cm^2)	9.55×10^{17}	1.42×10^{18}	1.16×10^{18}	1.65×10^{18}
Φ(E>0.1 MeV) (n/cm^2)	2.03×10^{18}	3.07×10^{18}	2.99×10^{18}	4.22×10^{18}
dpa	1.45×10^{-3}	2.15×10^{-3}	1.84×10^{-3}	2.57×10^{-3}
8.0 EFPY				
Φ(E>1.0 MeV) (n/cm^2)	2.46×10^{18}	3.65×10^{18}	2.98×10^{18}	4.24×10^{18}
Φ(E>0.1 MeV) (n/cm^2)	5.22×10^{18}	7.90×10^{18}	7.69×10^{18}	1.09×10^{19}
dpa	3.73×10^{-3}	5.53×10^{-3}	4.73×10^{-3}	6.61×10^{-3}
16.0 EFPY				
Φ(E>1.0 MeV) (n/cm^2)	4.91×10^{18}	7.31×10^{18}	5.97×10^{18}	8.49×10^{18}
Φ(E>0.1 MeV) (n/cm^2)	1.04×10^{19}	1.58×10^{19}	1.54×10^{19}	2.17×10^{19}
dpa	7.46×10^{-3}	1.11×10^{-2}	9.47×10^{-3}	1.32×10^{-2}

TABLE 6-13 (continued)
NEUTRON EXPOSURE PROJECTIONS AT KEY LOCATIONS
ON THE PRESSURE VESSEL CLAD/BASE METAL INTERFACE

	AZIMUTHAL ANGLE			
	0°	15°	30°	45°
32.0 EFPY				
Φ(E>1.0 MeV) (n/cm^2)	9.83×10^{18}	1.46×10^{19}	1.19×10^{19}	1.70×10^{19}
Φ(E>0.1 MeV) (n/cm^2)	2.09×10^{19}	3.16×10^{19}	3.08×10^{19}	4.34×10^{19}
dpa	1.49×10^{-2}	2.21×10^{-2}	1.89×10^{-2}	2.64×10^{-2}

TABLE 6-14

NEUTRON EXPOSURE VALUES FOR USE IN THE GENERATION OF HEATUP/COOLDOWN CURVES

8 EFPY

	NEUTRON FLUENCE (E > 1.0 MeV) SLOPE (n/cm^2)			dpa SLOPE (equivalent n/cm^2)		
	Surface	1/4 T	3/4 T	Surface	1/4 T	3/4 T
0°	2.46×10^{18}	1.34×10^{18}	2.86×10^{17}	2.46×10^{18}	1.55×10^{18}	5.38×10^{17}
15°	3.65×10^{18}	1.98×10^{18}	4.12×10^{17}	3.65×10^{18}	2.29×10^{18}	7.81×10^{17}
30°	2.98×10^{18}	1.63×10^{18}	3.56×10^{17}	2.98×10^{18}	1.99×10^{18}	7.60×10^{17}
45°	4.24×10^{18}	2.27×10^{18}	4.59×10^{17}	4.24×10^{18}	2.71×10^{18}	9.31×10^{17}

16 EFPY

	NEUTRON FLUENCE (E > 1.0 MeV) SLOPE (n/cm^2)			dpa SLOPE (equivalent n/cm^2)		
	Surface	1/4 T	3/4 T	Surface	1/4 T	3/4 T
0°	4.91×10^{18}	2.67×10^{18}	5.72×10^{17}	4.91×10^{18}	3.09×10^{18}	1.07×10^{18}
15°	7.31×10^{18}	3.96×10^{18}	8.25×10^{17}	7.31×10^{18}	4.58×10^{18}	1.56×10^{18}
30°	5.97×10^{18}	3.26×10^{18}	7.14×10^{17}	5.97×10^{18}	3.98×10^{18}	1.52×10^{18}
45°	8.49×10^{18}	4.54×10^{18}	9.21×10^{17}	8.49×10^{18}	5.42×10^{18}	1.87×10^{18}

TABLE 6-14 (continued)

NEUTRON EXPOSURE VALUES FOR USE IN THE GENERATION OF HEATUP/COOLDOWN CURVES

32 EFPY

	NEUTRON FLUENCE (E > 1.0 MeV) SLOPE (n/cm^2)			dpa SLOPE (equivalent n/cm^2)		
	Surface	1/4 T	3/4 T	Surface	1/4 T	3/4 T
0°	9.83×10^{18}	5.35×10^{18}	1.14×10^{18}	9.83×10^{18}	6.17×10^{18}	2.15×10^{18}
15°	1.46×10^{19}	7.96×10^{18}	1.64×10^{18}	1.46×10^{19}	9.14×10^{18}	3.13×10^{18}
30°	1.19×10^{19}	6.53×10^{18}	1.42×10^{18}	1.19×10^{19}	7.93×10^{18}	3.04×10^{18}
45°	1.70×10^{19}	9.14×10^{18}	1.84×10^{18}	1.70×10^{19}	1.09×10^{19}	3.73×10^{18}

TABLE 6-15

UPDATED LEAD FACTORS FOR DIABLO CANYON UNIT 2
SURVEILLANCE CAPSULES

Capsule	Lead Factor (a)
U	5.28
X	5.28
W	5.28
Z	5.28
V	4.62
Y	4.62

(a) Plant specific evaluation

SECTION 7.0
SURVEILLANCE CAPSULE REMOVAL SCHEDULE

The following removal schedule meets ASTM E185-82 and is recommended for future capsules to be removed from the Diablo Canyon Unit 2 reactor vessel:

Capsule	Location (deg.)	Capsule Lead Factor	Removal Time (b)	Estimated Fluence (n/cm^2)
U	56.0	5.28	0.99 (a)	3.51×10^{18} (a)
X	236.0	5.28	3.11 (a)	8.87×10^{18} (a)
Y	238.5	4.62	7.0	1.7×10^{19} (c)
W	124.0	5.28	10.0	2.8×10^{19}
V	58.5	4.62	Standby	- - -
Z	304.0	5.28	Standby	- - -

(a) Plant specific evaluation actual fluence and EFPY

(b) Effective full power years (EFPY) from plant startup.

(c) Approximate fluence at the reactor vessel clad/base metal interface at end of life (32 EFPY).

SECTION 8.0
REFERENCES

1. Davidson,J.A. and Yanichko,S.E., "Pacific Gas and Electric Company Diablo Canyon Unit No. 2 Reactor Vessel Radiation Surveillance Program," WCAP-8783, December 1976.

2. Yanichko, S.E., Anderson, S.L. and Albertin, L., "Analysis of Capsule U from the Pacific Gas and Electric Company Diablo Canyon Unit 2 Reactor Vessel Radiation Surveillance Program", WCAP-11851, May, 1988.

3. "Charpy Curve Fits for DCPP Unit 2 Surveillance Capsule X", Letter from M. D. Sullivan of Pacific Gas and Electric Company to E. Terek of Westinghouse, Dated November 2, 1990

4. Code of Federal Regulations, 10CFR50, Appendix G, "Fracture Toughness Requirements", and Appendix H, "Reactor Vessel Material Surveillance Program Requirements," U.S. Nuclear Regulatory Commission, Washington, D.C.

5. Regulatory Guide 1.99, Revision 2, "Radiation Embrittlement of Reactor Vessel Materials", U.S. Nuclear Regulatory Commission, May, 1988.

6. Section III of the ASME Boiler and Pressure Vessel Code, Appendix G, "Protection Against Nonductile Failure."

7. ASTM E208, "Standard Test Method for Conducting Drop-Weight Test to Determine Nil-Ductility Transition Temperature of Ferritic Steels."

8. ASTM E185-82, "Standard Practice for Light-Water Cooled Nuclear Power Reactor Vessels, E706 (IF)."

9. ASTM E23-88, "Standard Test Methods for Notched Bar Impact Testing of Metallic Materials."

10. ASTM A370-89, "Standard Test Methods and Definitions for Mechanical Testing of Steel Products."

11. ASTM E8-89b, "Standard Test Methods of Tension Testing of Metallic Materials."

12. ASTM E21-79 (1988), "Standard Practice for Elevated Temperature Tension Tests of Metallic Materials."

13. ASTM E83-85, "Standard Practice for Verification and Classification of Extensometers."

14. R. G. Soltesz, R. K. Disney, J. Jedruch, and S. L. Ziegler, "Nuclear Rocket Shielding Methods, Modification, Updating and Input Data Preparation. Vol. 5--Two-Dimensional Discrete Ordinates Transport Technique", WANL-PR(LL)-034, Vol. 5, August 1970.

15. "ORNL RSCI Data Library Collection DLC-76, SAILOR Coupled Self-Shielded, 47 Neutron, 20 Gamma-Ray, P3, Cross Section Library for Light Water Reactors".

16. Vestovich, J.A., Lancaster, D.B , Signorella, T.L. and Radcliffe, R.E., "The Nuclear Design and Core Phsics Characteristics of the Diablo Canyon Unit 2 Cycle 1" WCAP-10593, July 1984, (Westinghouse Proprietary)

17. Fecteau, M.W., Piplica, A.N., Radcliff, R.E. and Zimmermann, M. W., "The Nuclear Design and Core Phsics Characteristics of the Diablo Canyon Power Plant Unit 2 Cycle 2" WCAP-11450, May 1987, (Westinghouse Proprietary)

18. Fecteau, M.W., Piplica, A.N. and Radcliff, R.E. "The Nuclear Design and Core Phsics Characteristics of the Diablo Canyon Power Plant Unit 2 Cycle 3" WCAP-11962, October, 1988 (Westinghouse Proprietary)

19. ASTM Designation E482-82, "Standard Guide for Application of Neutron Transport Methods for Reactor Vessel Surveillance", in ASTM Standards, Section 12, American Society for Testing and Materials, Philadelphia, PA, 1984.

20. ASTM Designation E560-77, "Standard Recommended Practice for Extrapolating Reactor Vessel Surveillance Dosimetry Results", in ASTM Standards, Section 12, American Society for Testing and Materials, Philadelphia, PA, 1984.

21. ASTM Designation E693-79, "Standard Practice for Characterizing Neutron Exposures in Ferritic Steels in Terms of Displacements per Atom (dpa)", in ASTM Standards, Section 12, American Society for Testing and Materials, Philadelphia, PA, 1984.

22. ASTM Designation E706-81a, "Standard Master Matrix for Light-Water Reactor Pressure Vessel Surveillance Standard", in ASTM Standards, Section 12, American Society for Testing and Materials, Philadelphia, PA, 1984.

23. ASTM Designation E853-84, "Standard Practice for Analysis and Interpretation of Light-Water Reactor Surveillance Results", in ASTM Standards, Section 12, American Society for Testing and Materials, Philadelphia, PA, 1984.

24. ASTM Designation E261-77, "Standard Method for Determining Neutron Flux, Fluence, and Spectra by Radioactivation Techniques", in ASTM Standards, Section 12, American Society for Testing and Materials, Philadelphia, PA, 1984.

25. ASTM Designation E262-77, "Standard Method for Measuring Thermal Neutron Flux by Radioactivation Techniques", in ASTM Standards, Section 12, American Society for Testing and Materials, Philadelphia, PA, 1984.

26. ASTM Designation E263-82, "Standard Method for Determining Fast-Neutron Flux Density by Radioactivation of Iron", in ASTM Standards, Section 12, American Society for Testing and Materials, Philadelphia, PA, 1984.

27. ASTM Designation E264-82, "Standard Method for Determining Fast-Neutron Flux Density by Radioactivation of Nickel", in ASTM Standards, Section 12, American Society for Testing and Materials, Philadelphia, PA, 1984.

28. ASTM Designation E481-78, "Standard Method for Measuring Neutron-Flux Density by Radioactivation of Cobalt and Silver", in ASTM Standards, Section 12, American Society for Testing and Materials, Philadelphia, PA, 1984.

29. ASTM Designation E523-82, "Standard Method for Determining Fast-Neutron Flux Density by Radioactivation of Copper", in ASTM Standards, Section 12, American Society for Testing and Materials, Philadelphia, PA, 1984.

30. ASTM Designation E704-84, "Standard Method for Measuring Reaction Rates by Radioactivation of Uranium-238", in ASTM Standards, Section 12, American Society for Testing and Materials, Philadelphia, PA, 1984.

31. ASTM Designation E705-79, "Standard Method for Measuring Fast-Neutron Flux Density by Radioactivation of Neptunium-237", in ASTM Standards, Section 12, American Society for Testing and Materials, Philadelphia, PA, 1984.

32. ASTM Designation E1005-84, "Standard Method for Application and Analysis of Radiometric Monitors for Reactor Vessel Surveillance", in ASTM Standards, Section 12, American Society for Testing and Materials, Philadelphia, PA, 1984.

33. F. A. Schmittroth, FERRET Data Analysis Code, HEDL-TME 79-40, Hanford Engineering Development Laboratory, Richland, WA, September 1979.

34. W. N. McElroy, S. Berg and T. Crocket, A Computer-Automated Iterative Method of Neutron Flux Spectra Determined by Foil Activation, AFWL-TR-7-41, Vol. I-IV, Air Force Weapons Laboratory, Kirkland AFB, NM, July 1967.

35. EPRI-NP-2188, "Development and Demonstration of an Advanced Methodology for LWR Dosimetry Applications", R. E. Maerker, et al., 1981.

APPENDIX A

Load-Time Records for Charpy Specimen Tests

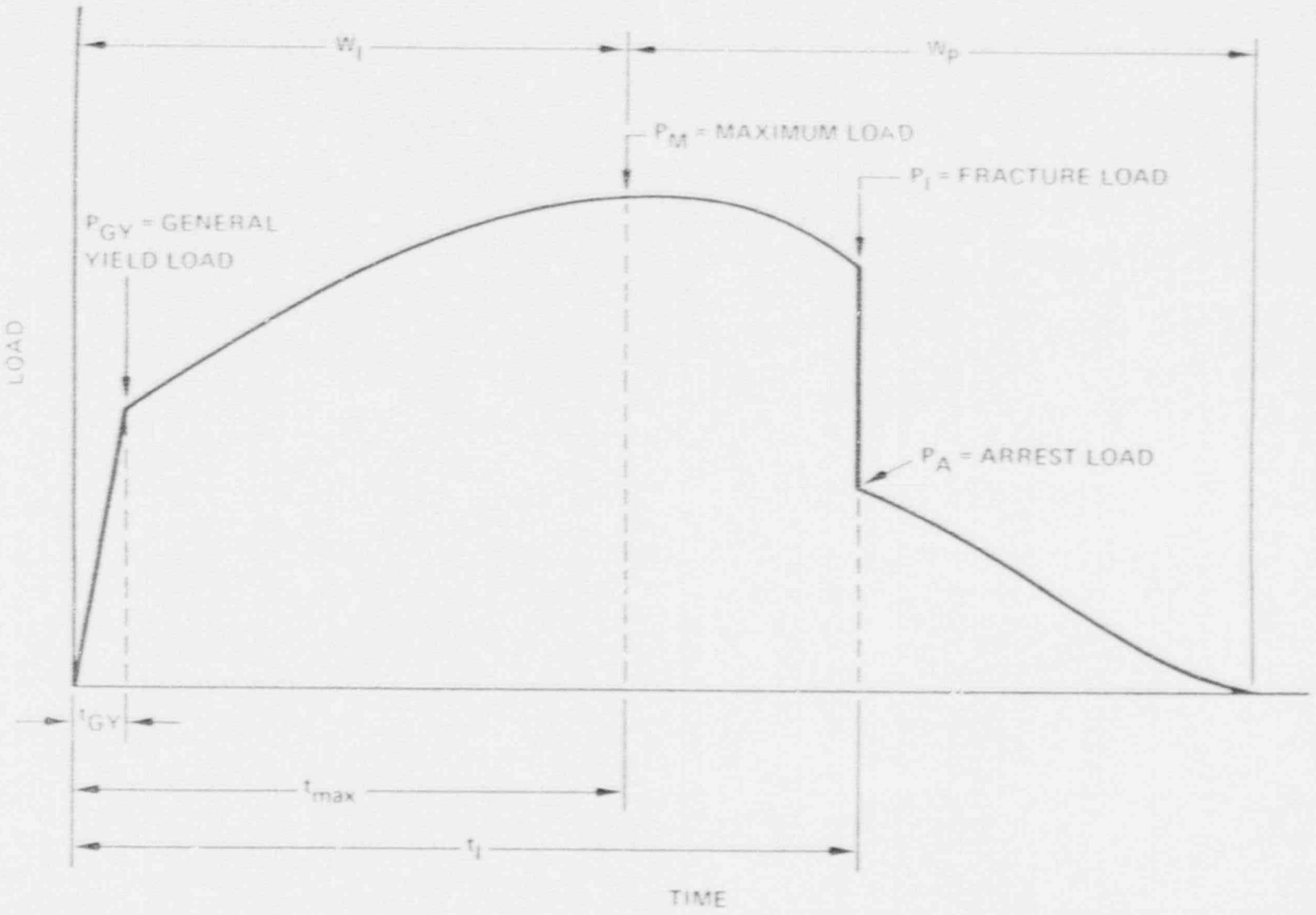

Figure A-1. Idealized load-time record.

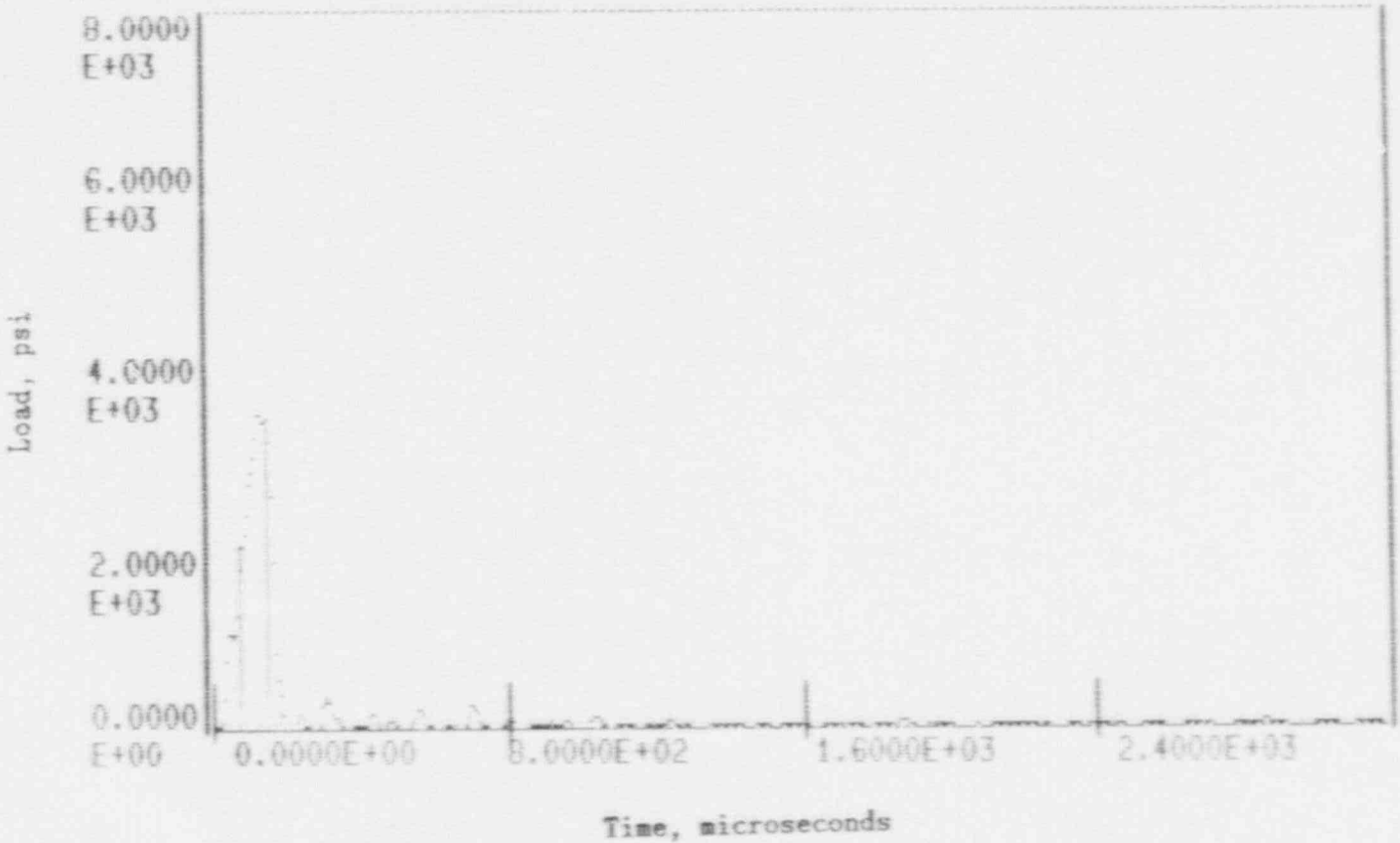

Figure A-2. Load-time record for Specimen PL54.

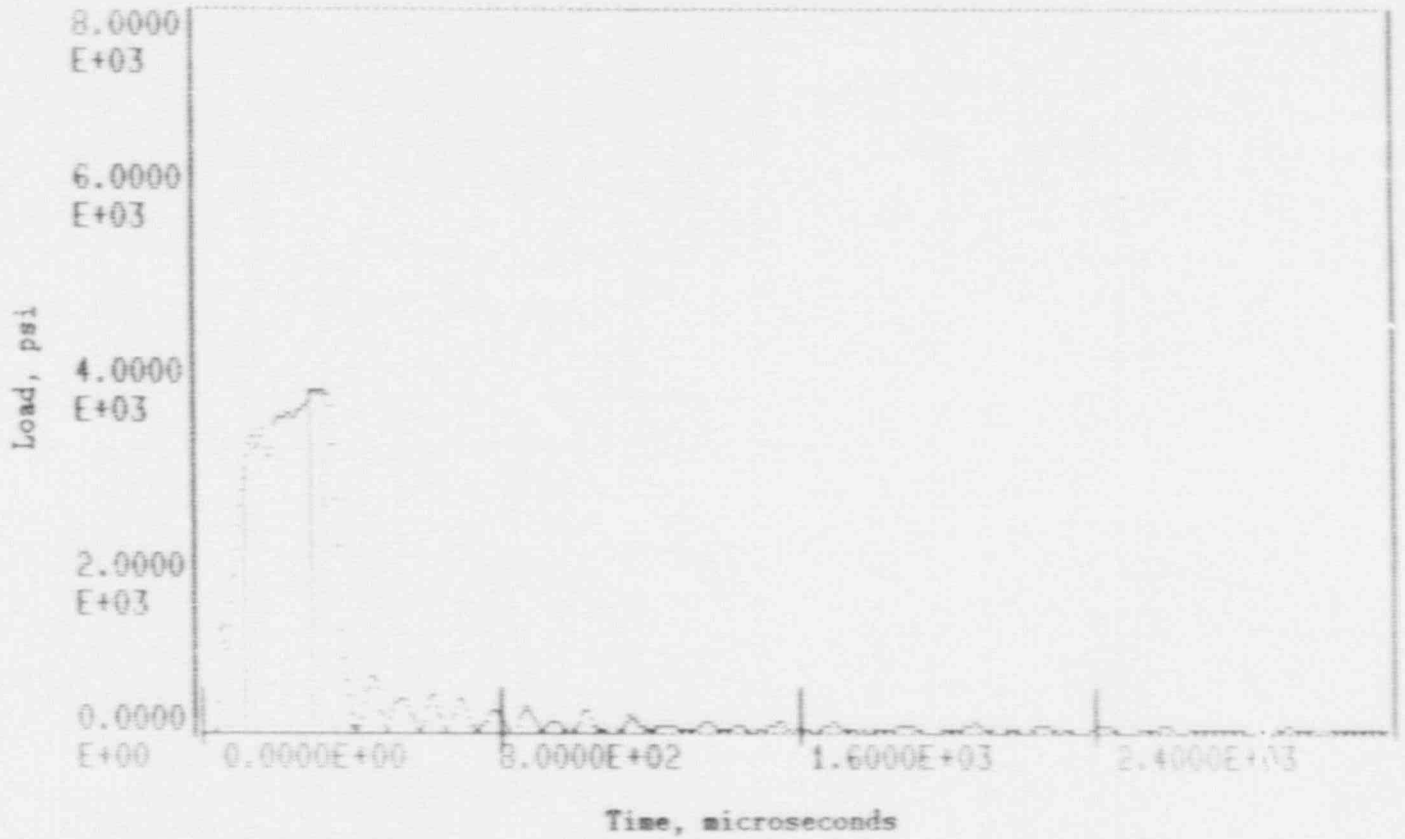

Figure A-3. Load-time record for Specimen PL47.

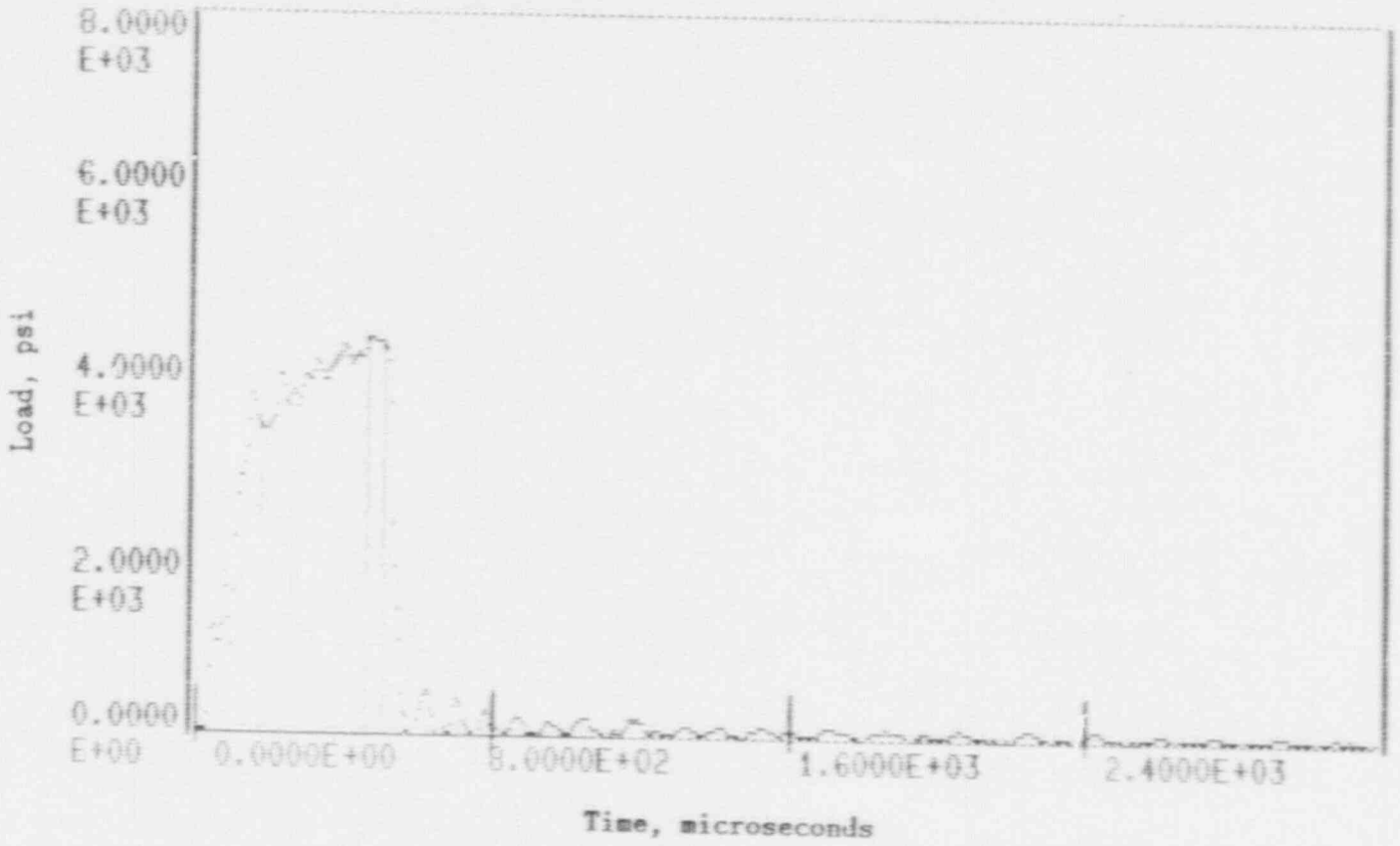

Figure A-4. Load-time record for Specimen PL57

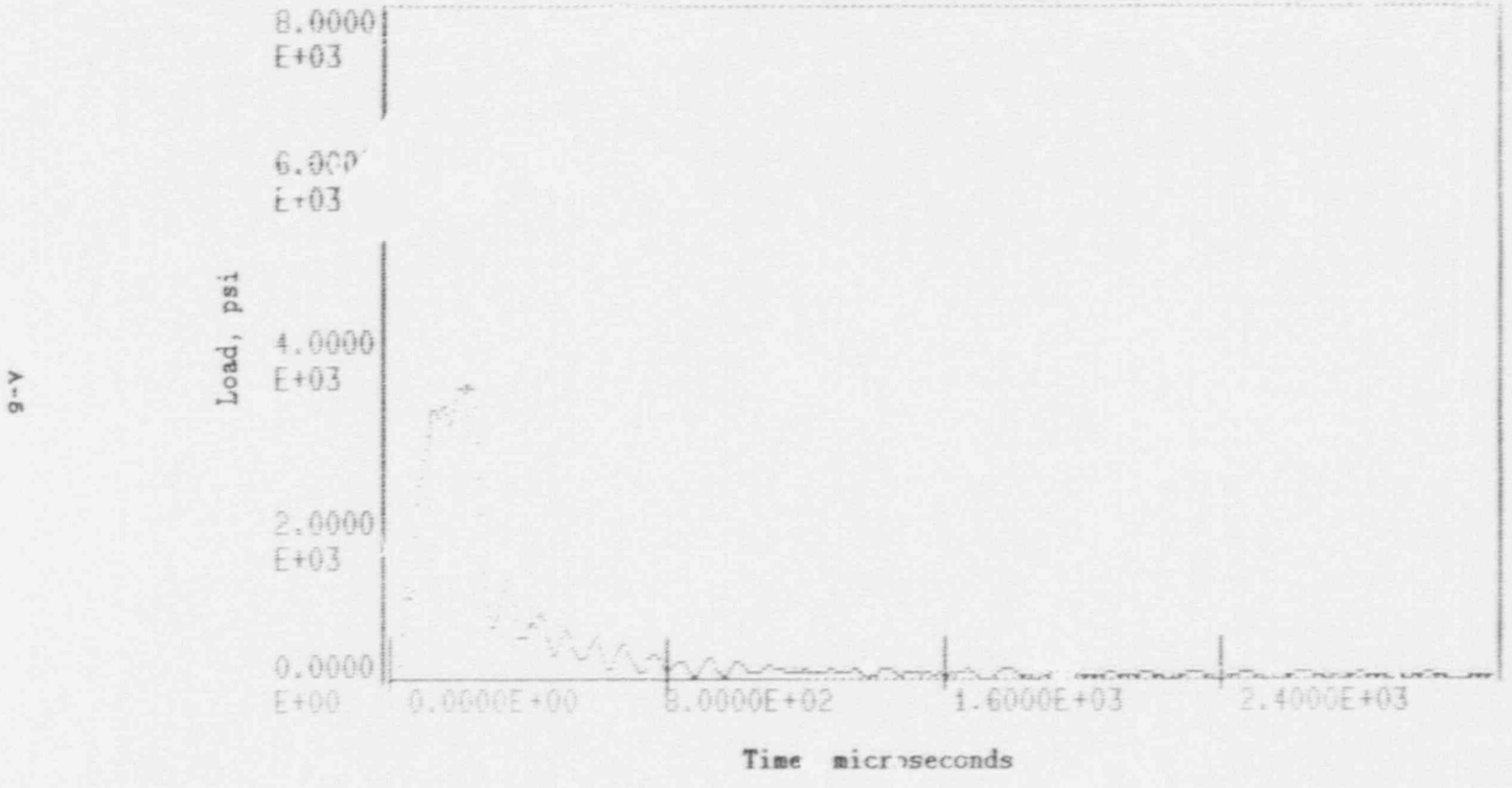

Figure A-5. Load-time record for Specimen PL60.

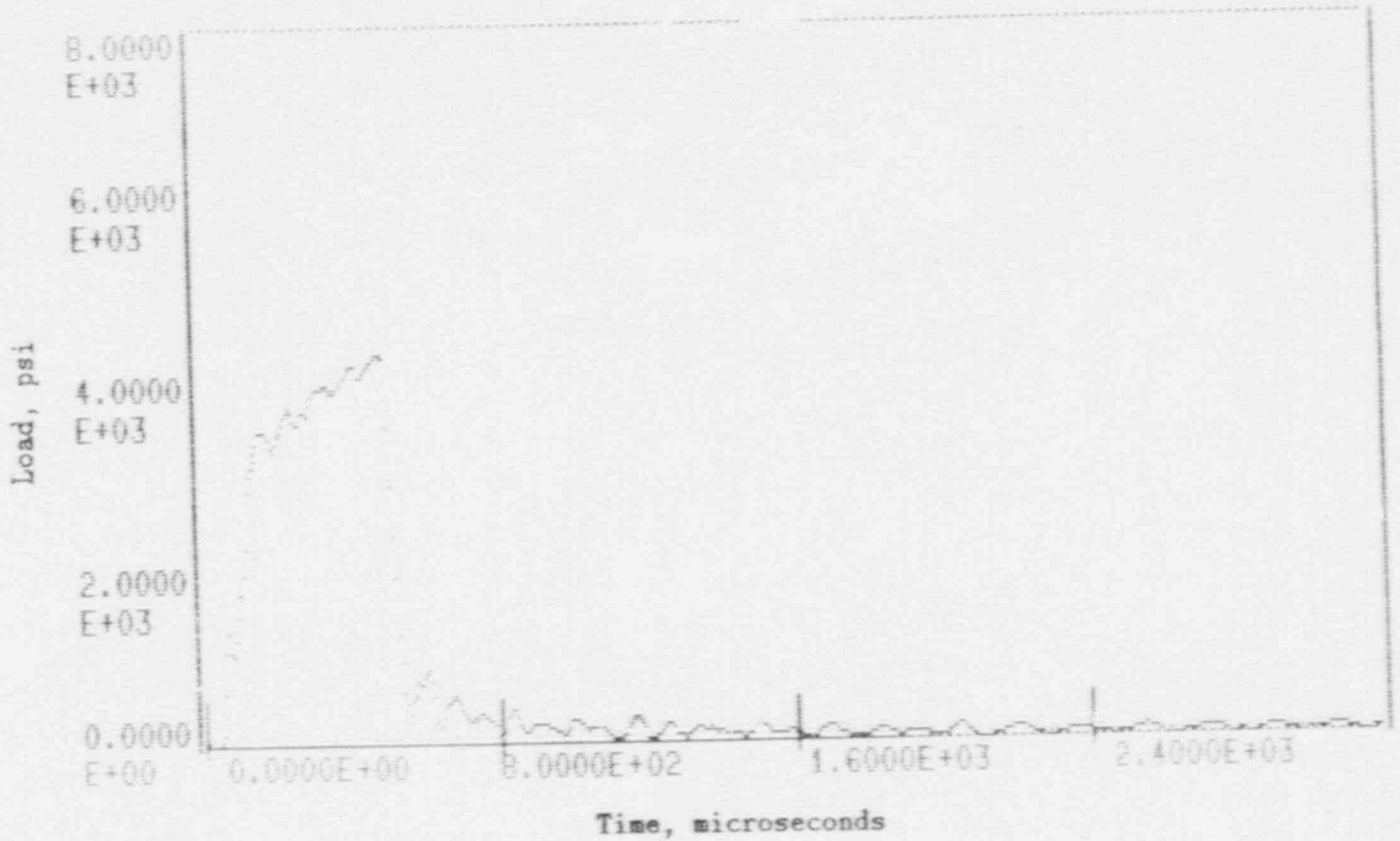

Figure A-6. Load-time record for Specimen PL58.

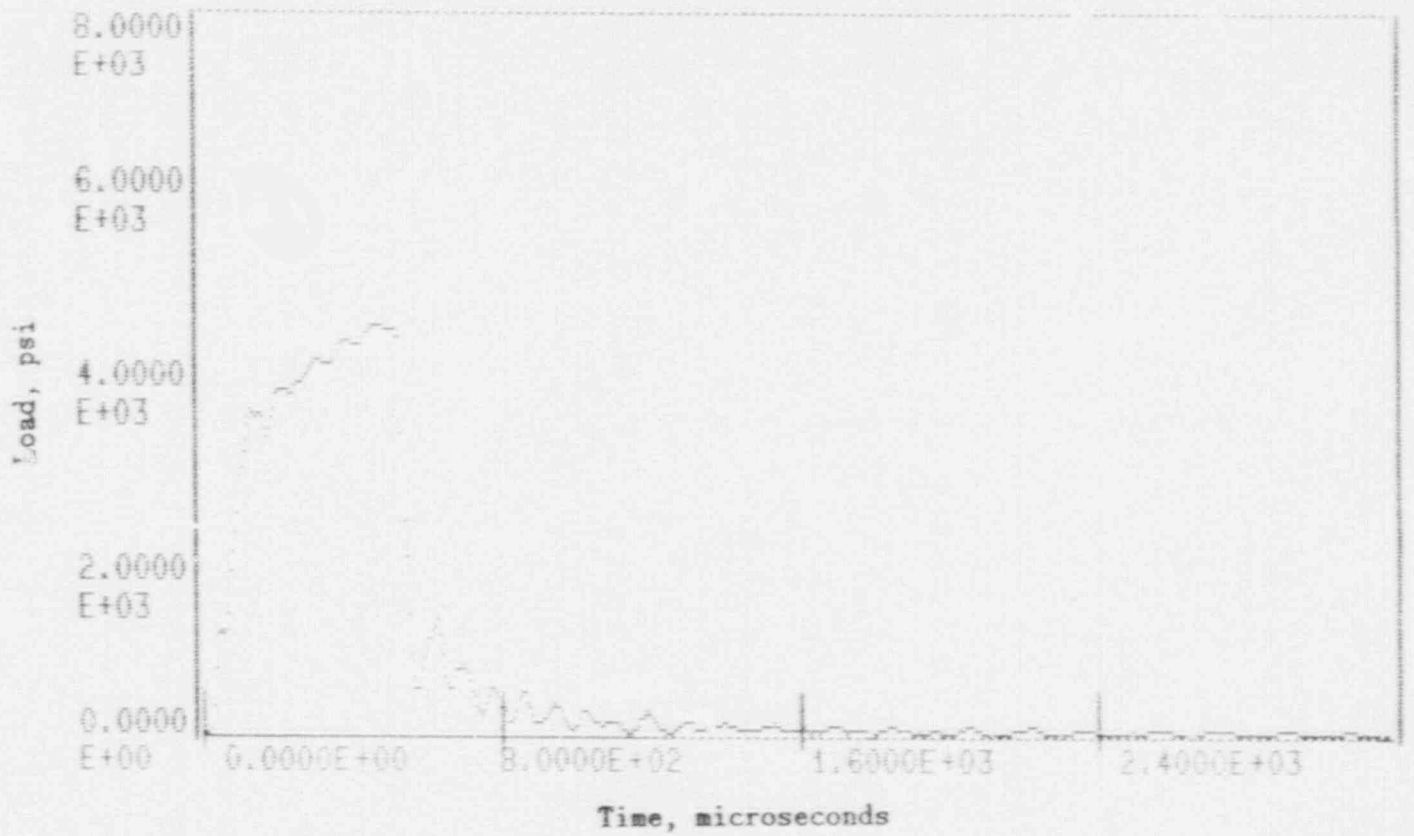

Figure A-7. Load-time record for Specimen PL51.

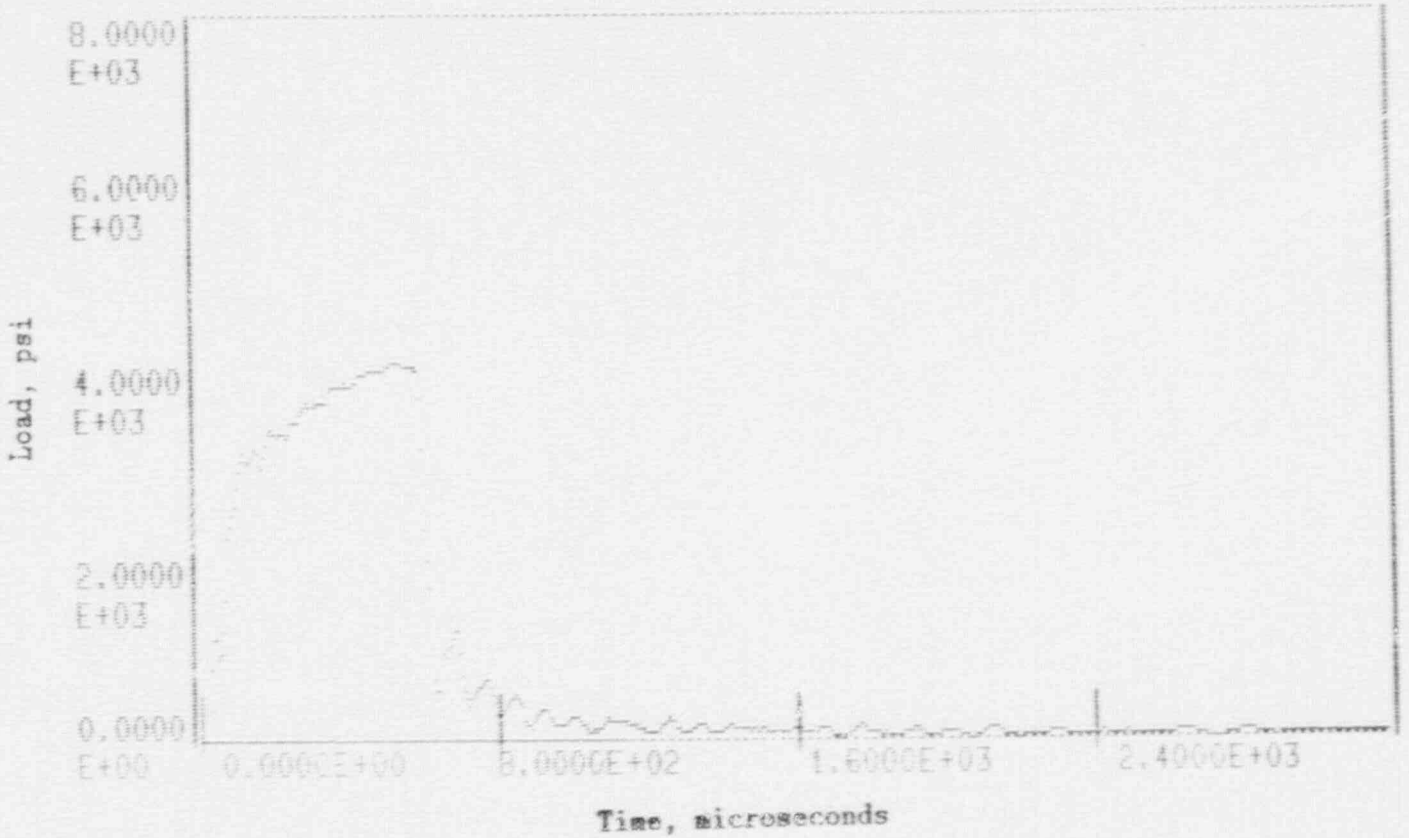

Figure A-8. Load-time record for Specimen PL49.

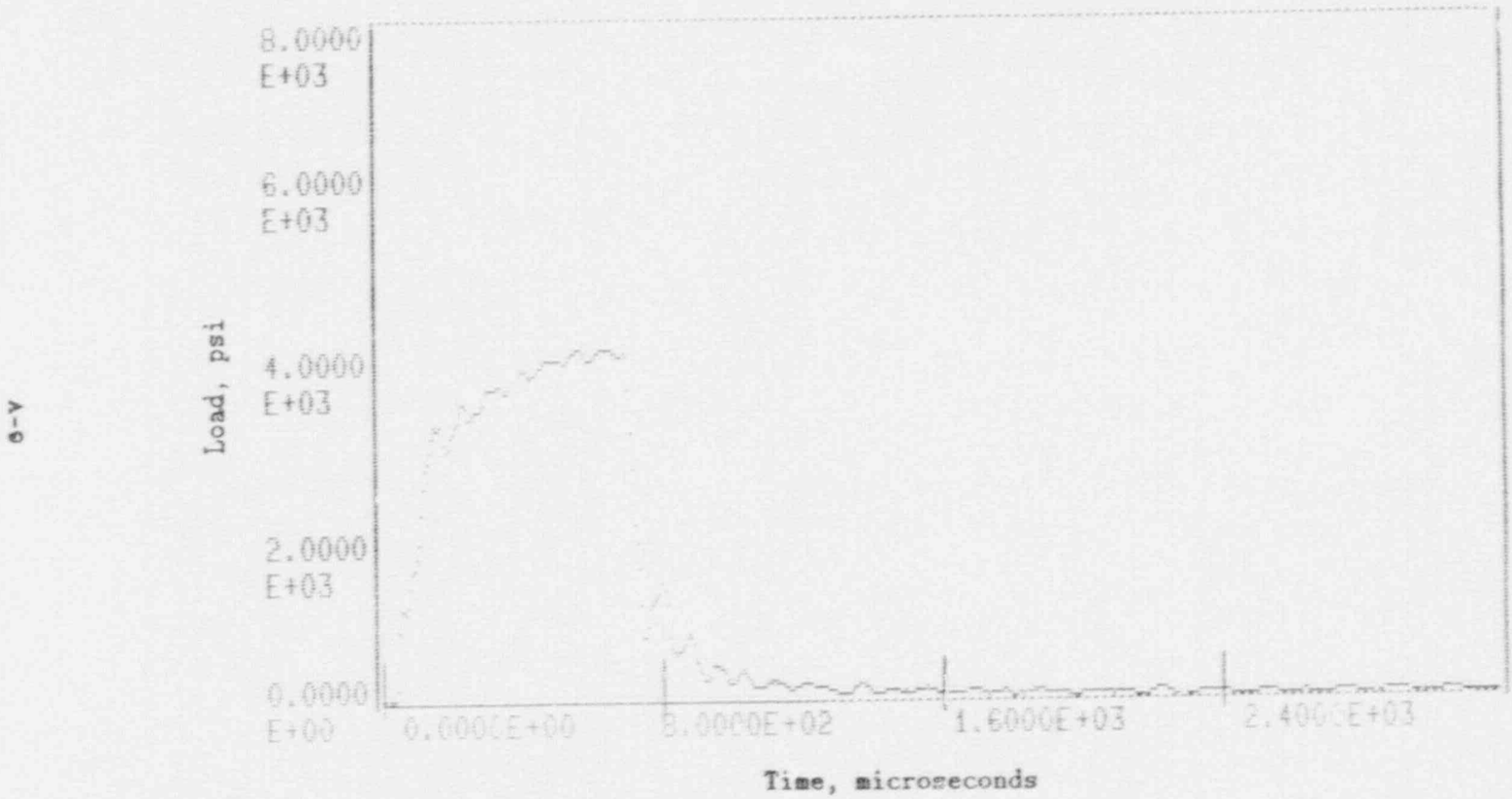

Figure A-9. Load-time record for Specimen PL59.

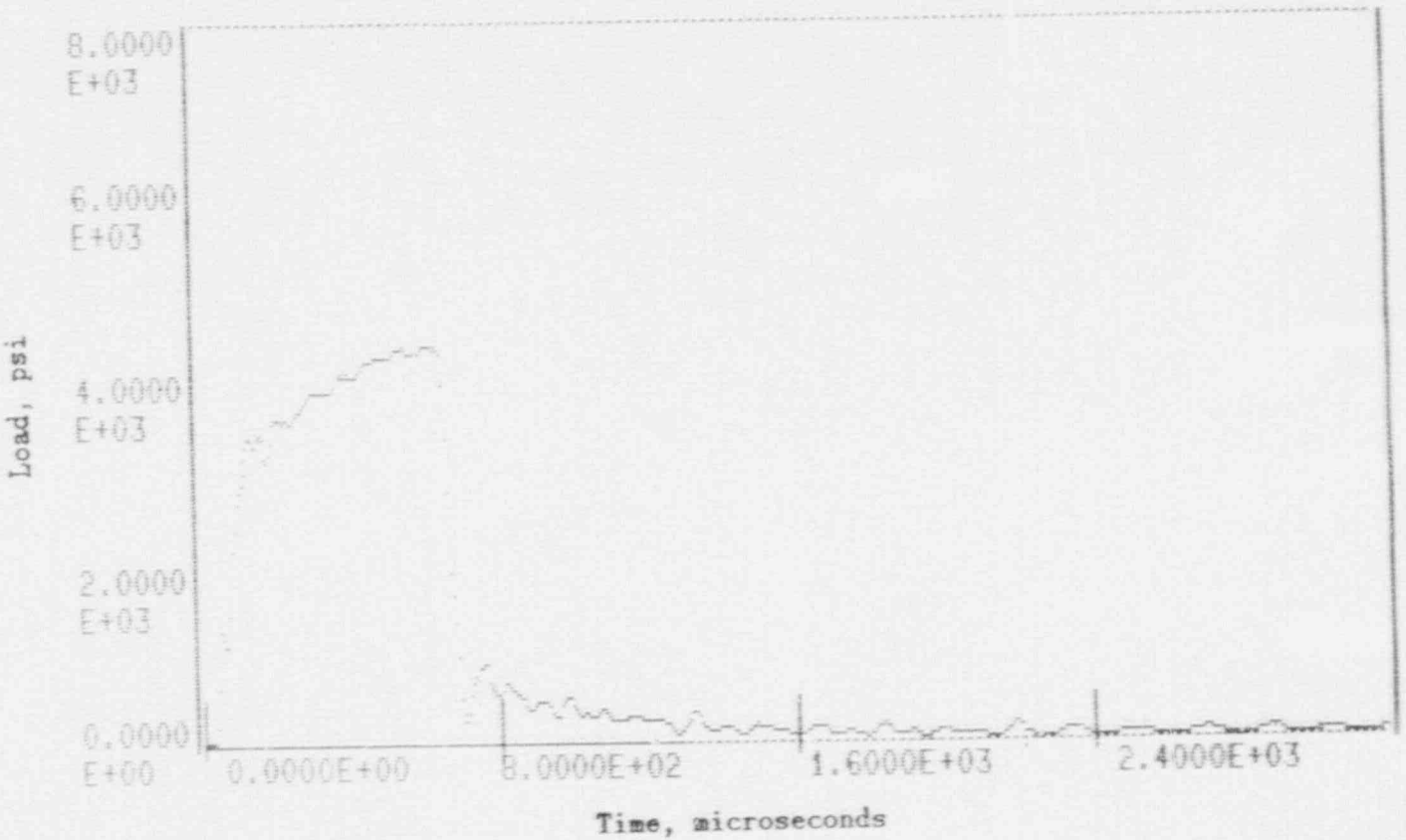

Figure A-10. Load-time record for Specimen PL48.

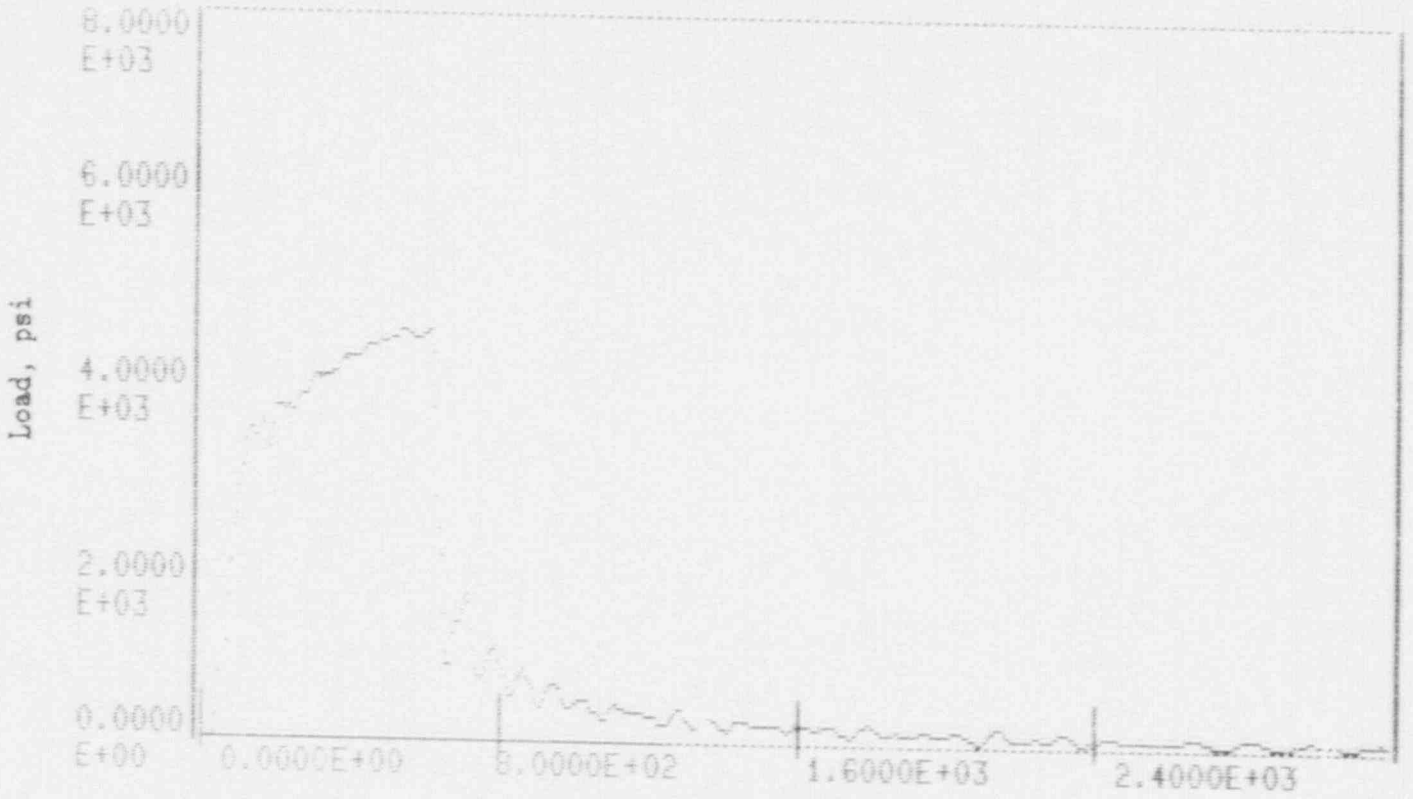

Figure A-11. Load-time record for Specimen PL53.

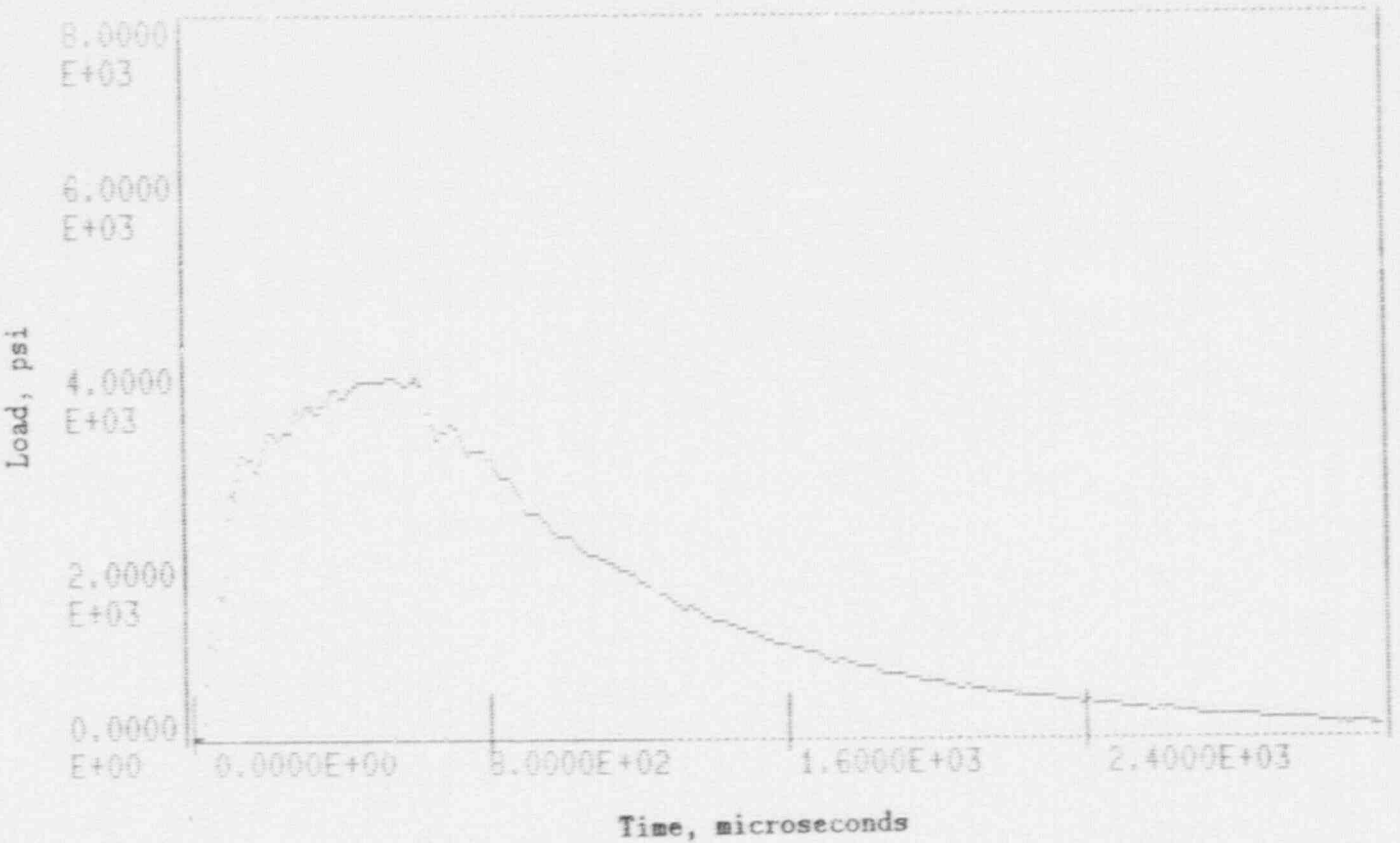

Figure A-12. Load-time record for Specimen PL55.

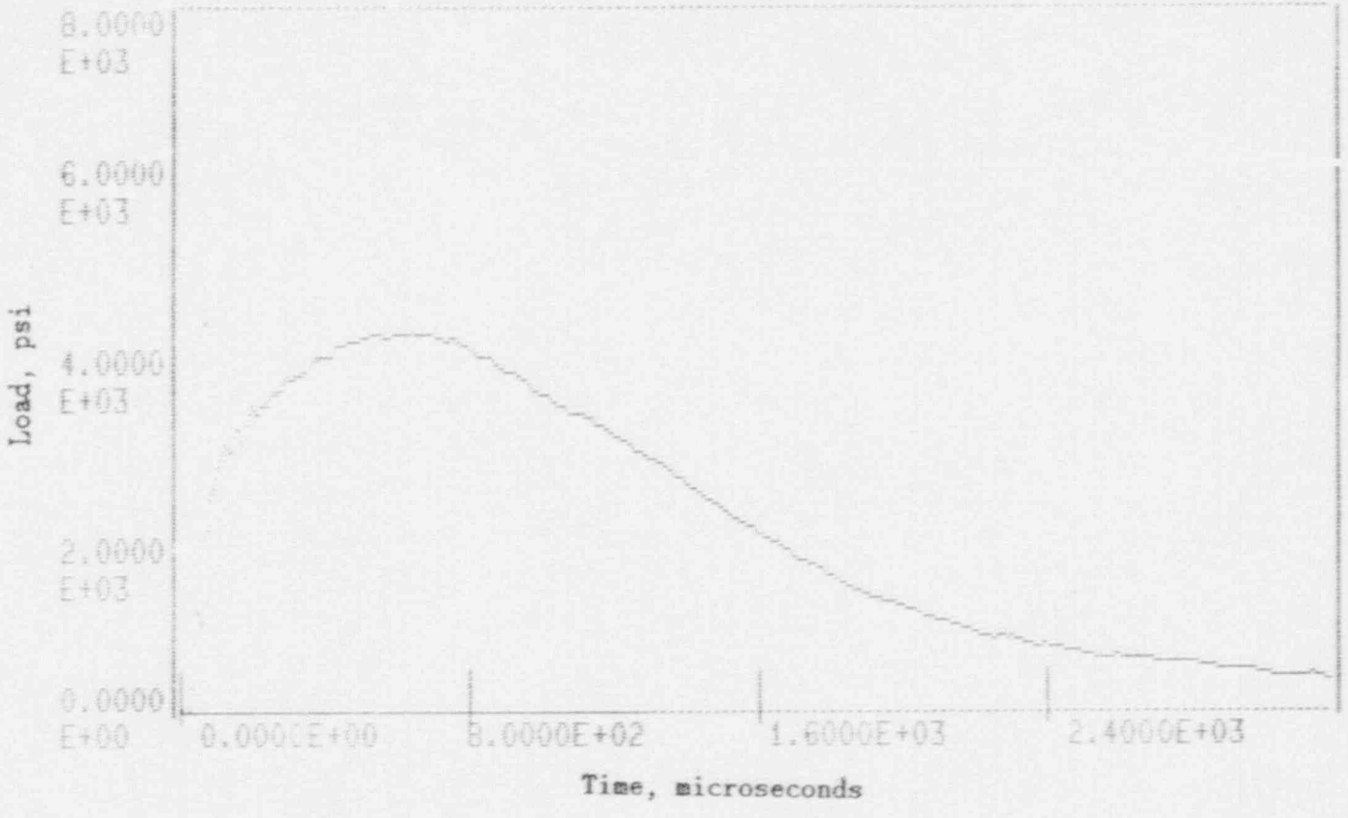

Figure A-13. Load-time record for Specimen PL50.

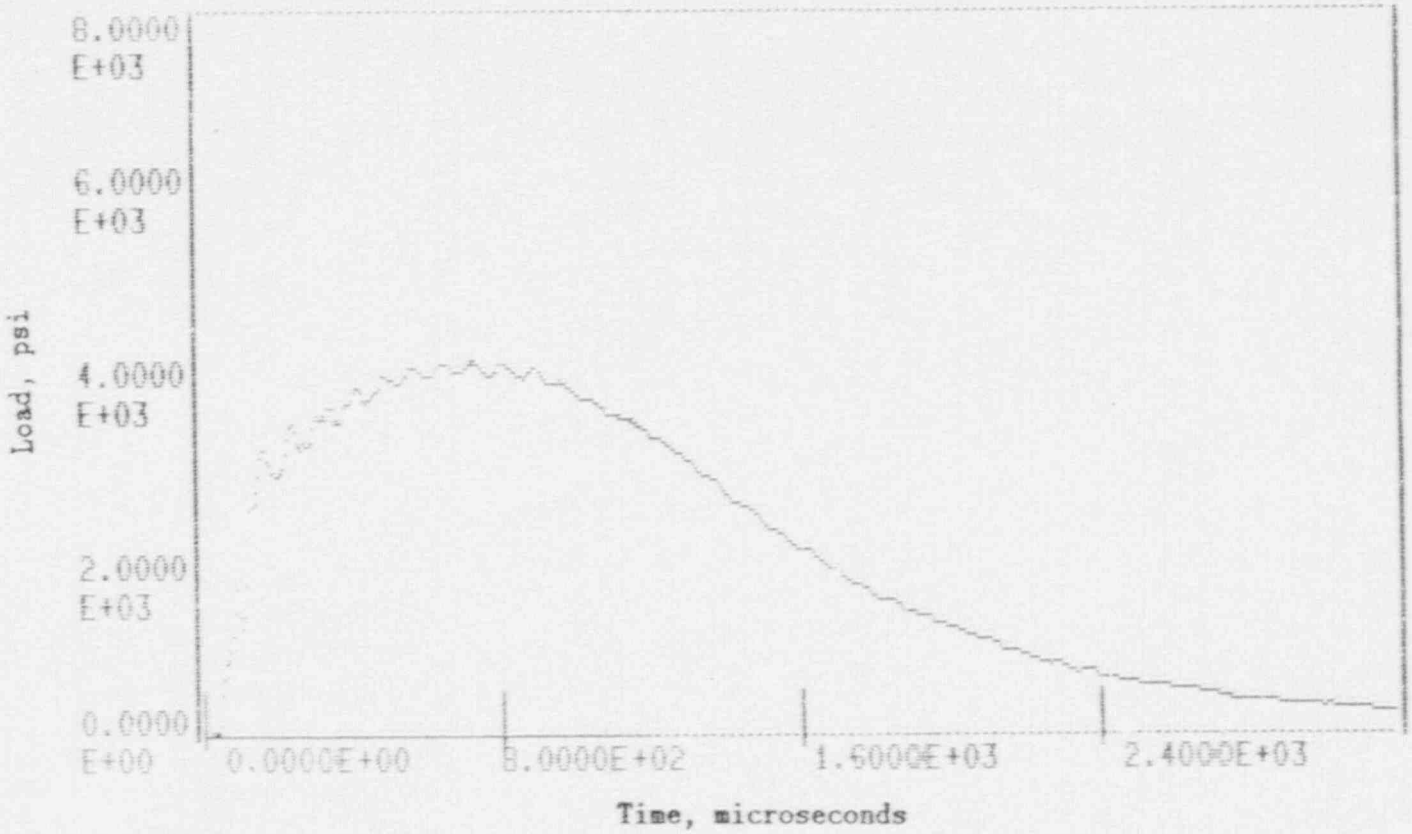

Figure A-14. Load-time record for Specimen PL46.

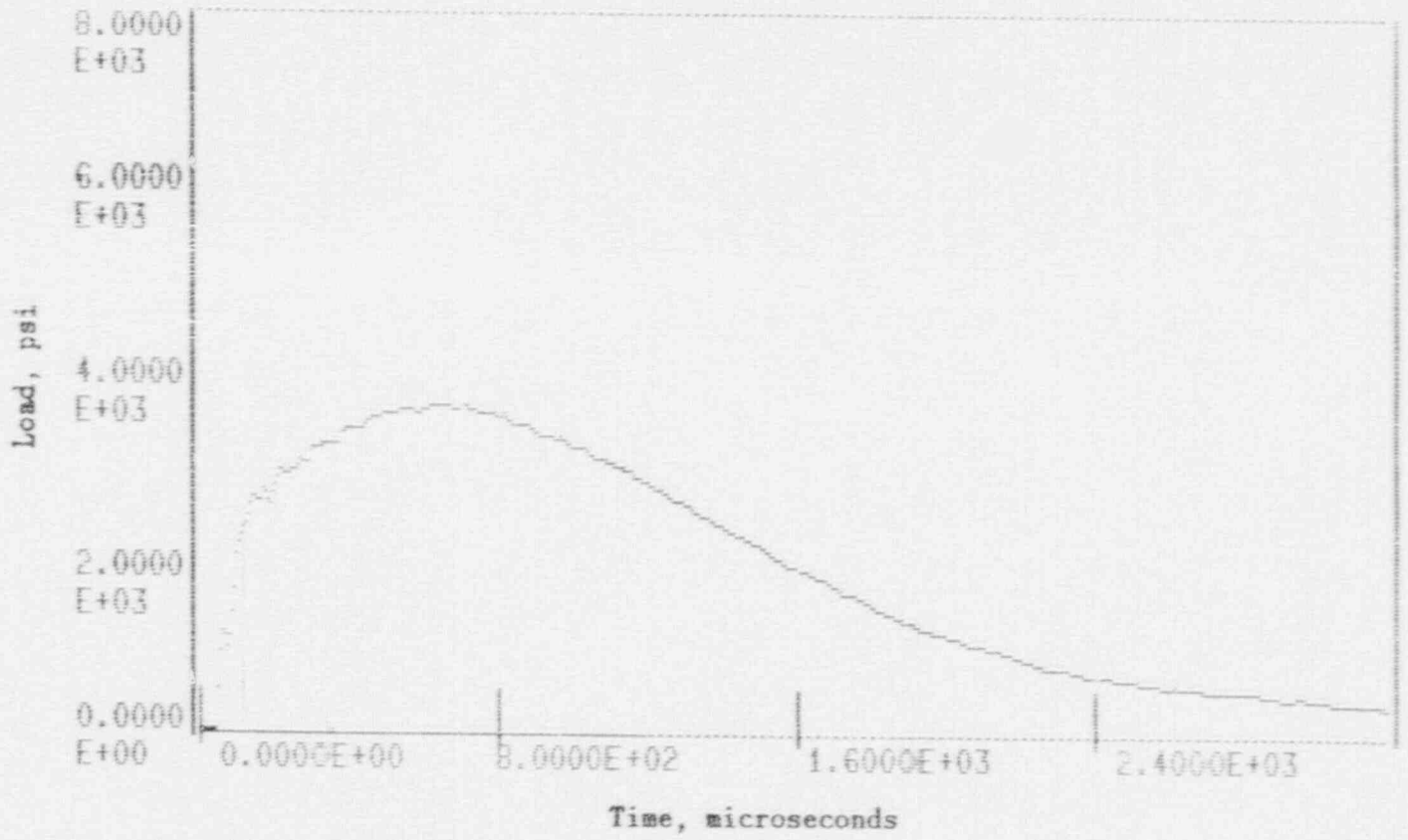

Figure A-15. Load-time record for Specimen PL56.

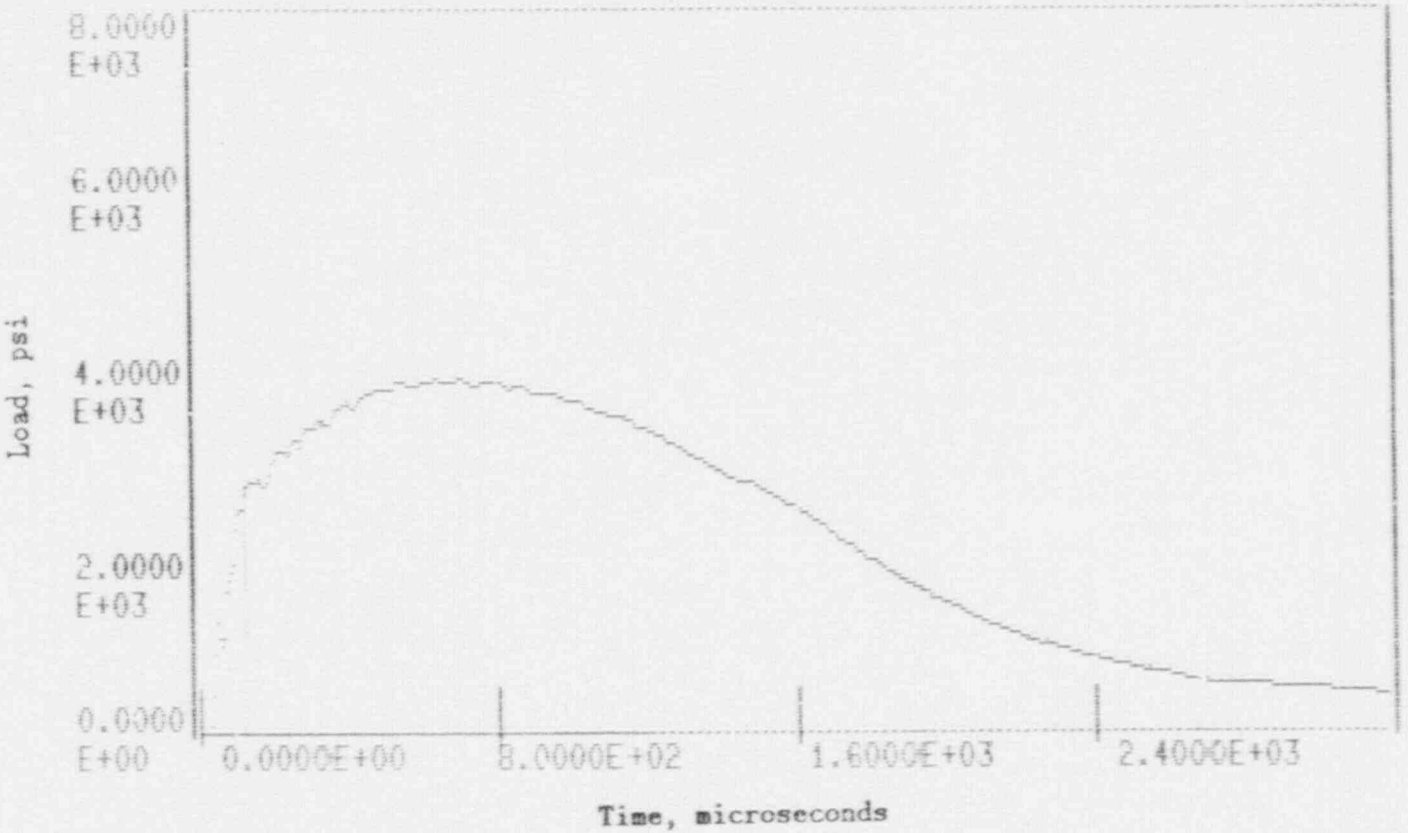

Figure A-16. Load-time record for Specimen PL52.

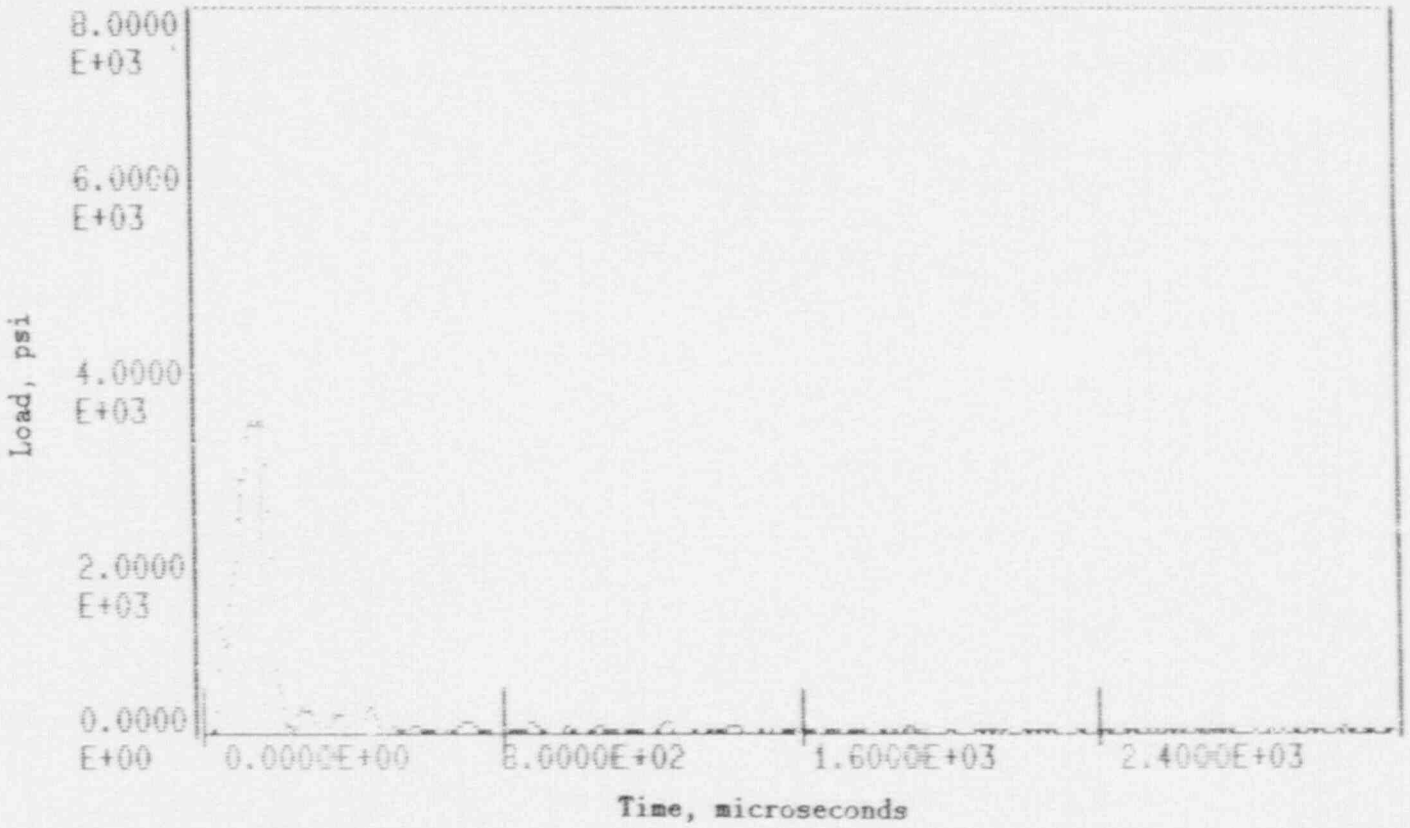

Figure A-17. Load-time record for Specimen PT56.

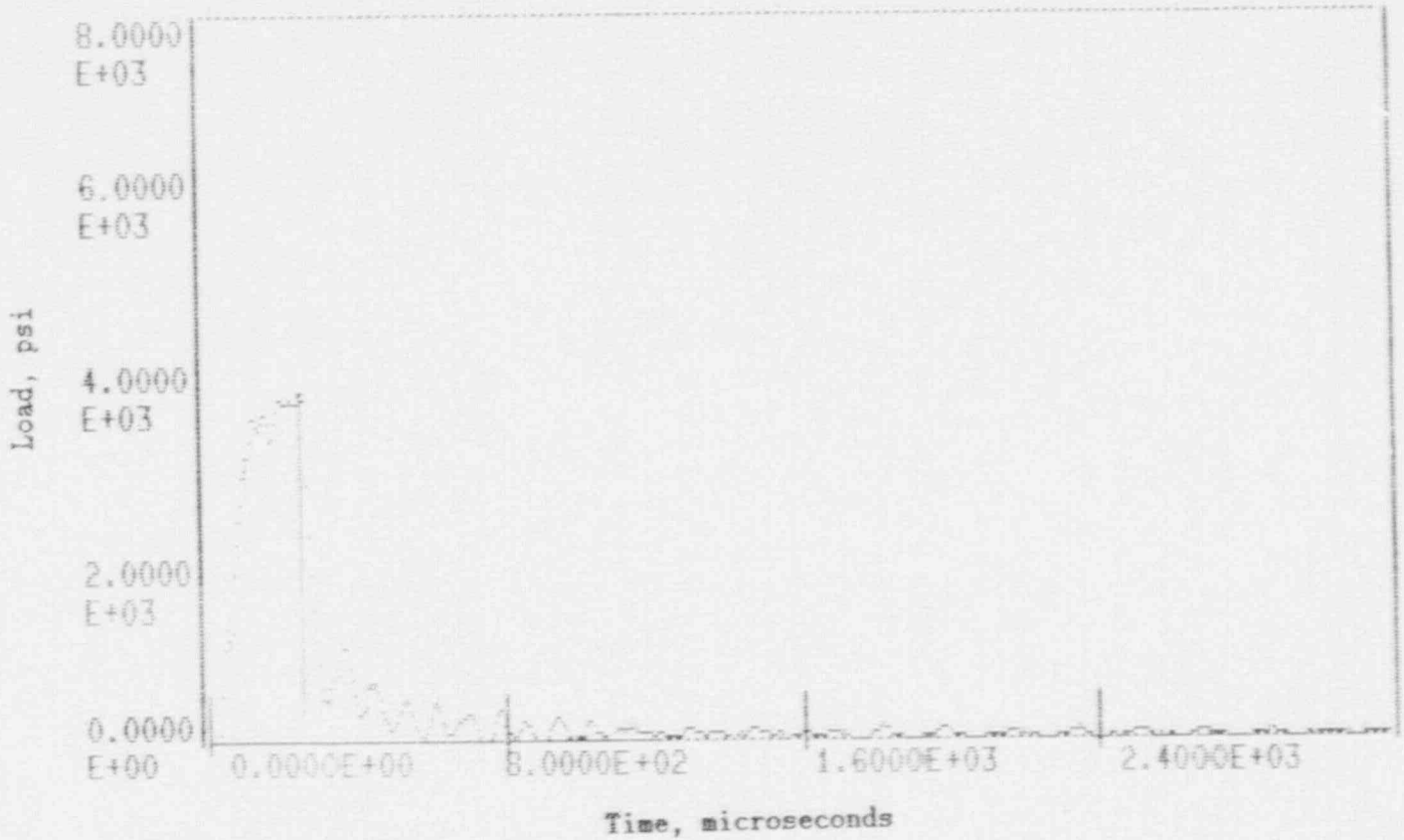

Figure A-18. Load-time record for Specimen PT59.

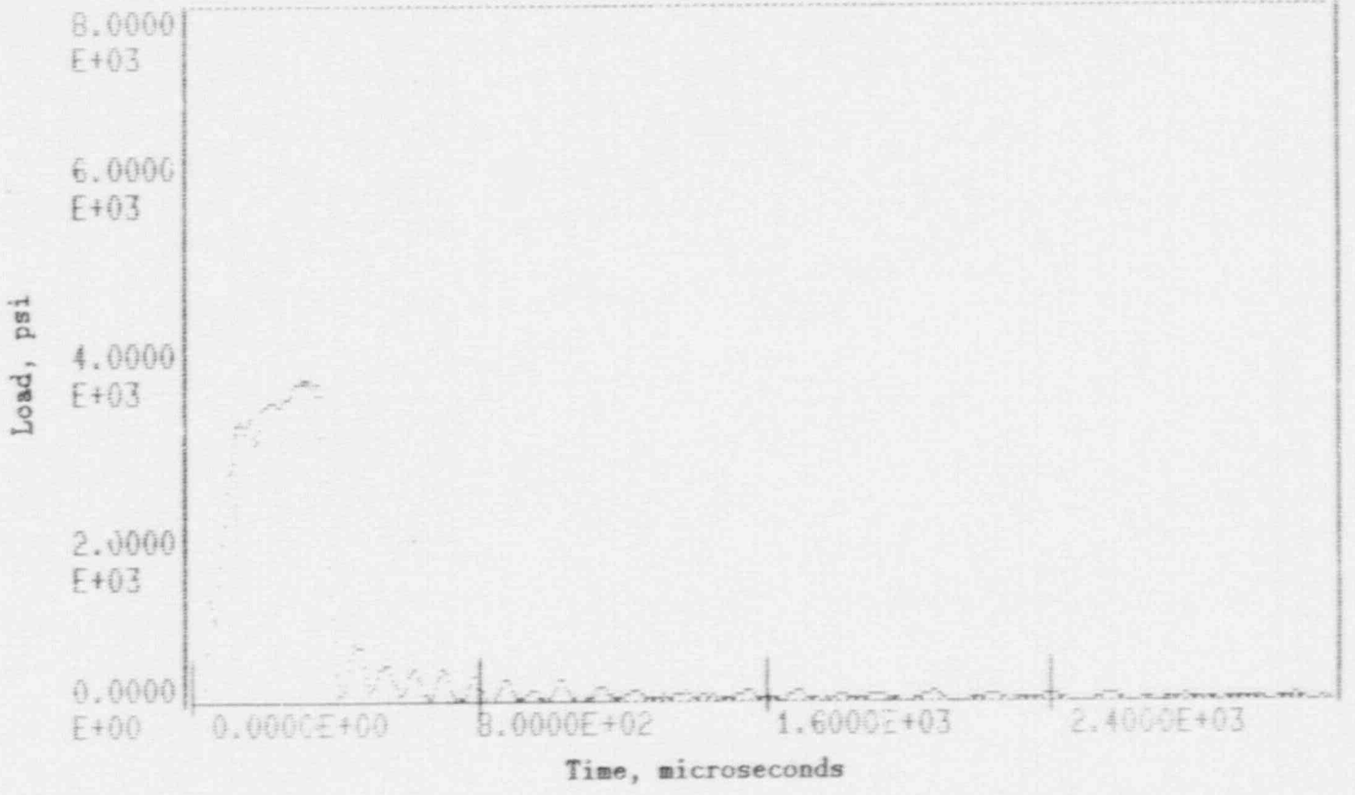

Figure A-19. Load-time record for Specimen PT48.

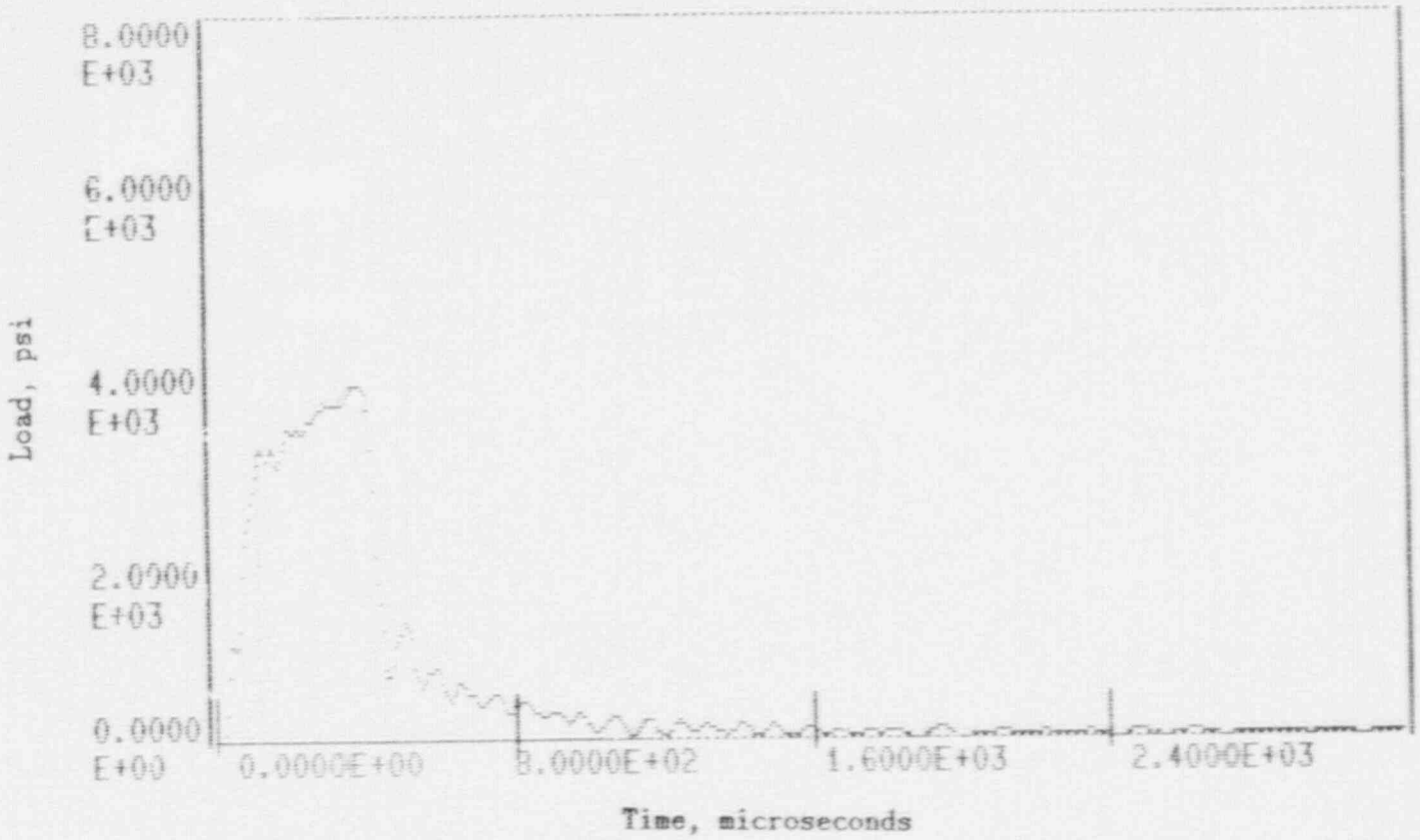

Figure A-20. Load-time record for Specimen PT54.

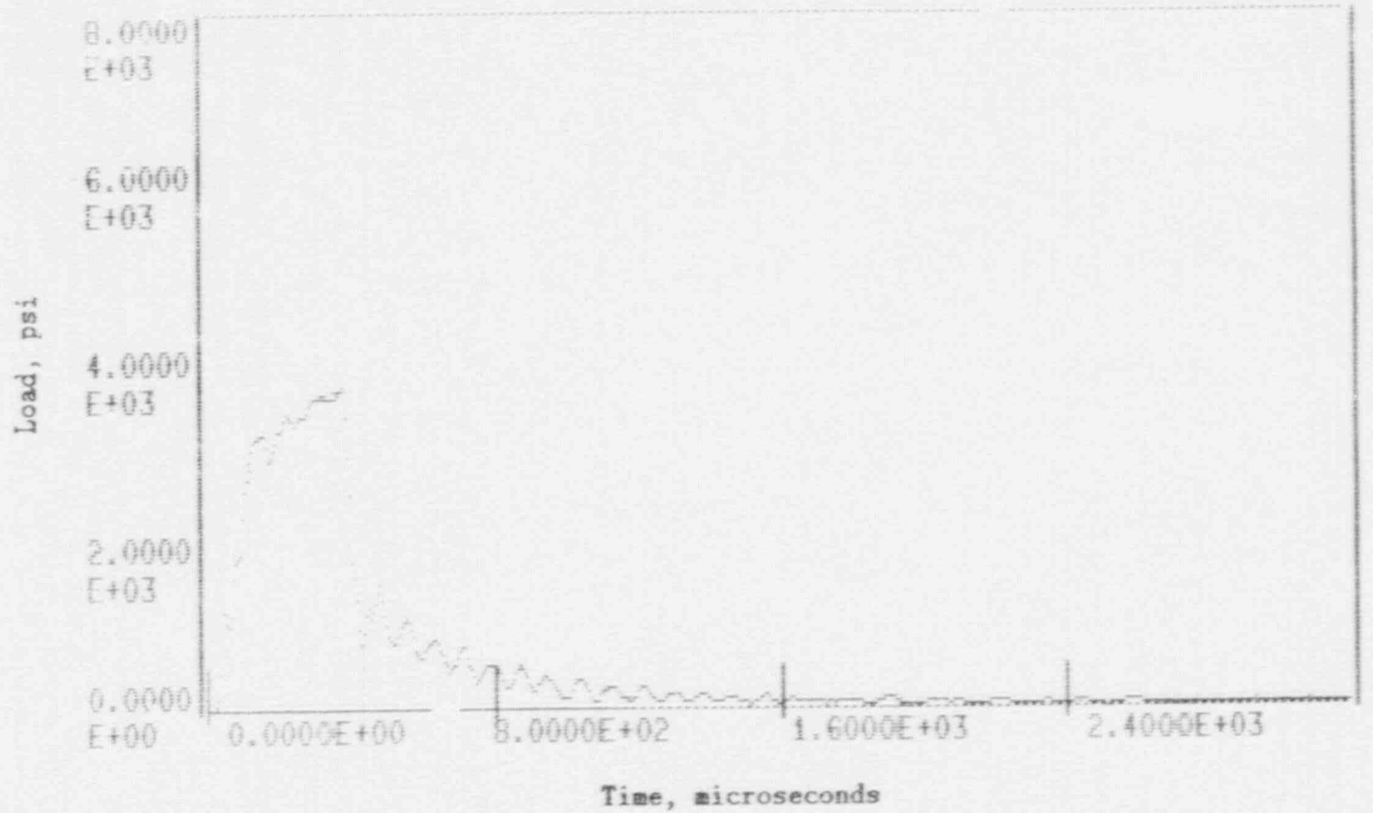

Figure A-21. Load-time record for Specimen PT52.

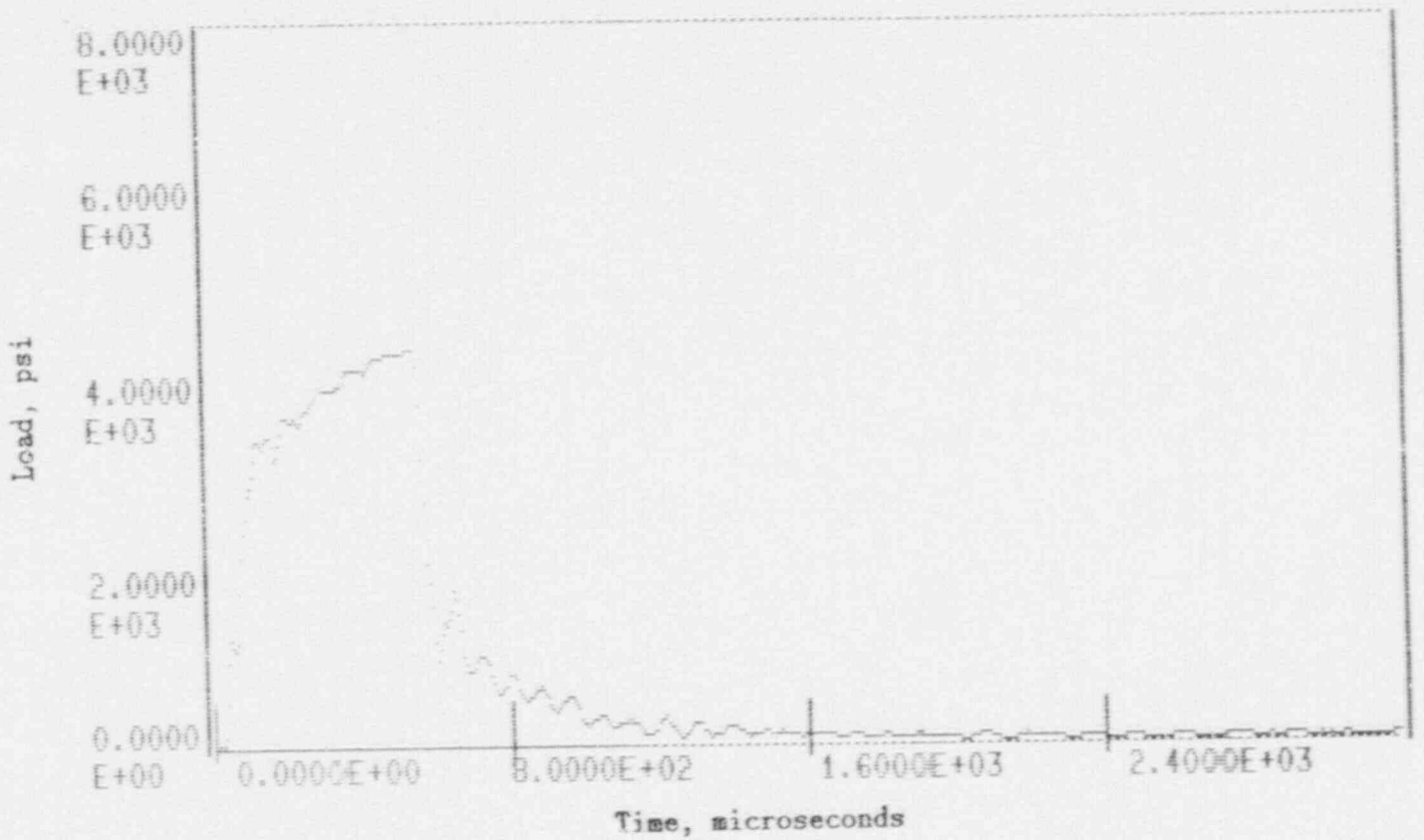

Figure A-22. Load-time record for Specimen PT46.

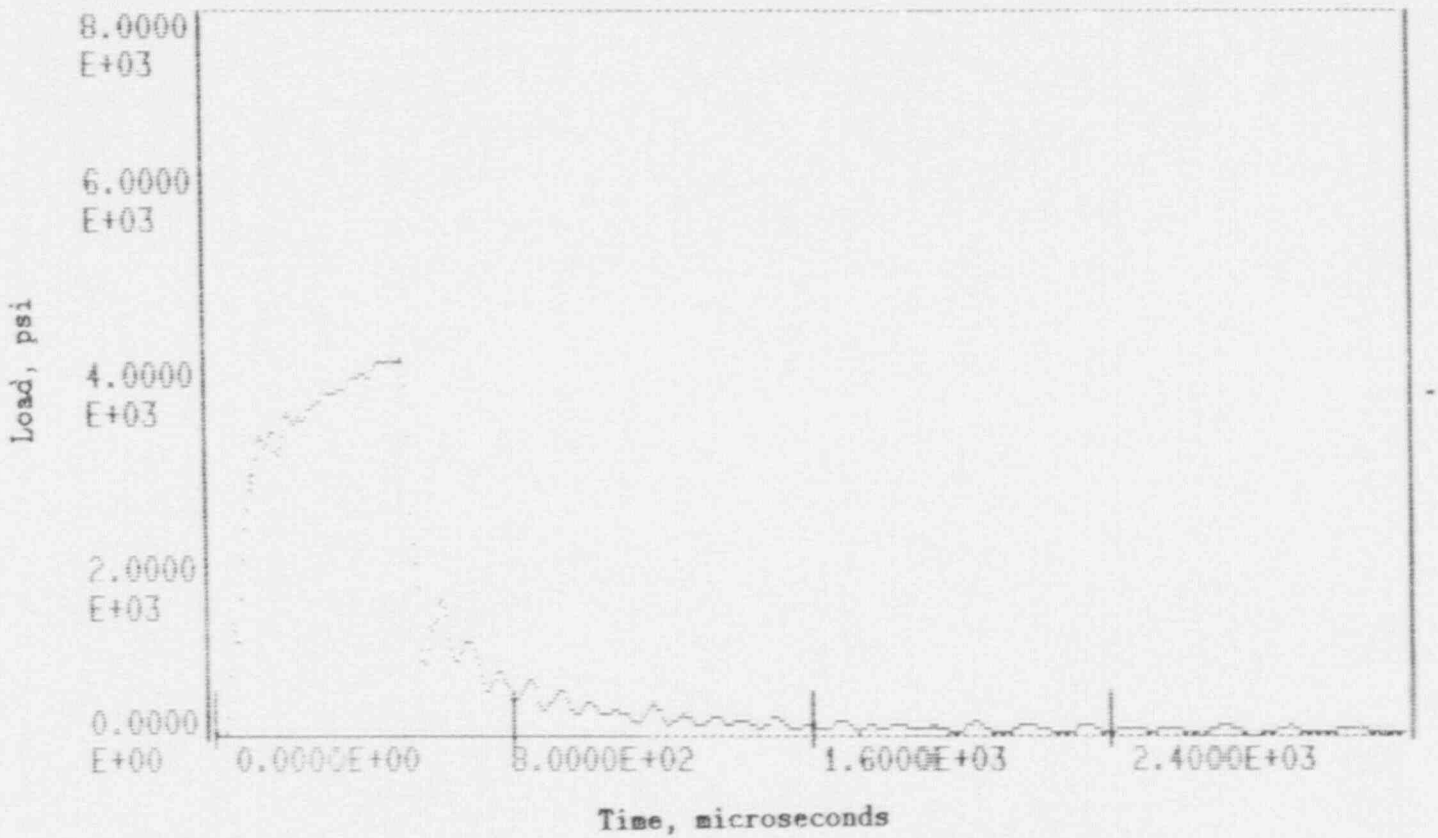

Figure A-23. Load-time record for Specimen PT60.

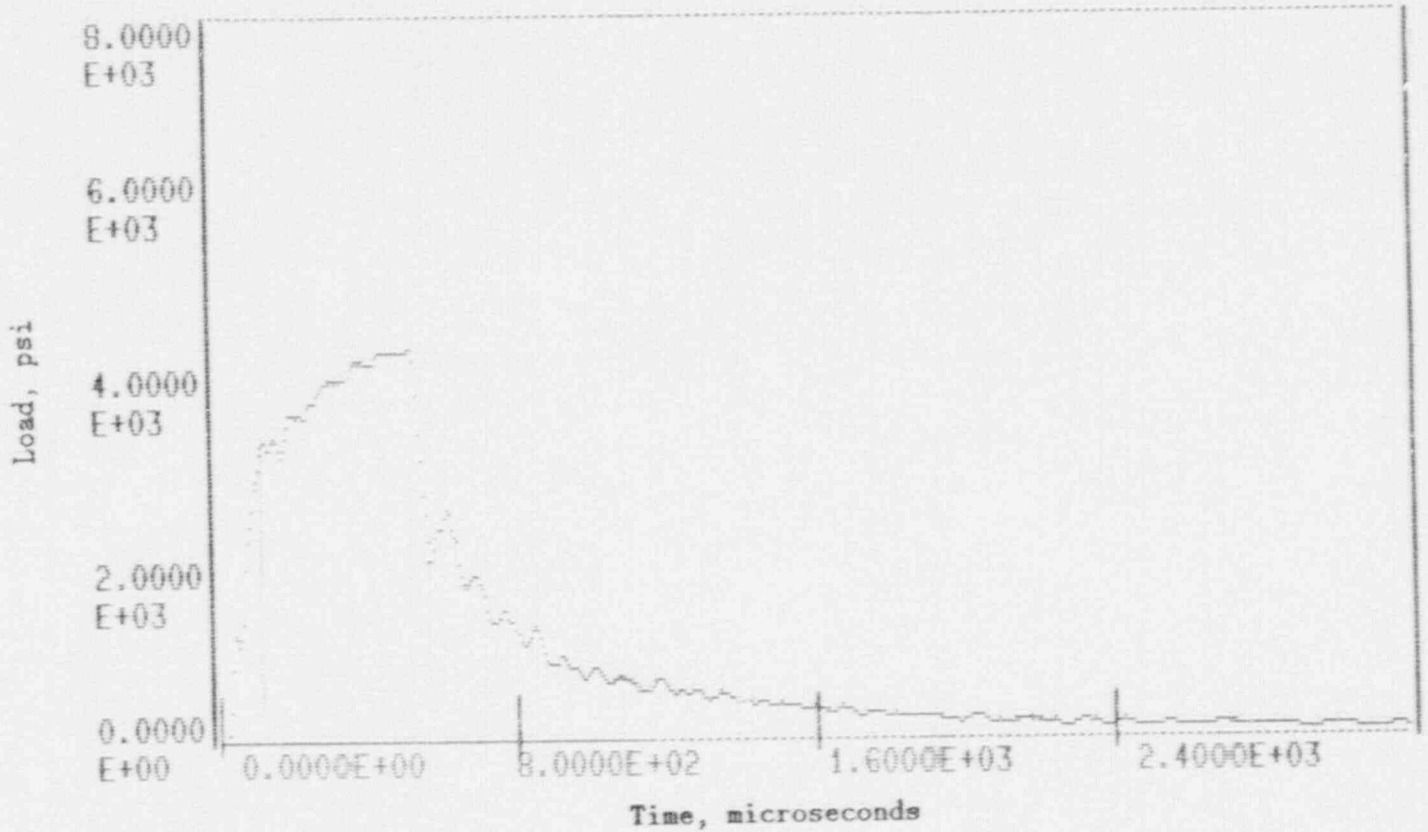

Figure A-24. Load-time record for Specimen PT53.

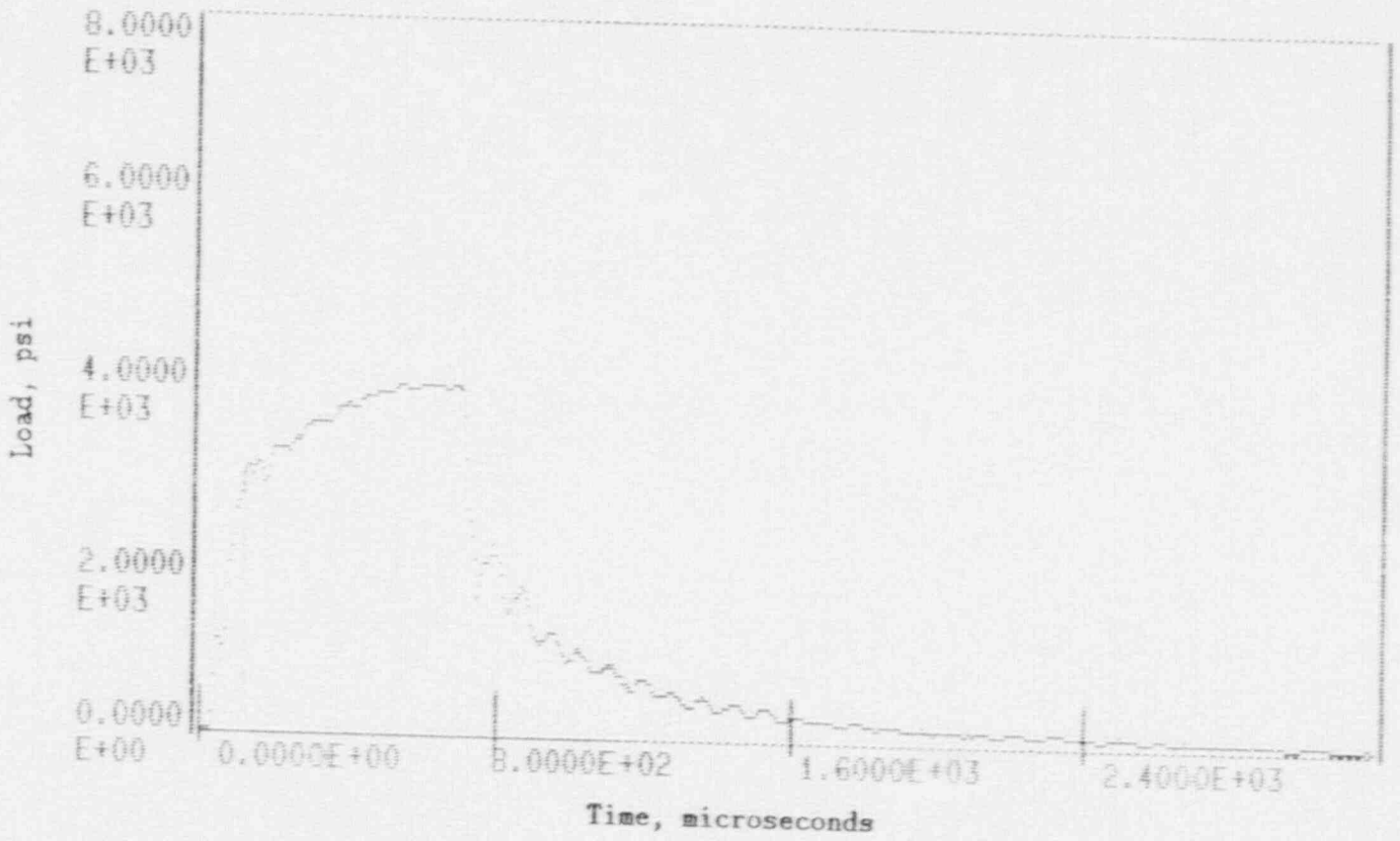

Figure A-25. Load-time record for Specimen PT51.

No record - computer malfunction

Figure A-26. Load-time record for Specimen PT58.

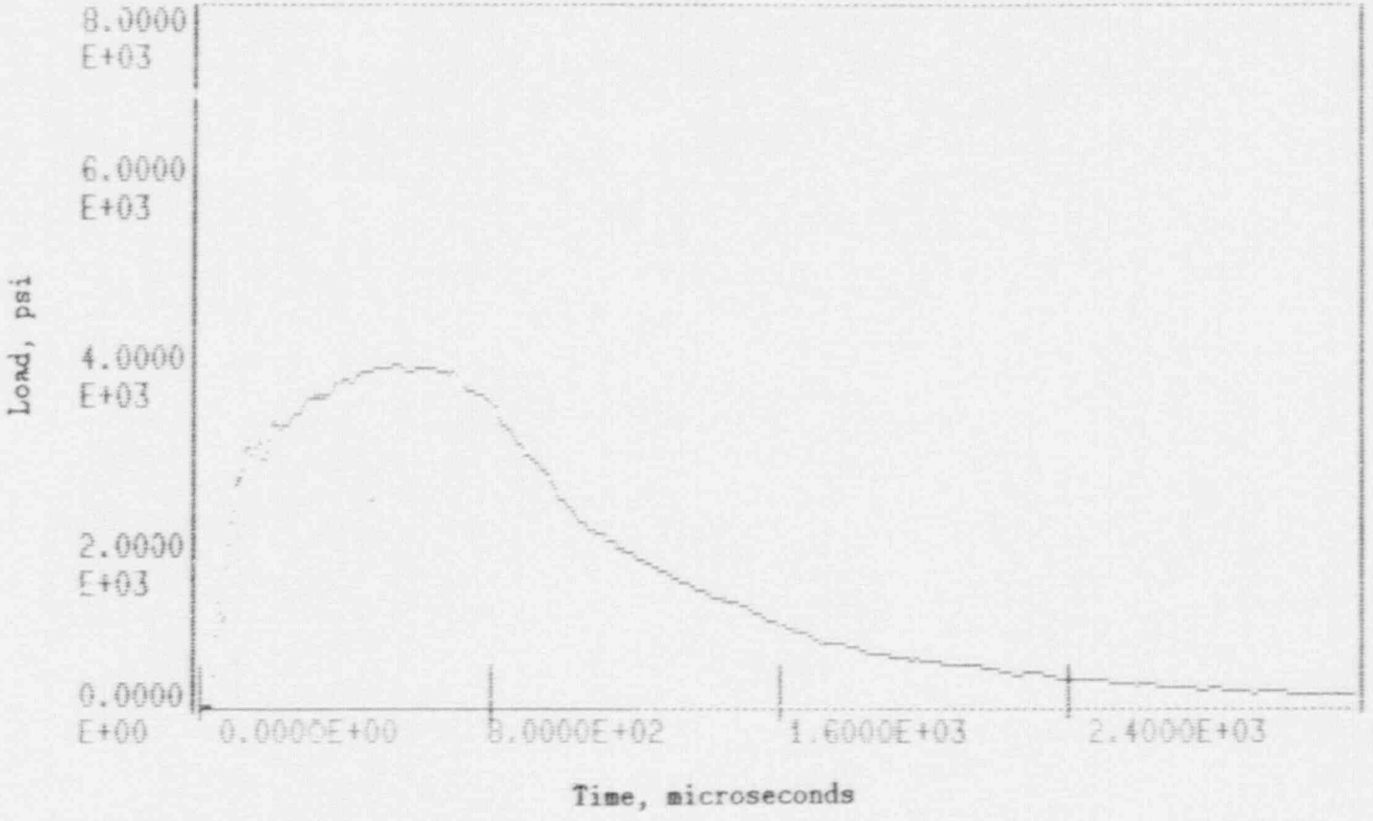

Figure A-27. Load-time record for Specimen PT49.

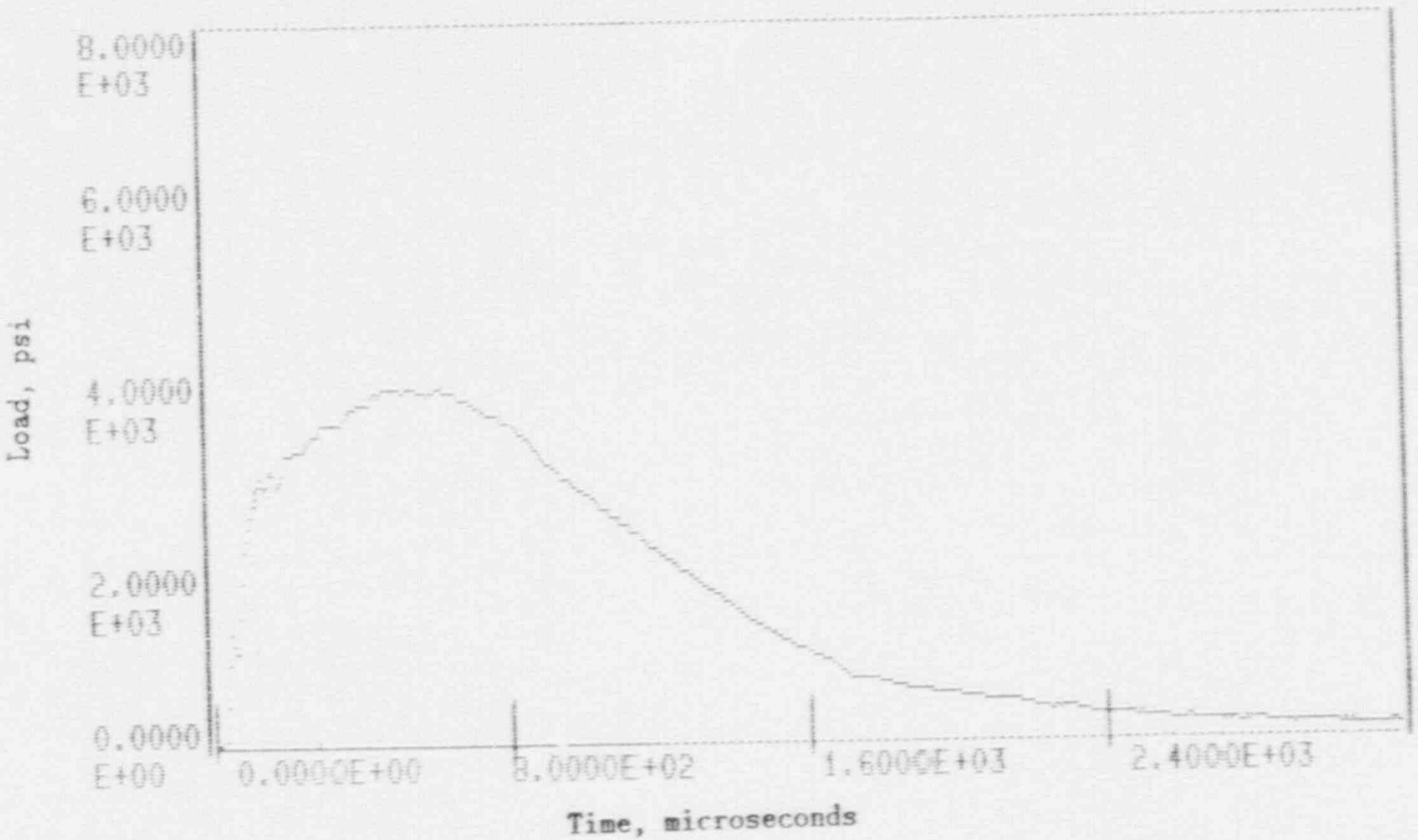

Figure A-28. Load-time record for Specimen PT55.

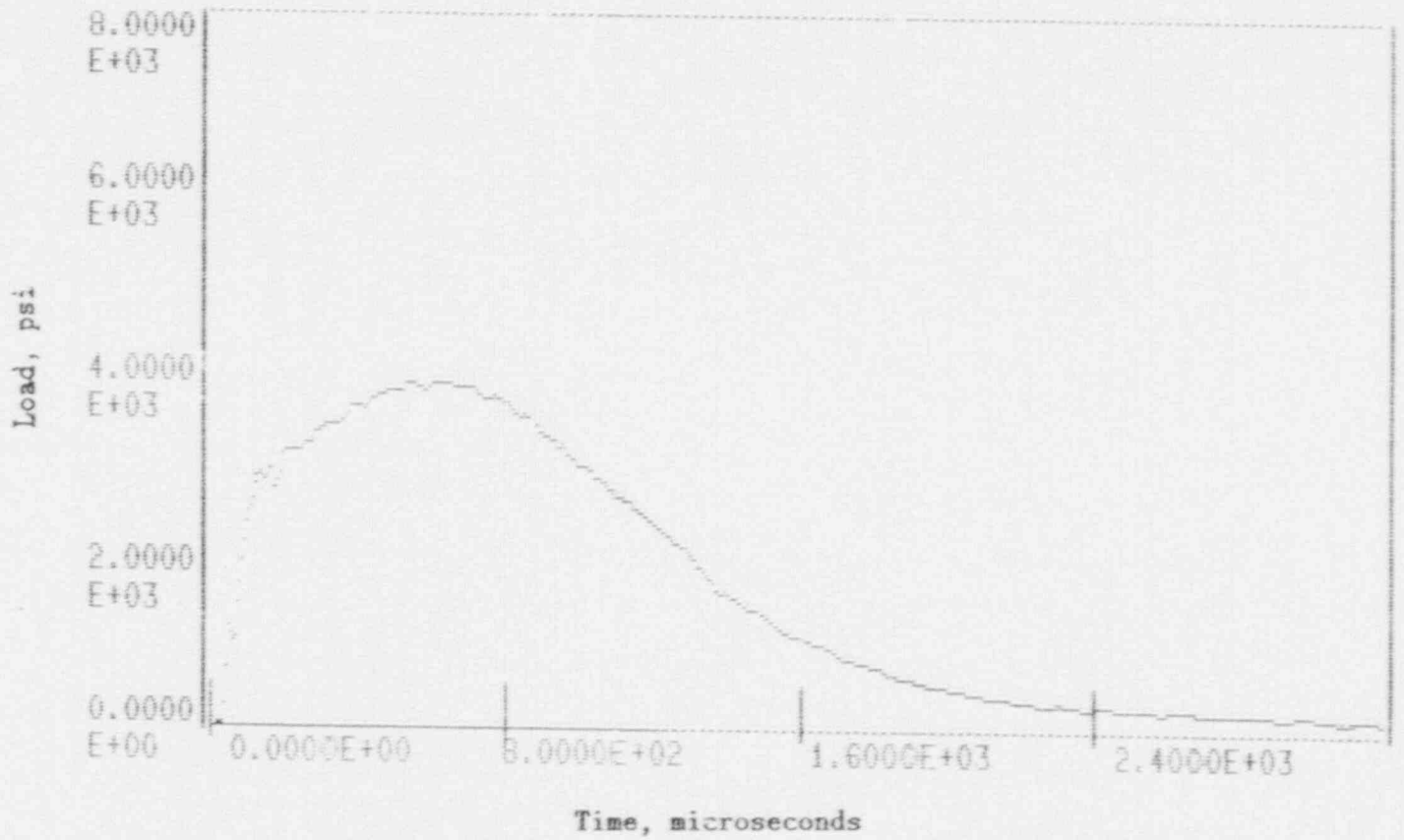

Figure A-29. Load-time record for Specimen PT47.

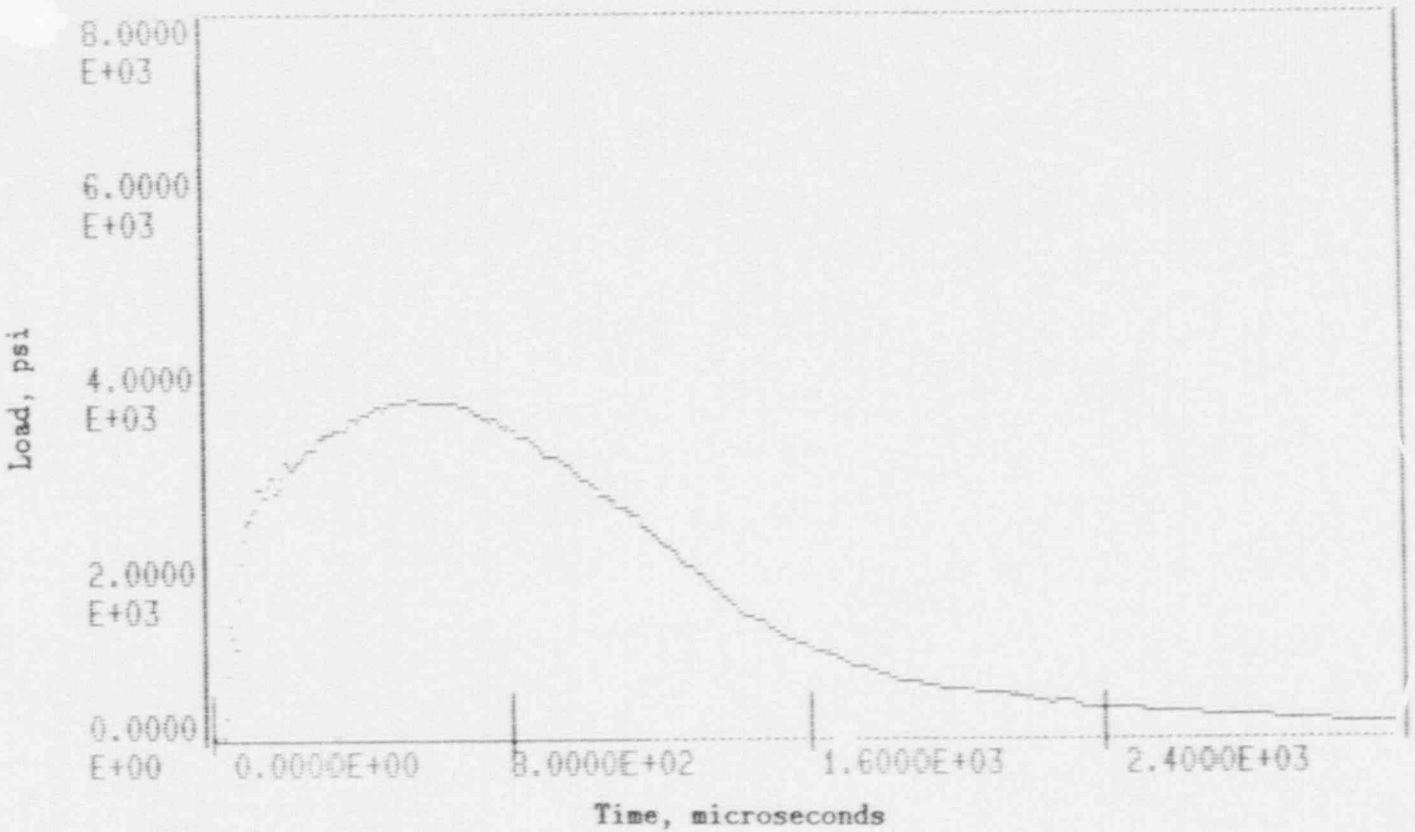

Figure A-30. Load-time record for Specimen PT57.

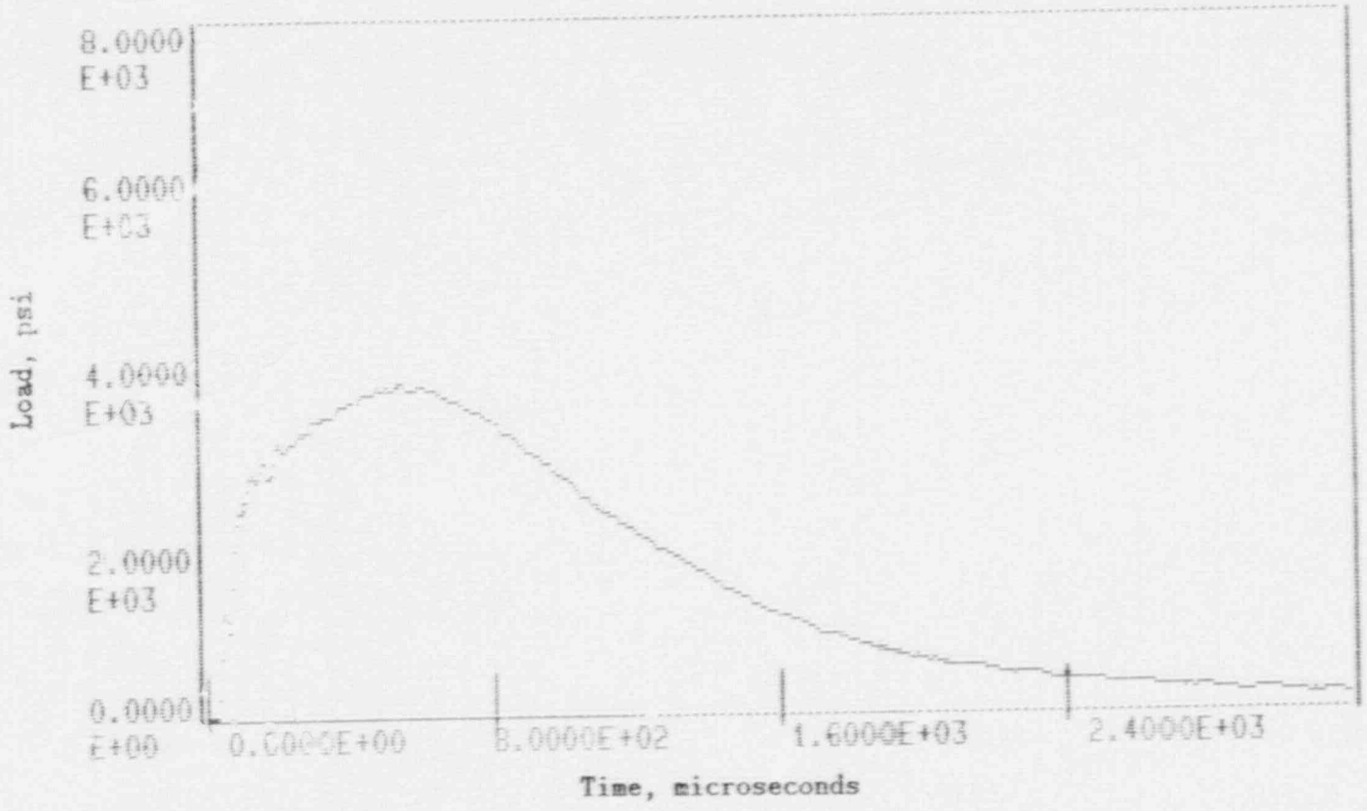

Figure A-31. Load-time record for Specimen PT50.

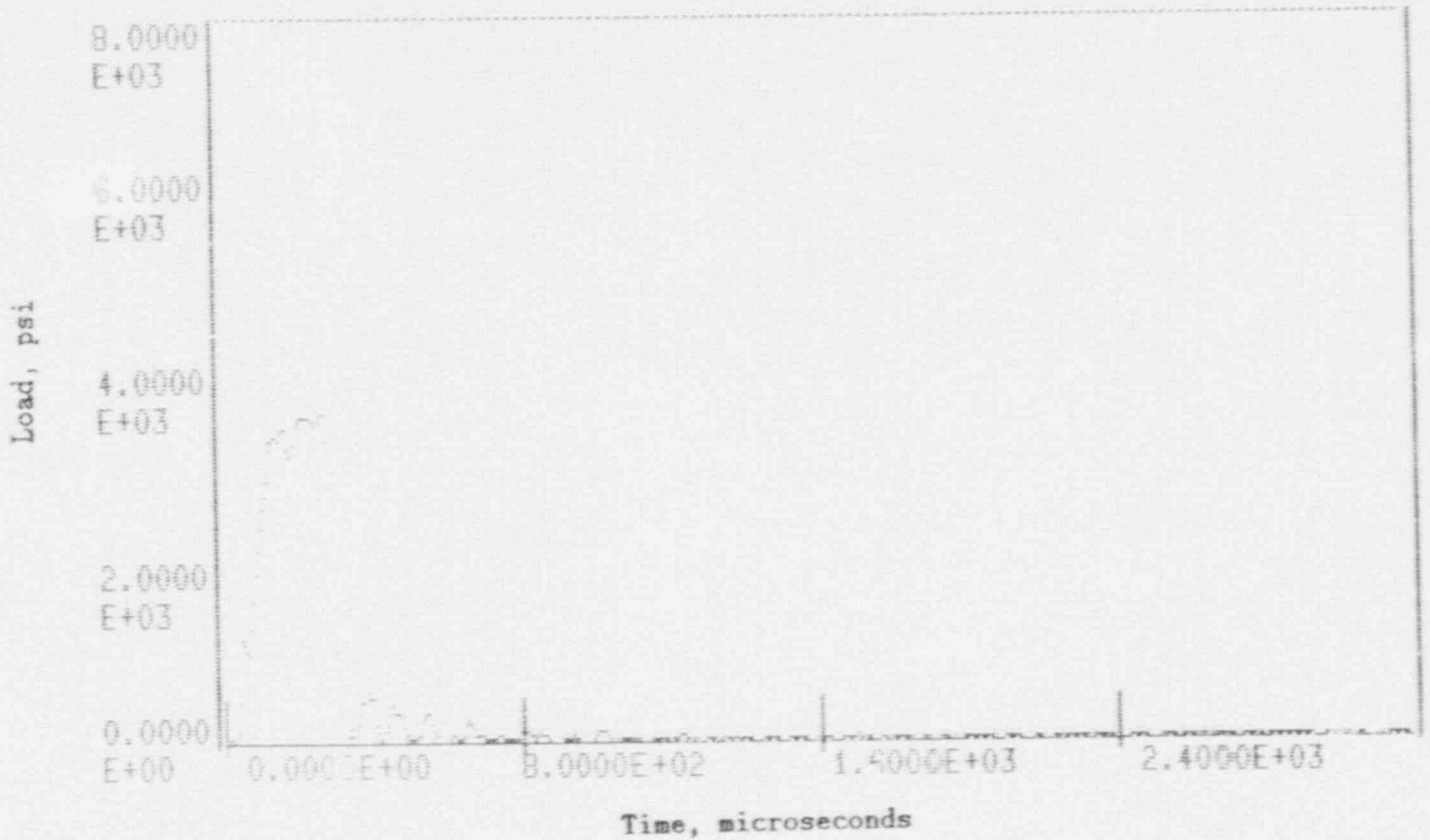

Figure A-32. Load-time record for Specimen PW58.

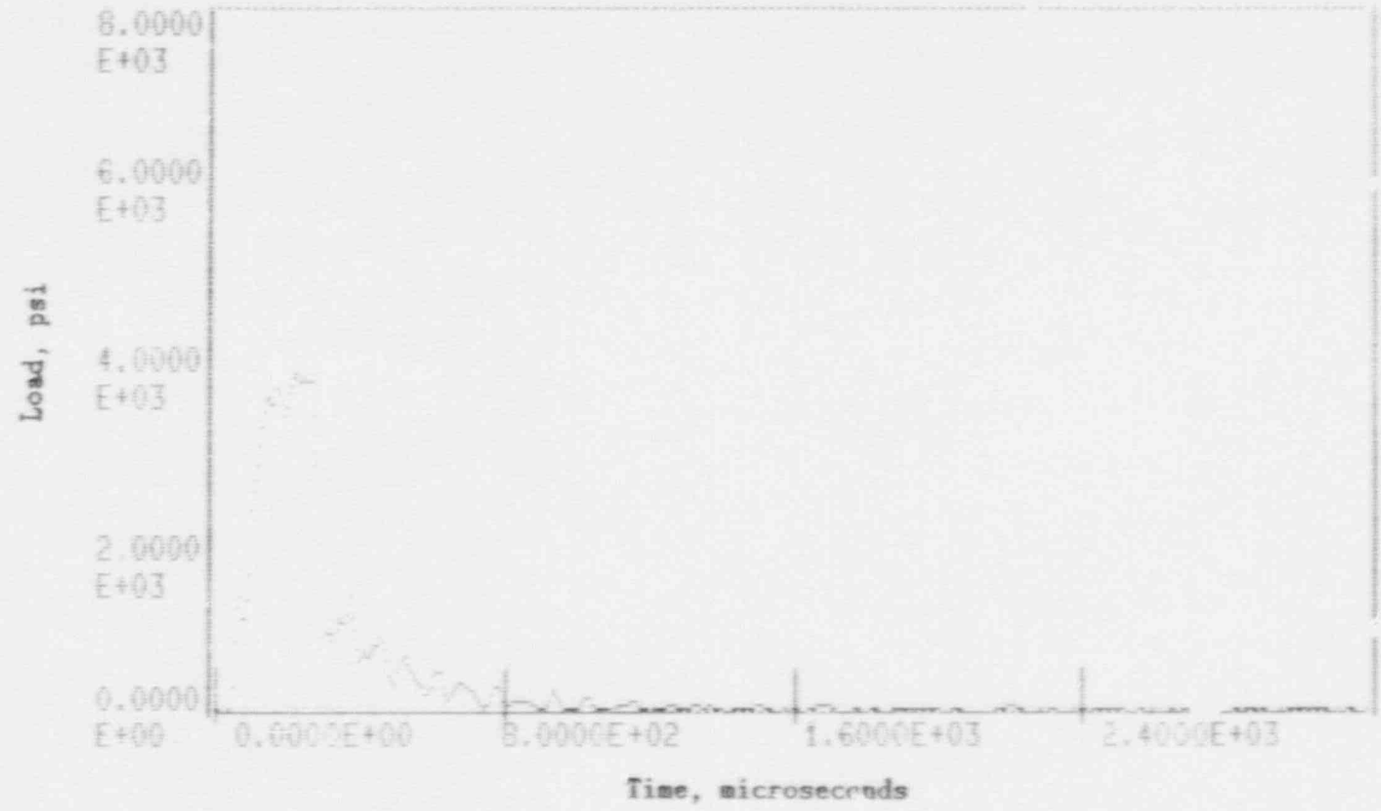

Figure A-33. Load-time record for Specimen PW57.

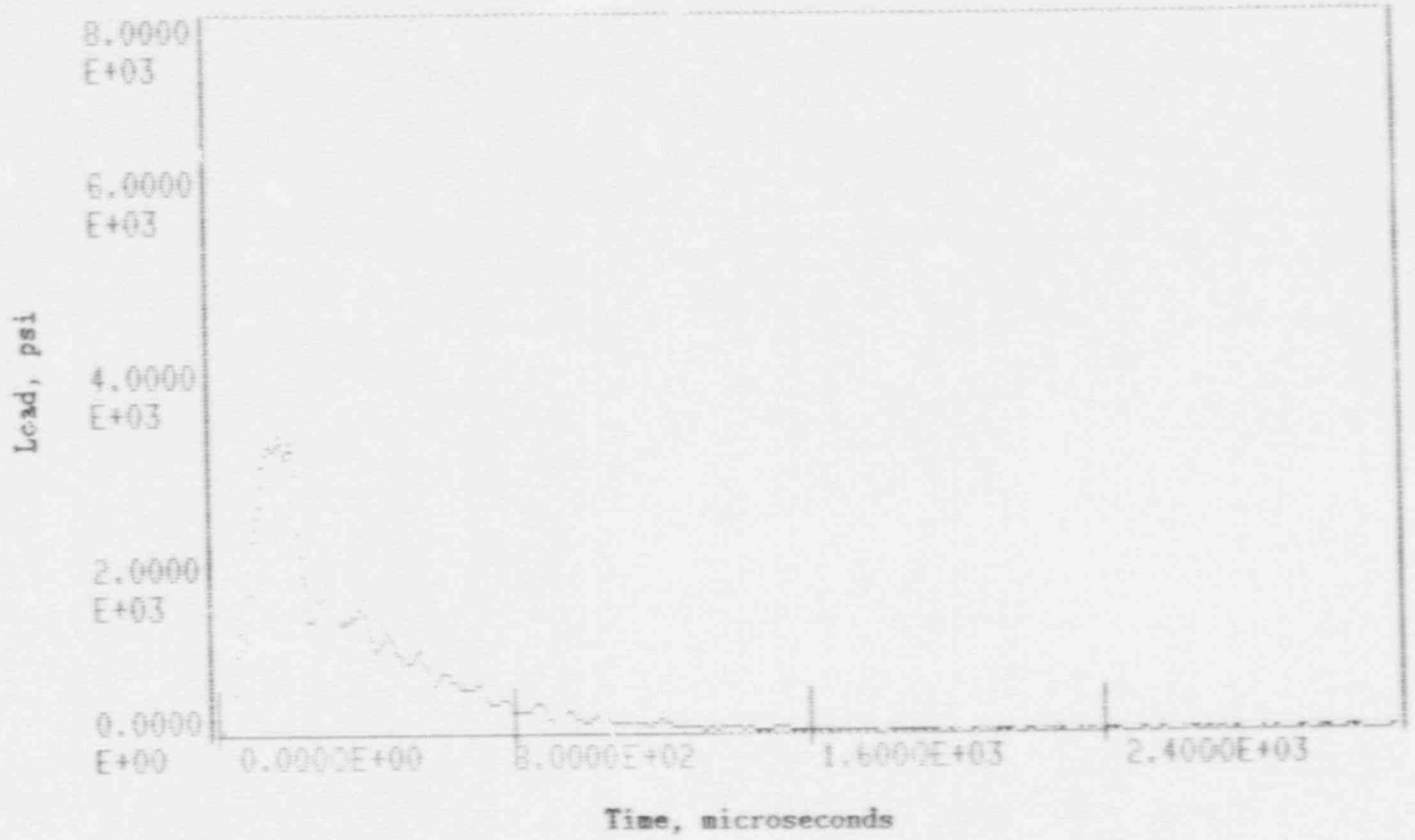

Figure A-34. Load-time record for Specimen PW55.

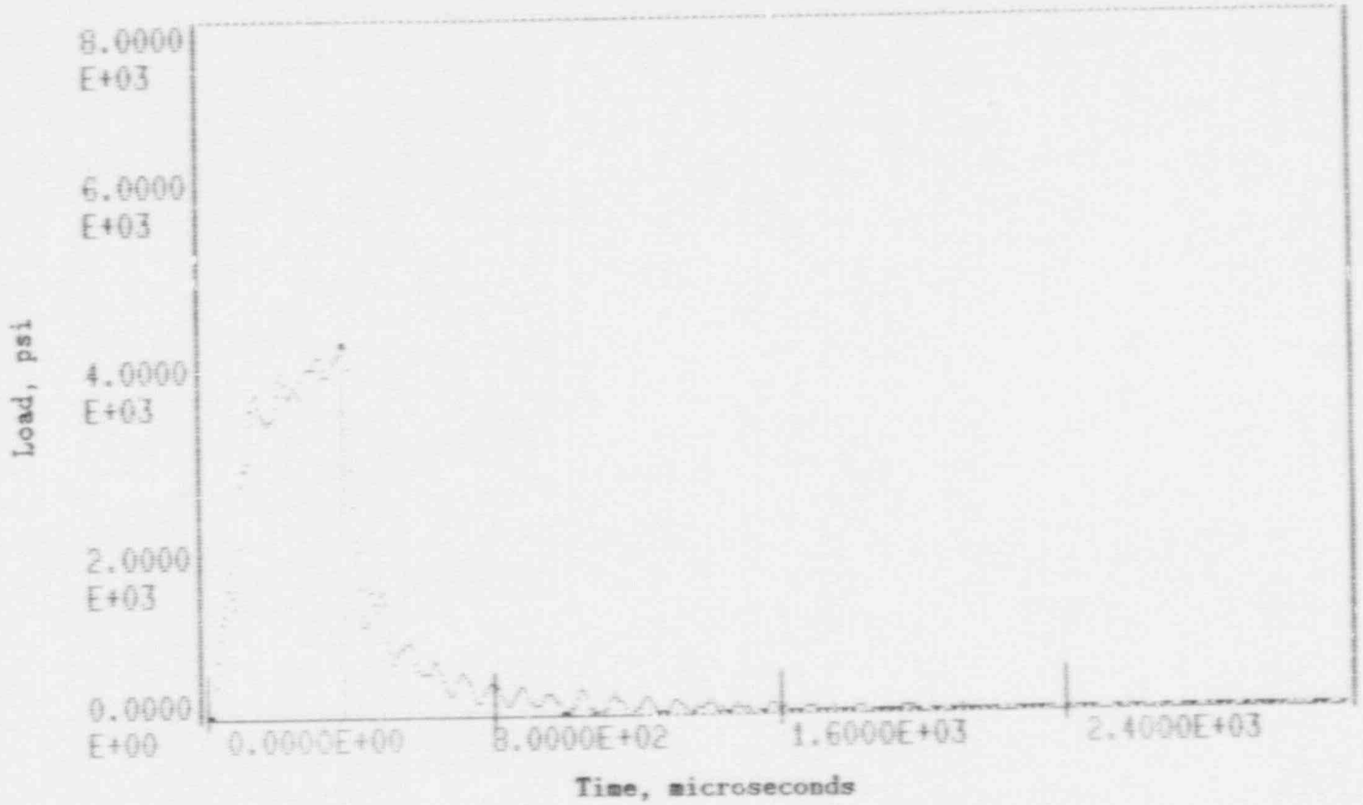

Figure A-35. Load-time record for Specimen PW60.

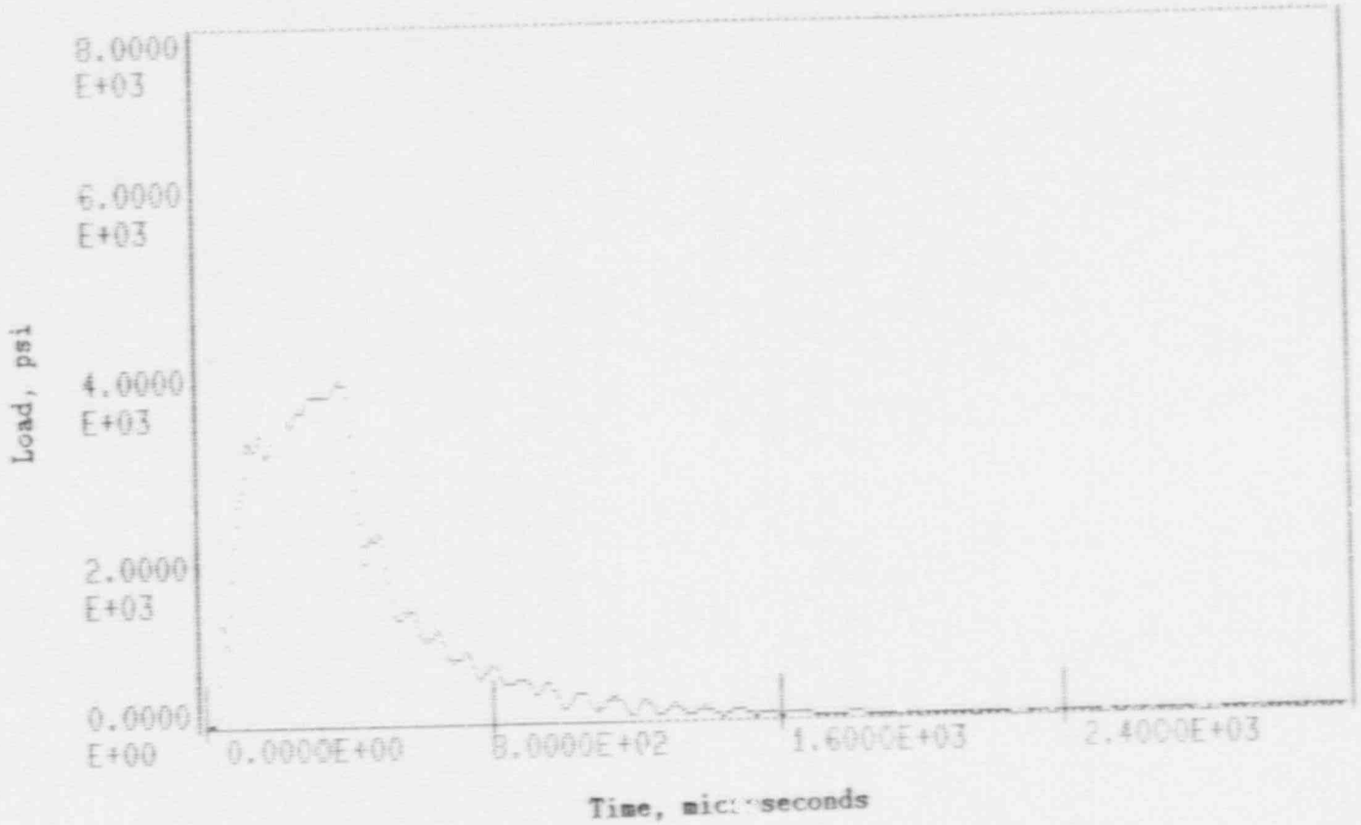

Figure A-36. Load-time record for Specimen PW49.

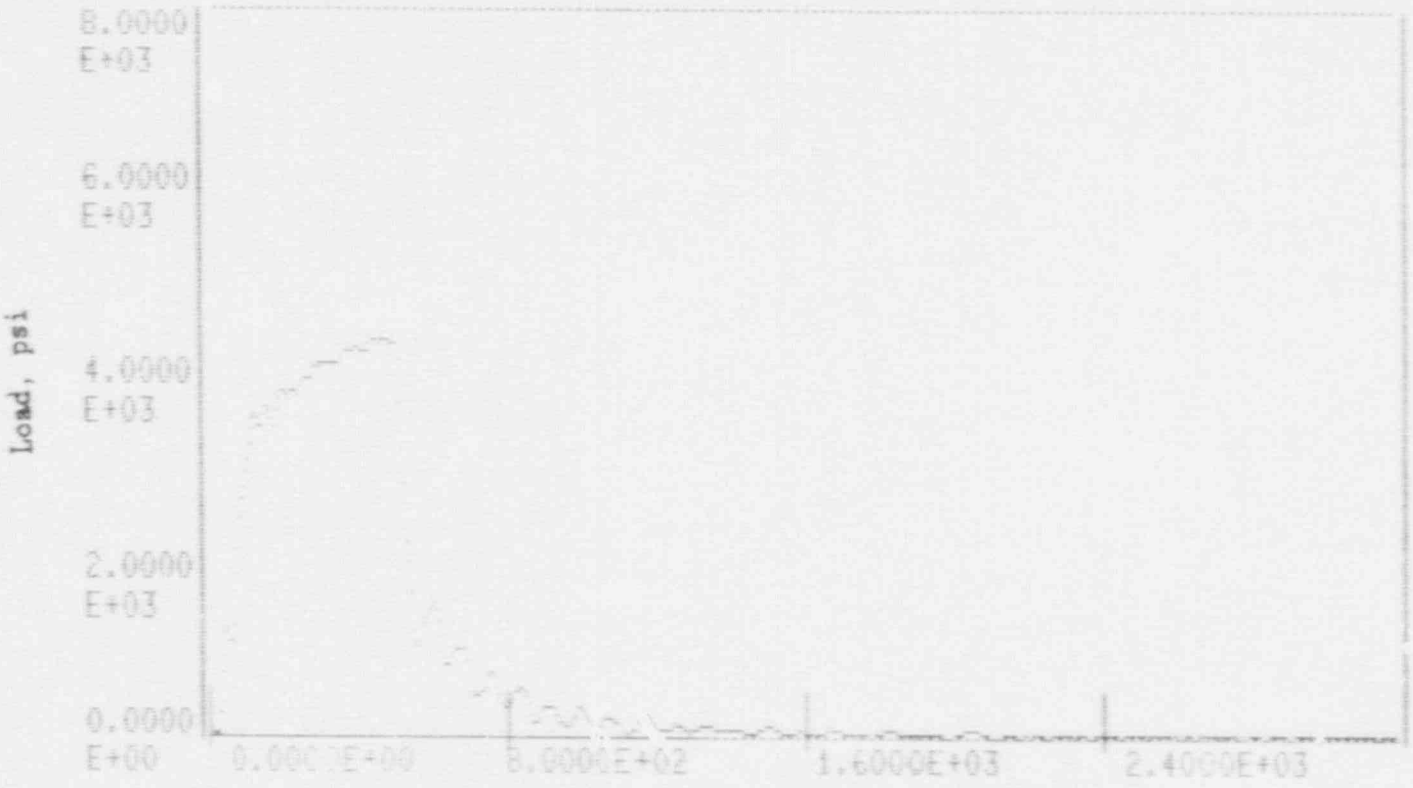

Figure A-37. Load-time record for Specimen PW-0.

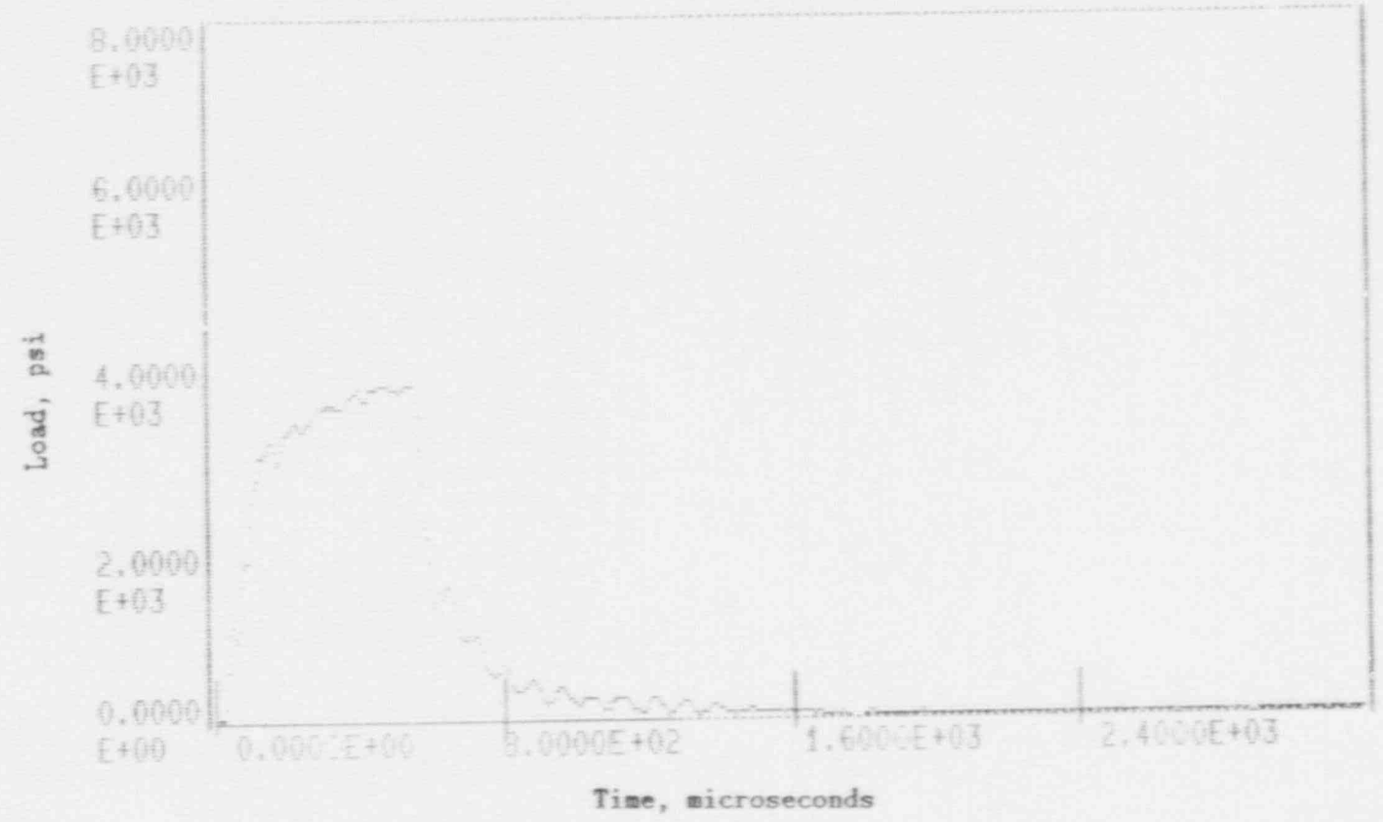

Figure A-38. Load-time record for Specimen PW59.

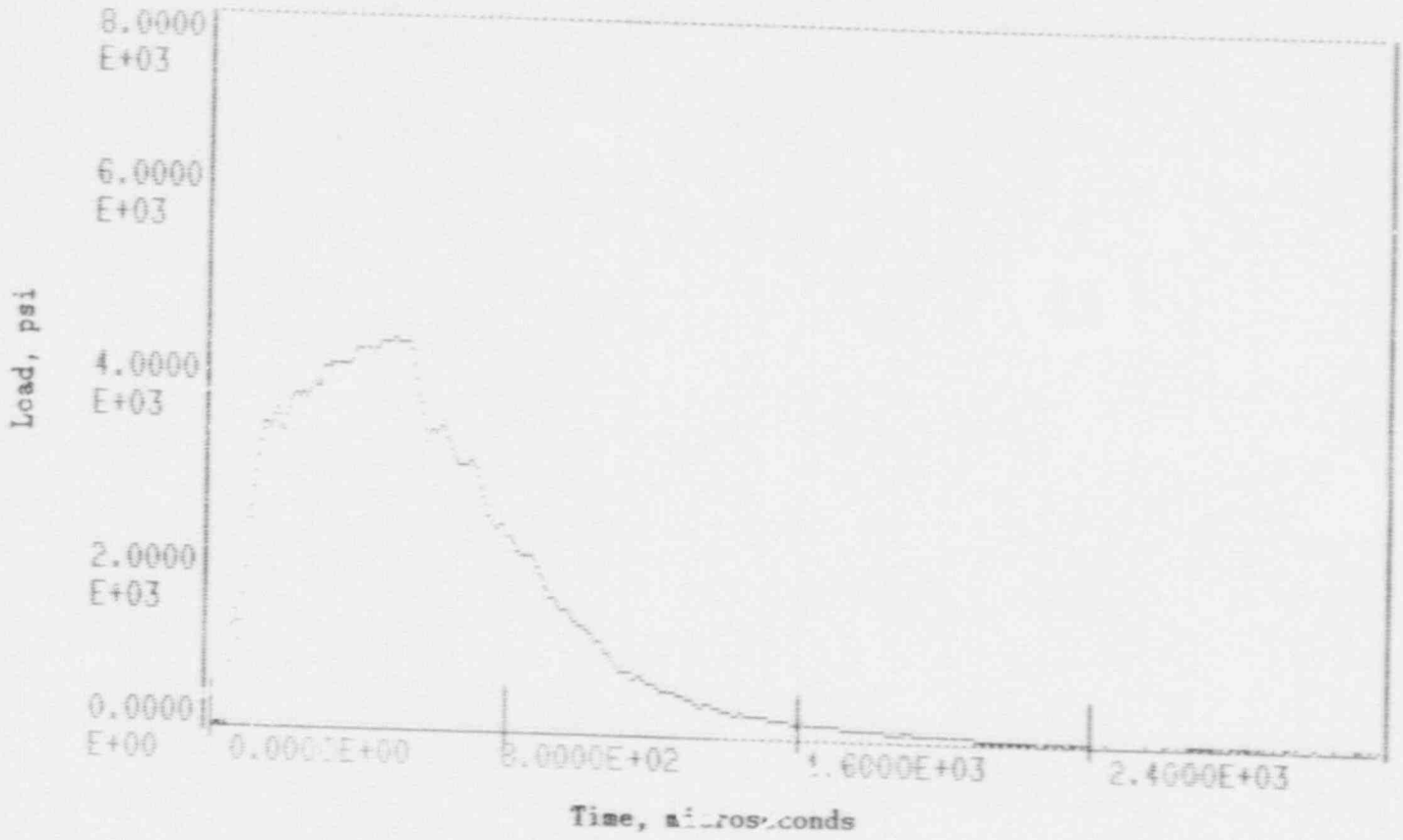

Figure A-39. Load-time record for Specimen PW47.

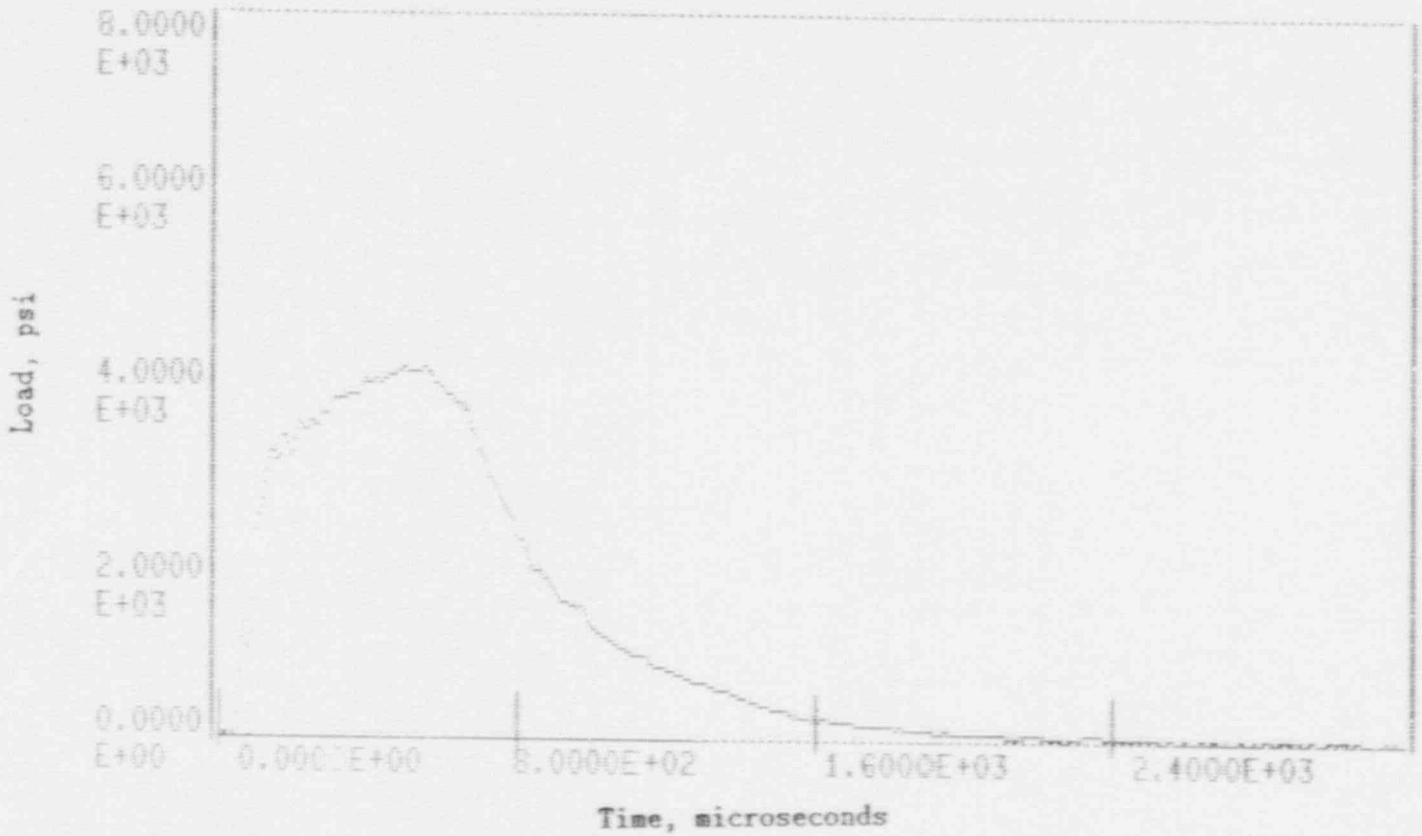

Figure A-40. Load-time record for Specimen PW56.

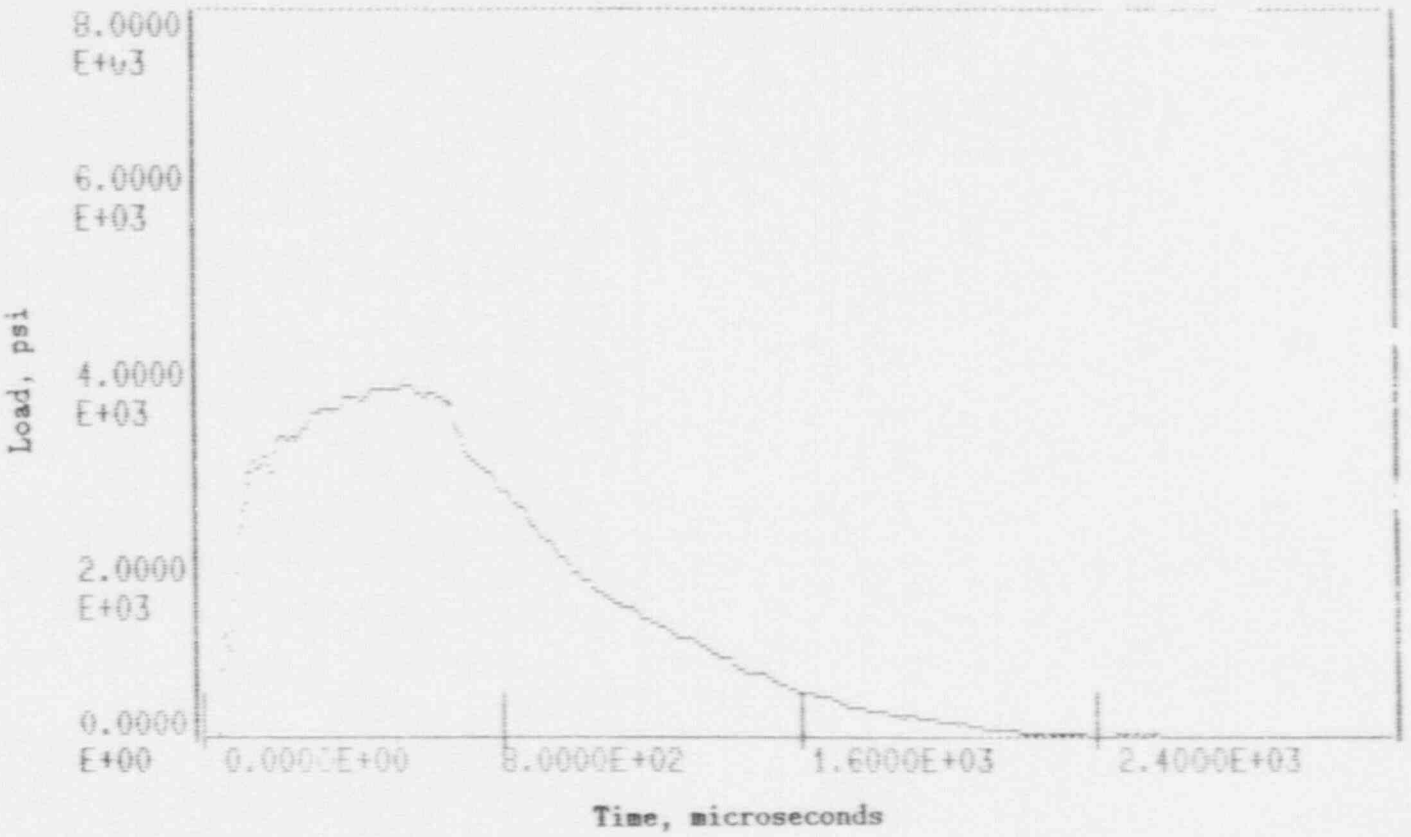

Figure A-41. Load-time record for Specimen P#46.

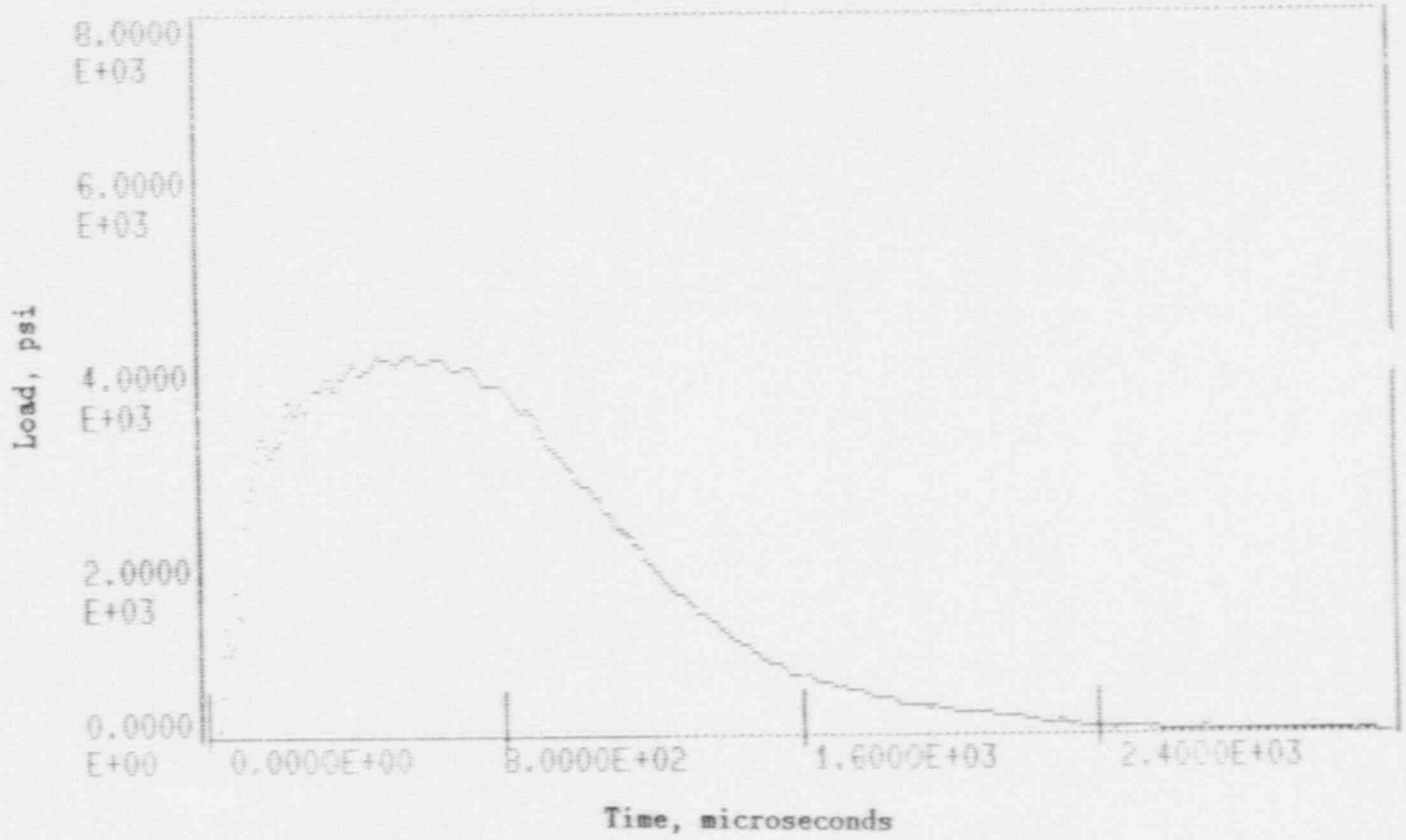

Figure A-42. Load-time record for Specimen PW53.

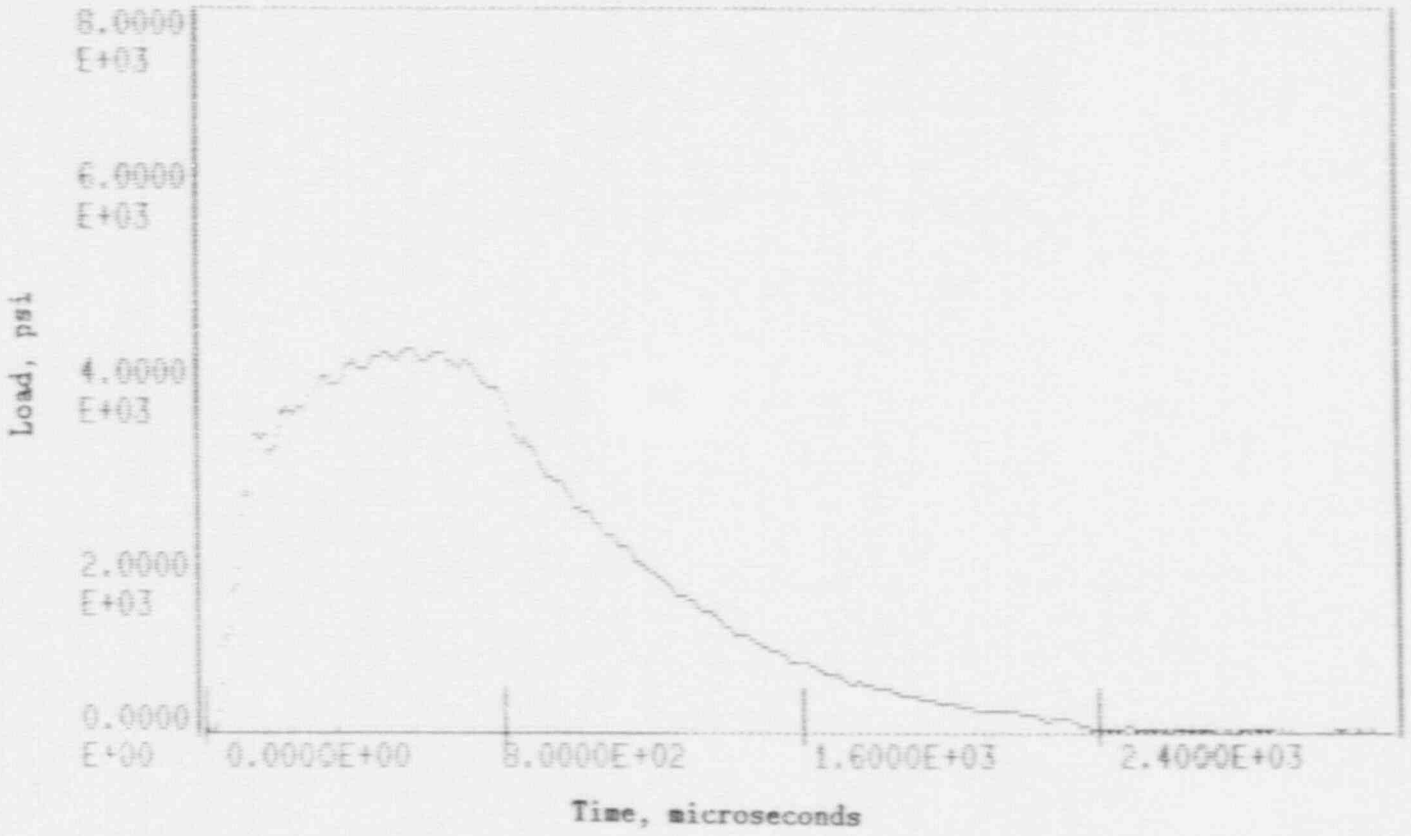

Figure A-43. Load-time record for Specimen PW51.

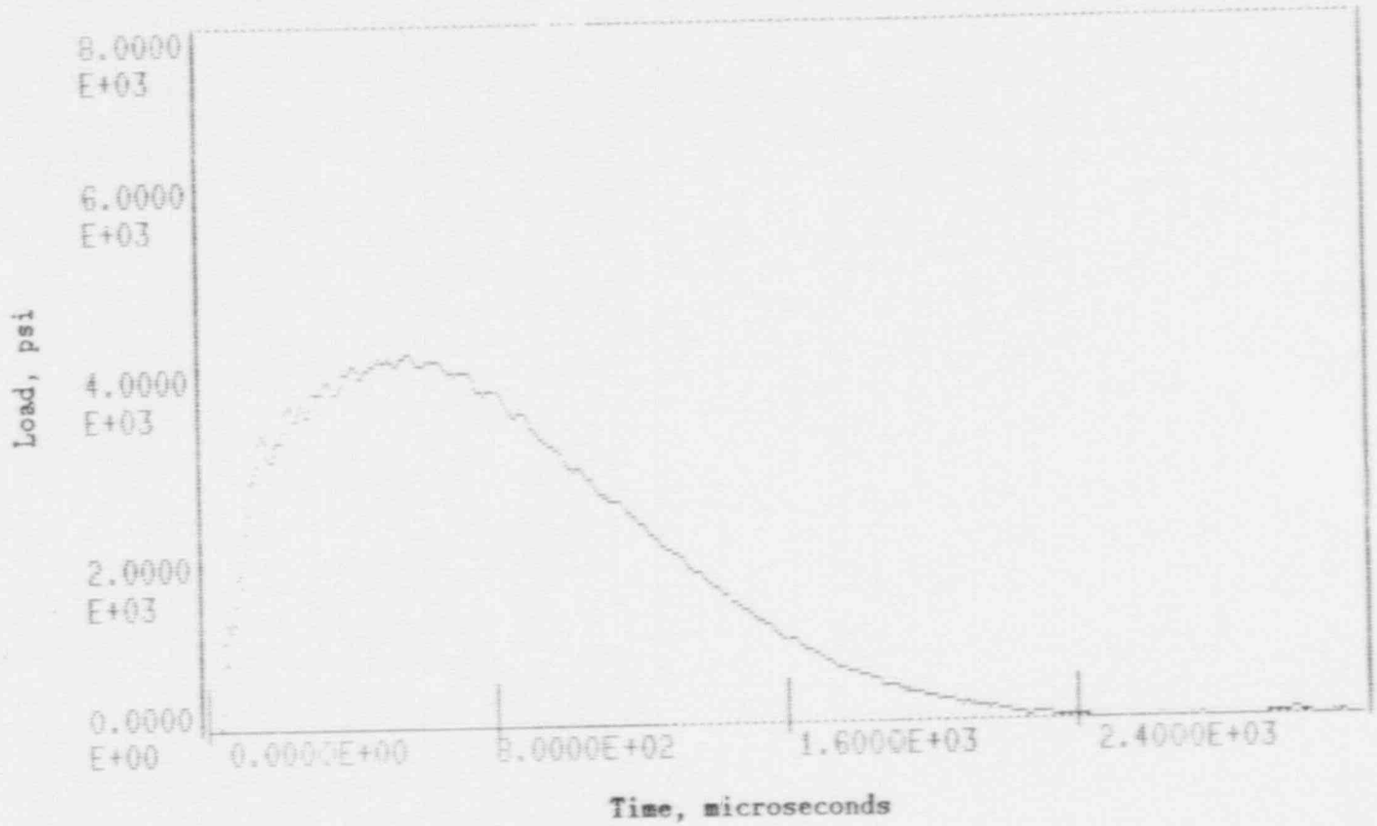

Figure A-44. Load-time record for Specimen PW52.

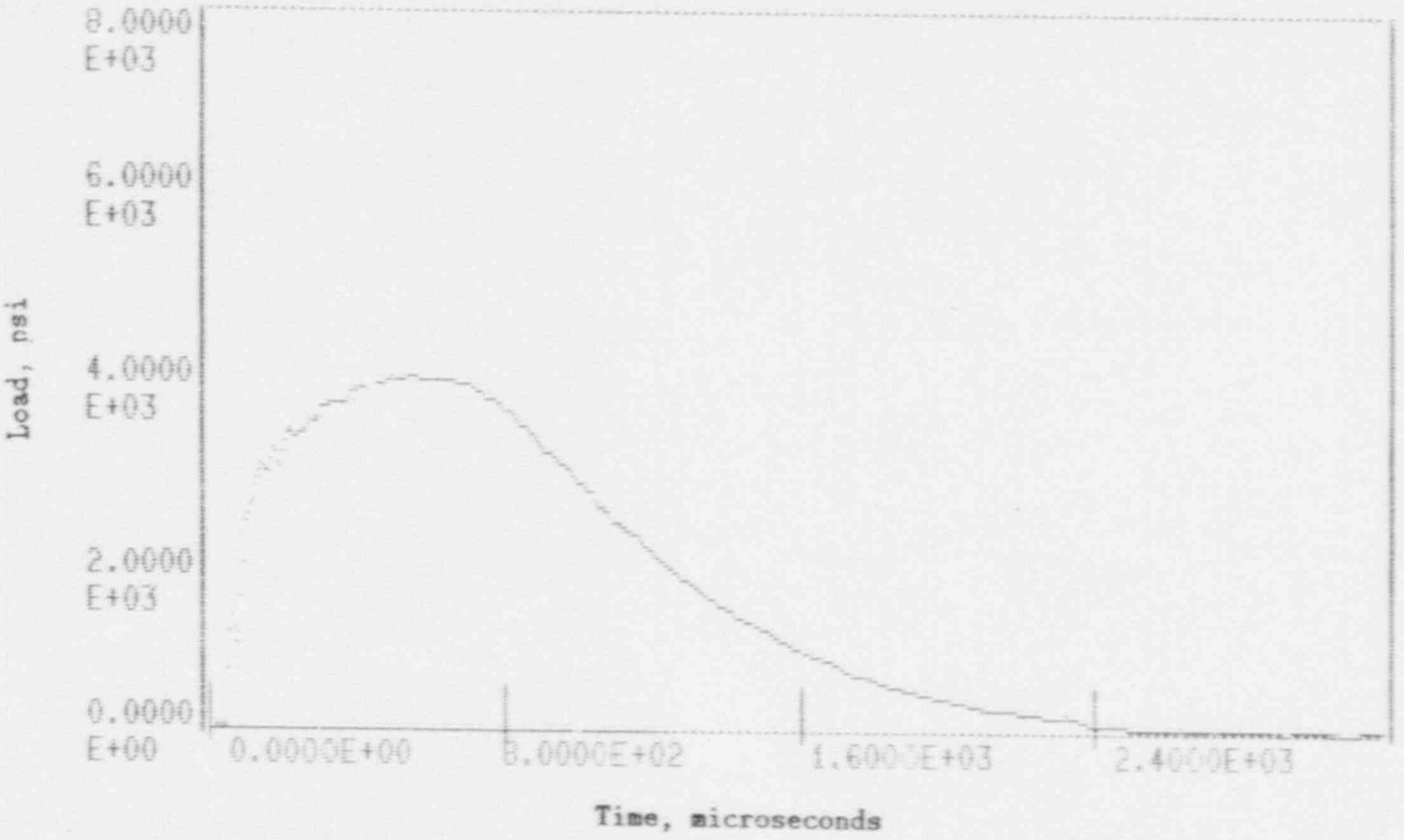

Figure A-45. Load-time record for Specimen PW54.

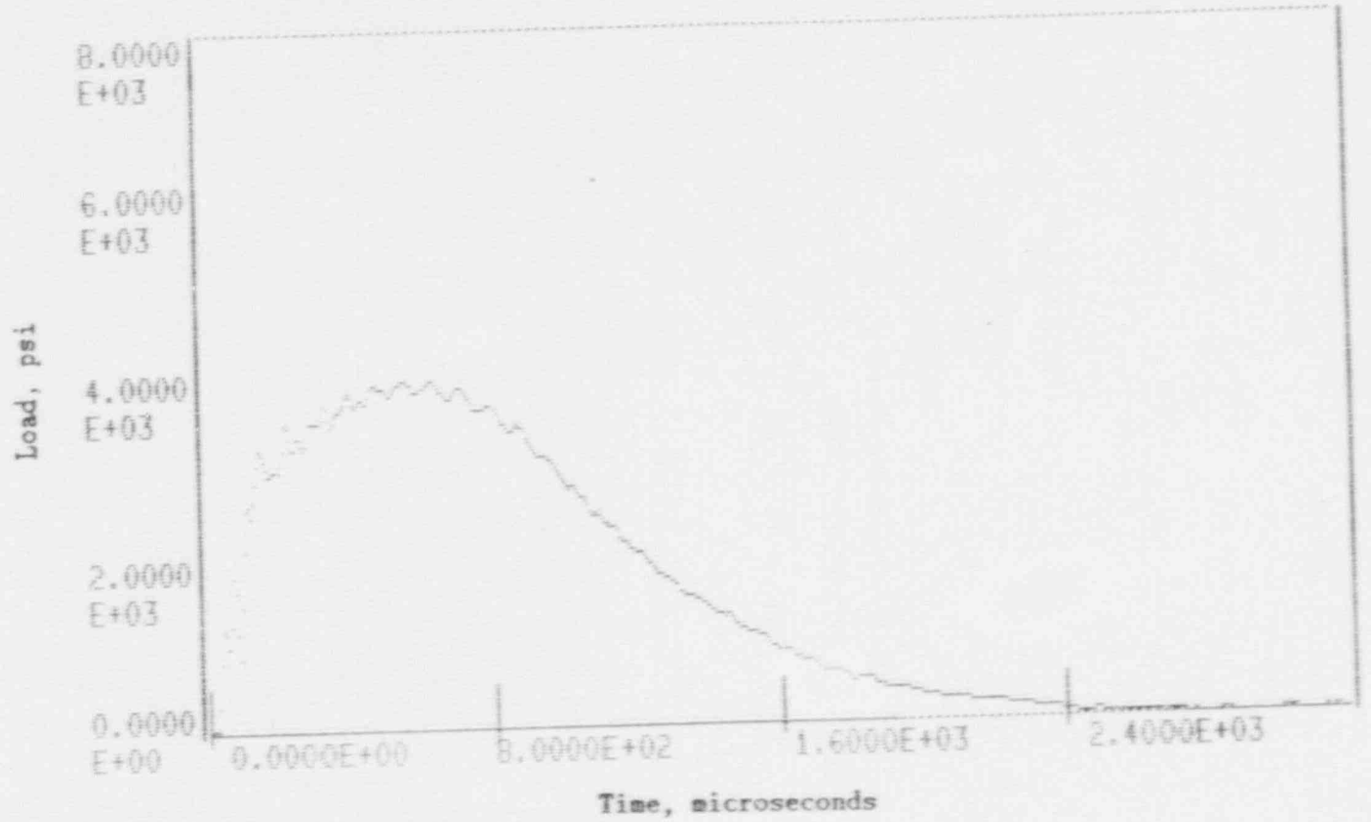

Figure A-46. Load-time record for Specimen PW48

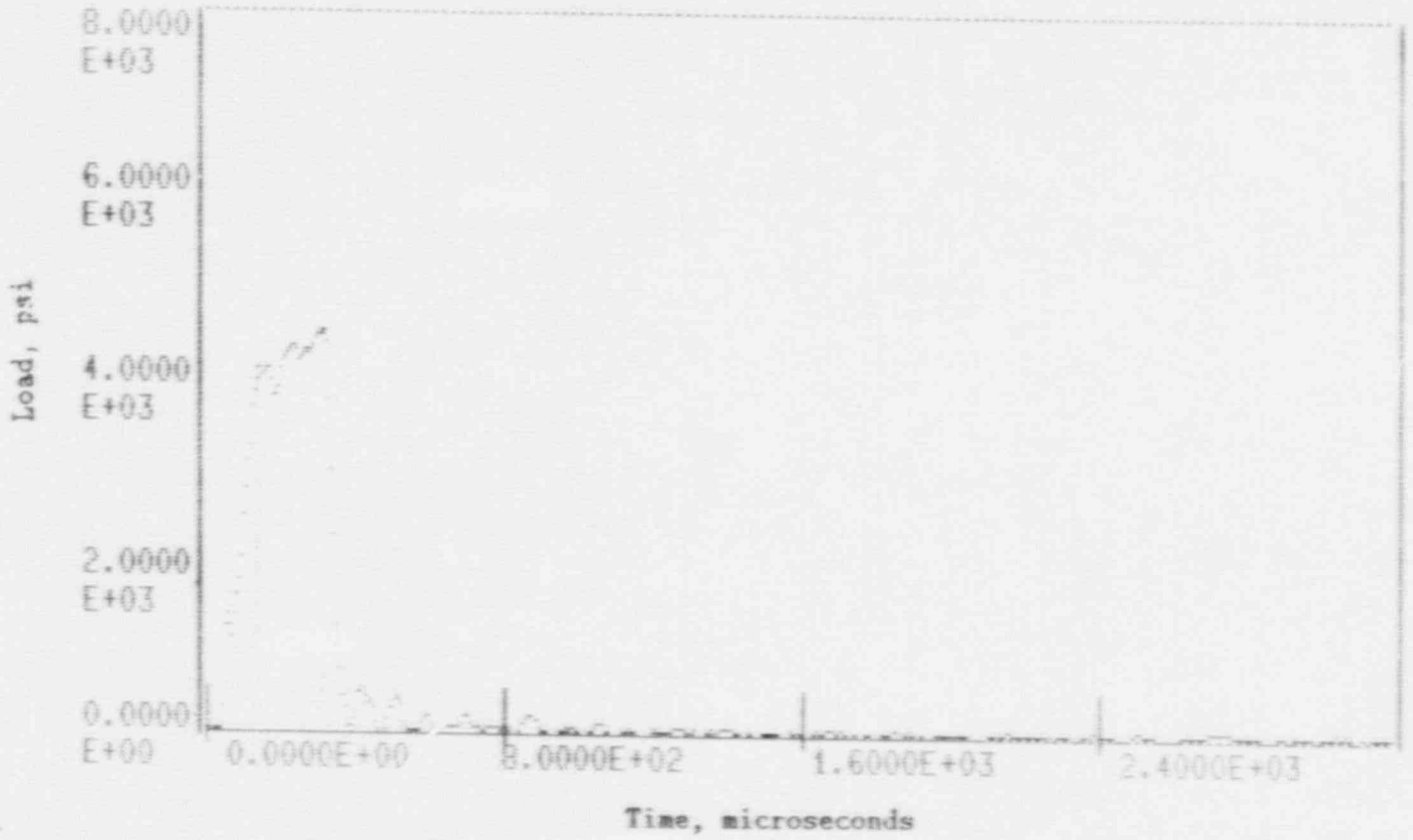

Figure A-47. Load-time record for Specimen PH59.

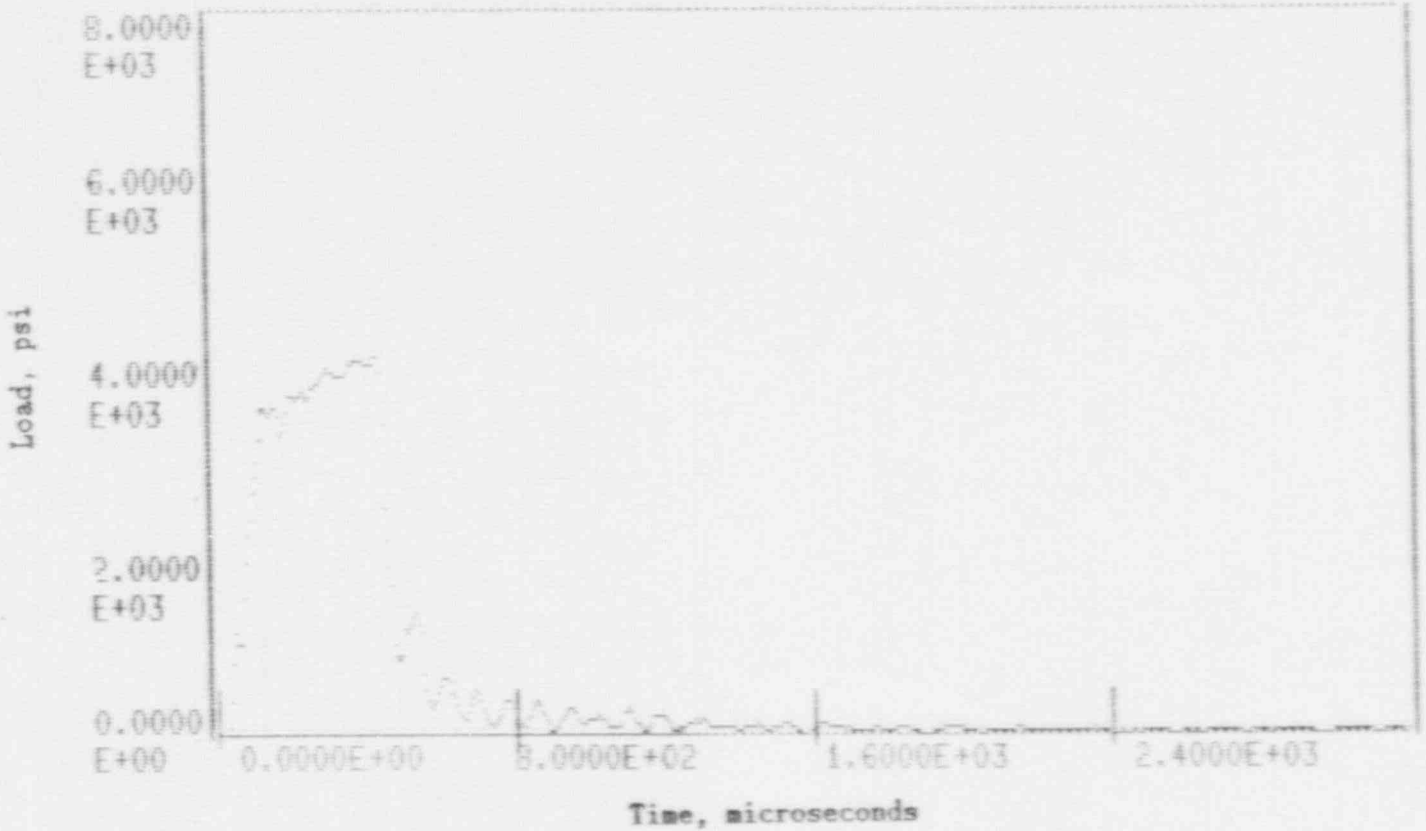

Figure A-48. Load-time record for Specimen PH53.

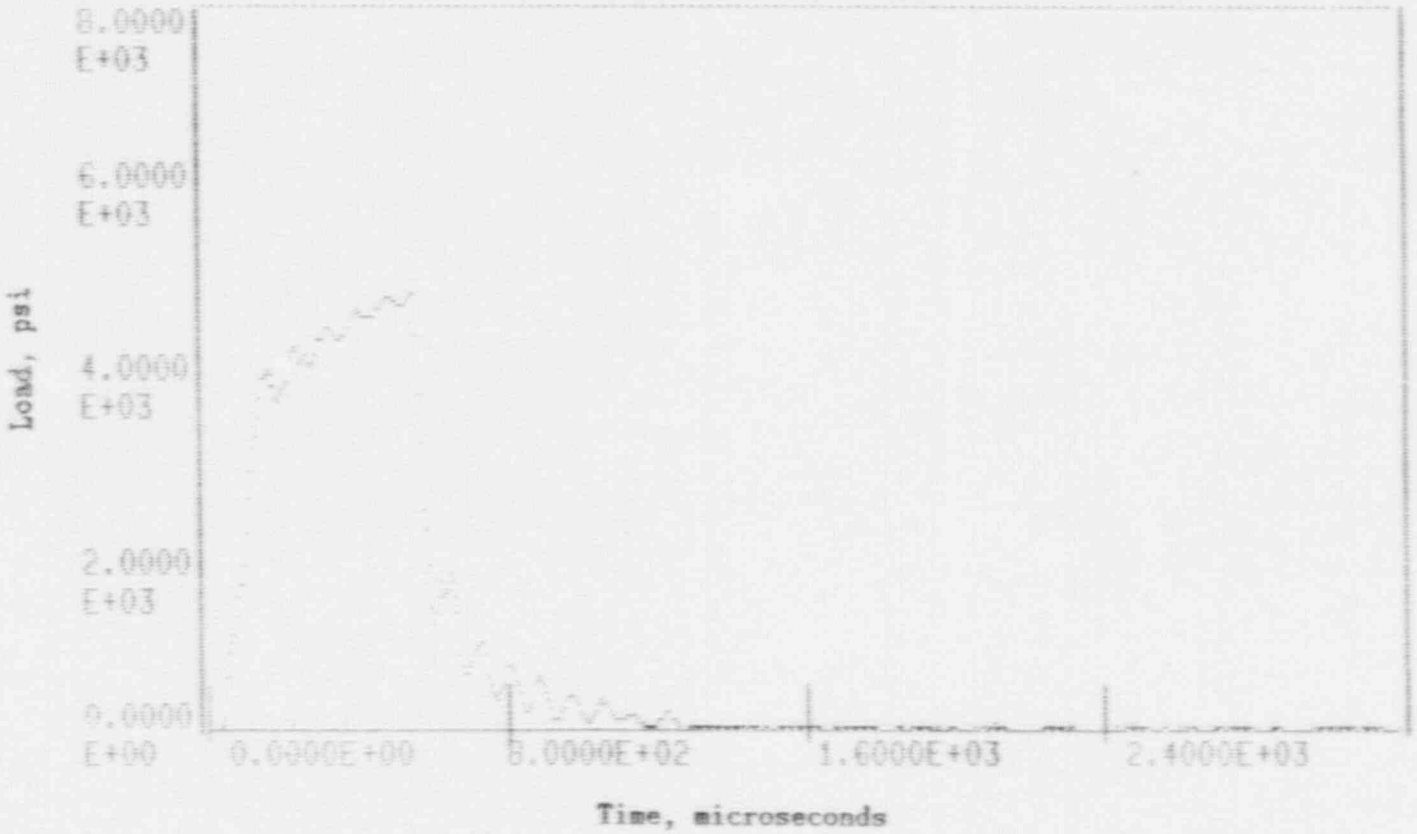

Figure A-49. Load-time record for Specimen PH51

No record - computer malfunction

Figure A-50. Load-time record for Specimen PH55.

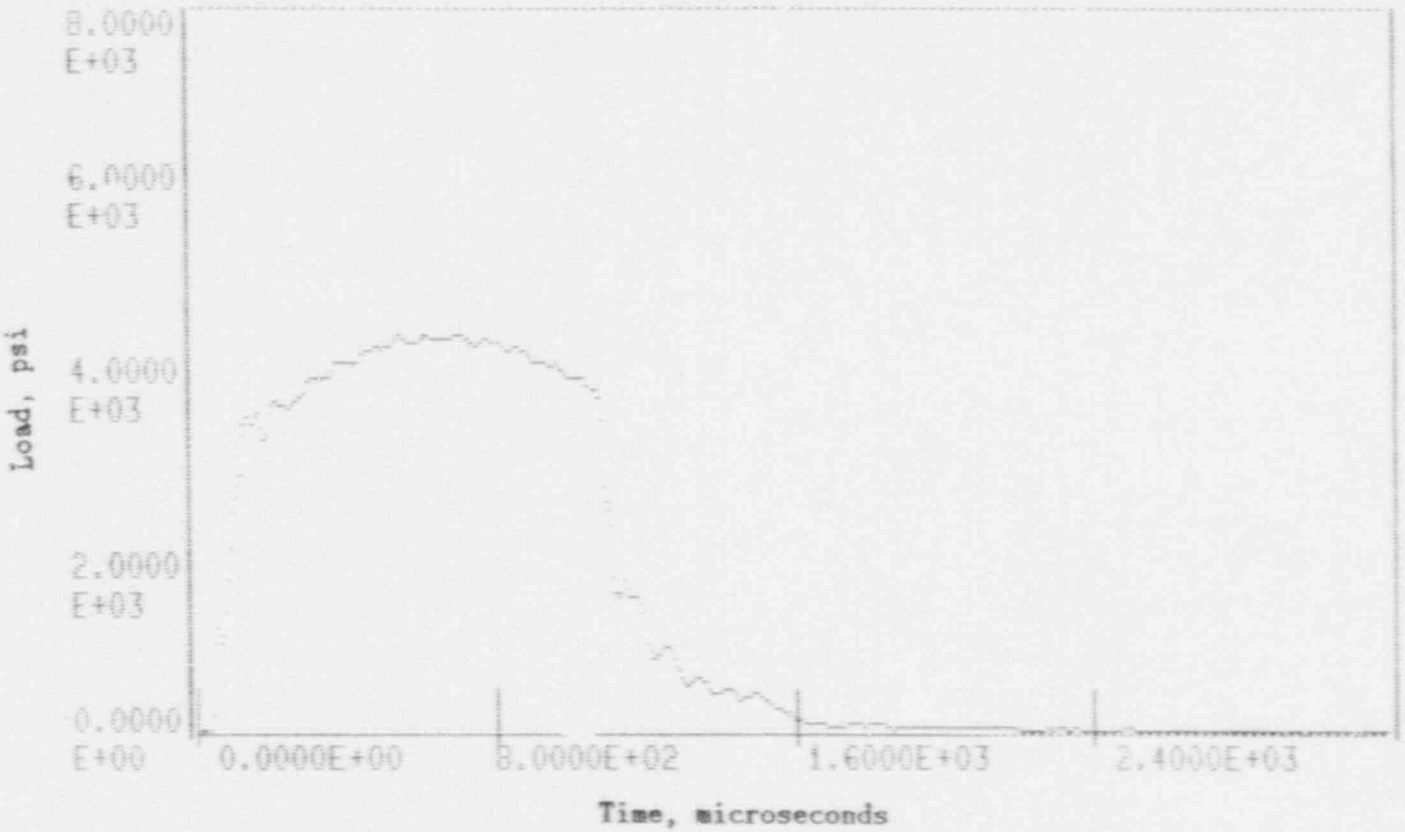

Figure A-51. Load-time record for Specimen PH54.

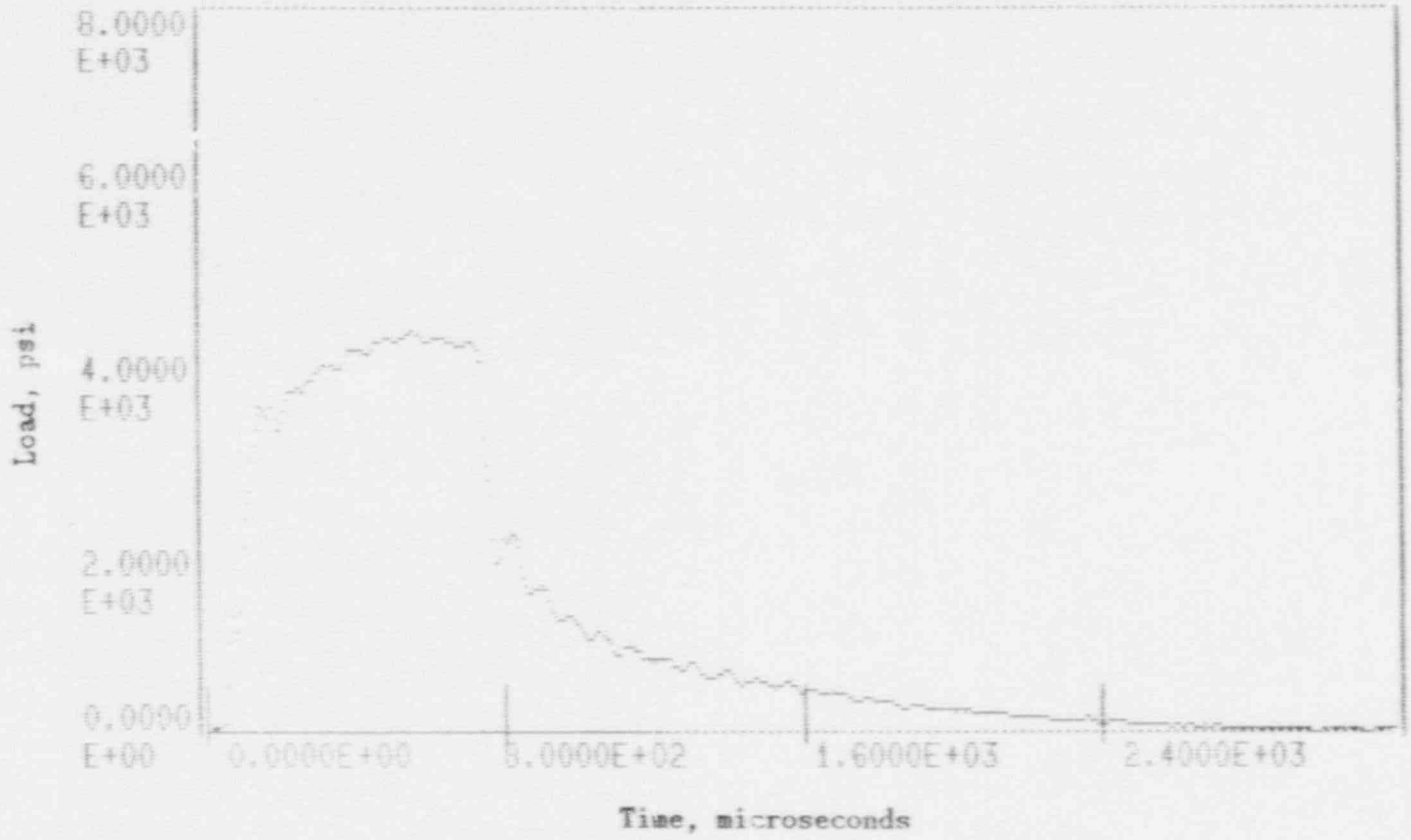

Figure A-52. Load-time record for Specimen PH52.

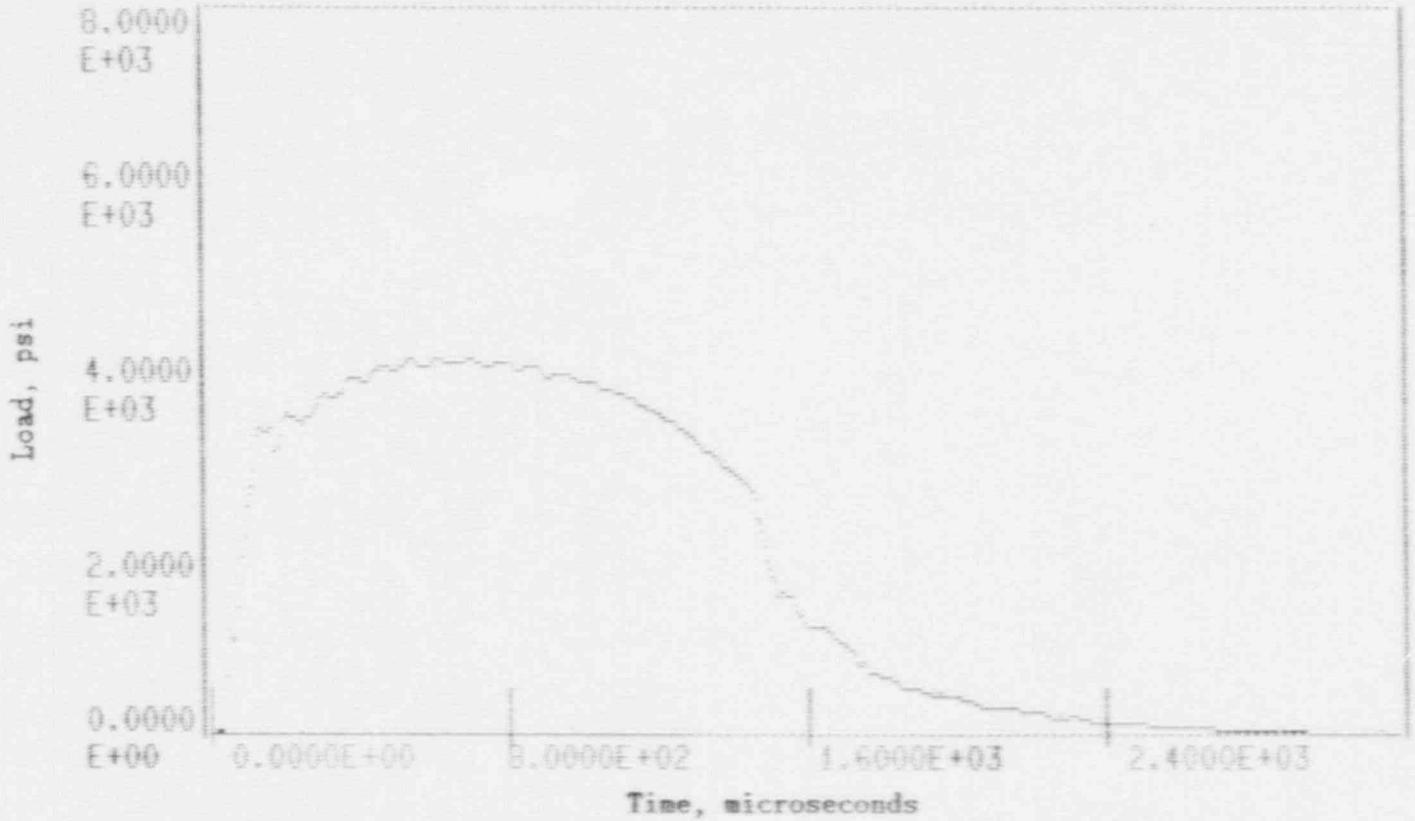

Figure A-53. Load-time rec[illegible] Spe[illegible]

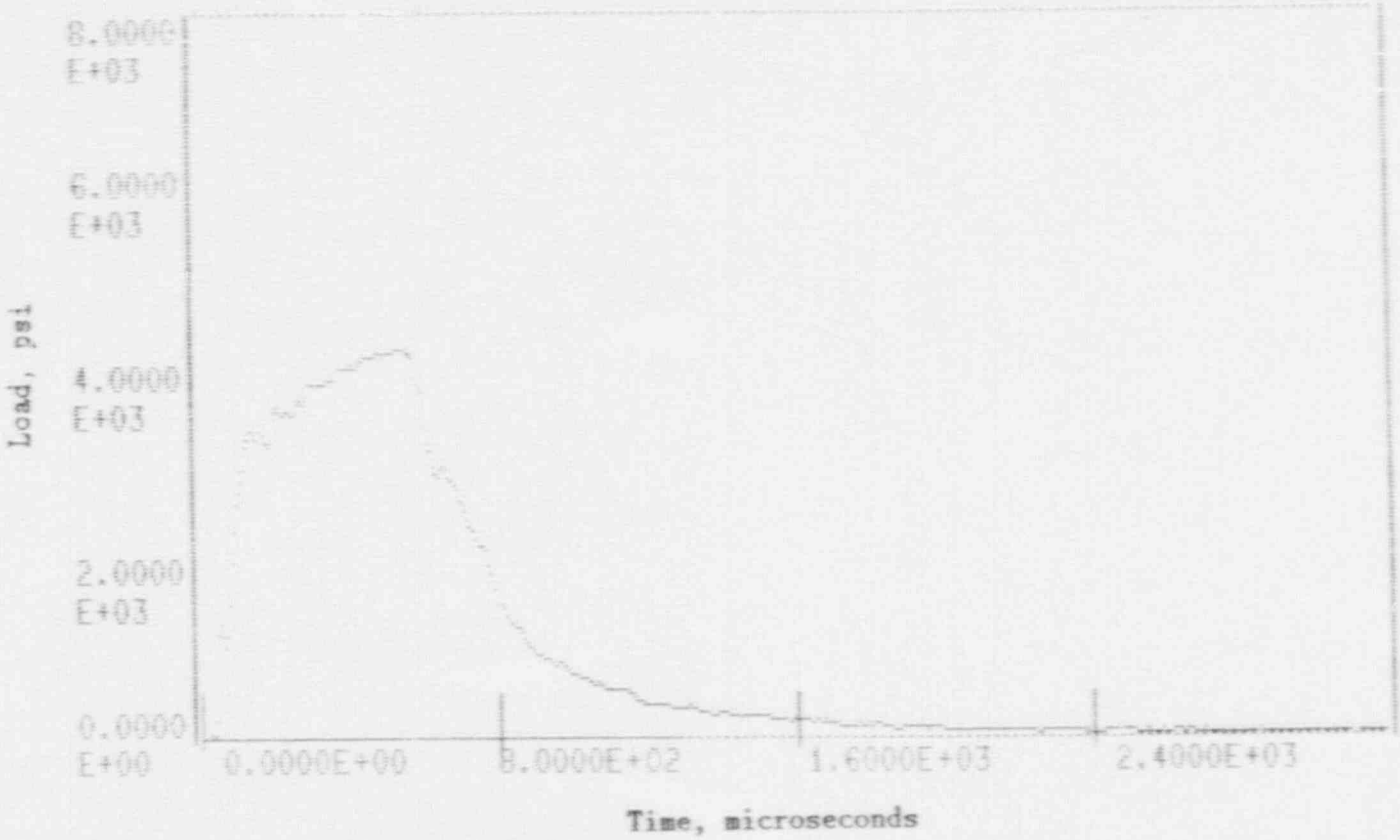

Figure A-54. Load-time record for Specimen PH57.

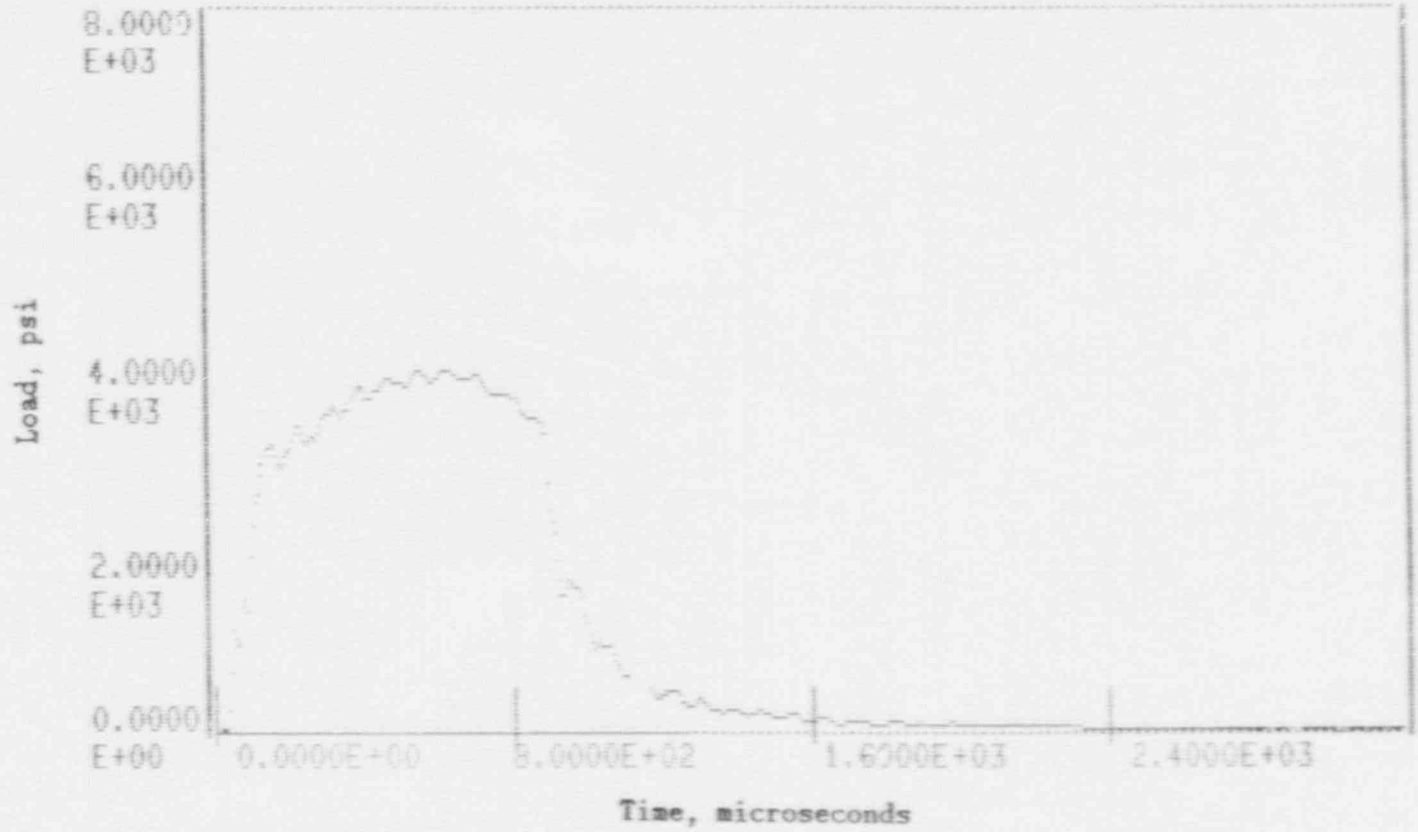

Figure A-55. Load-time record for Specimen PH58.

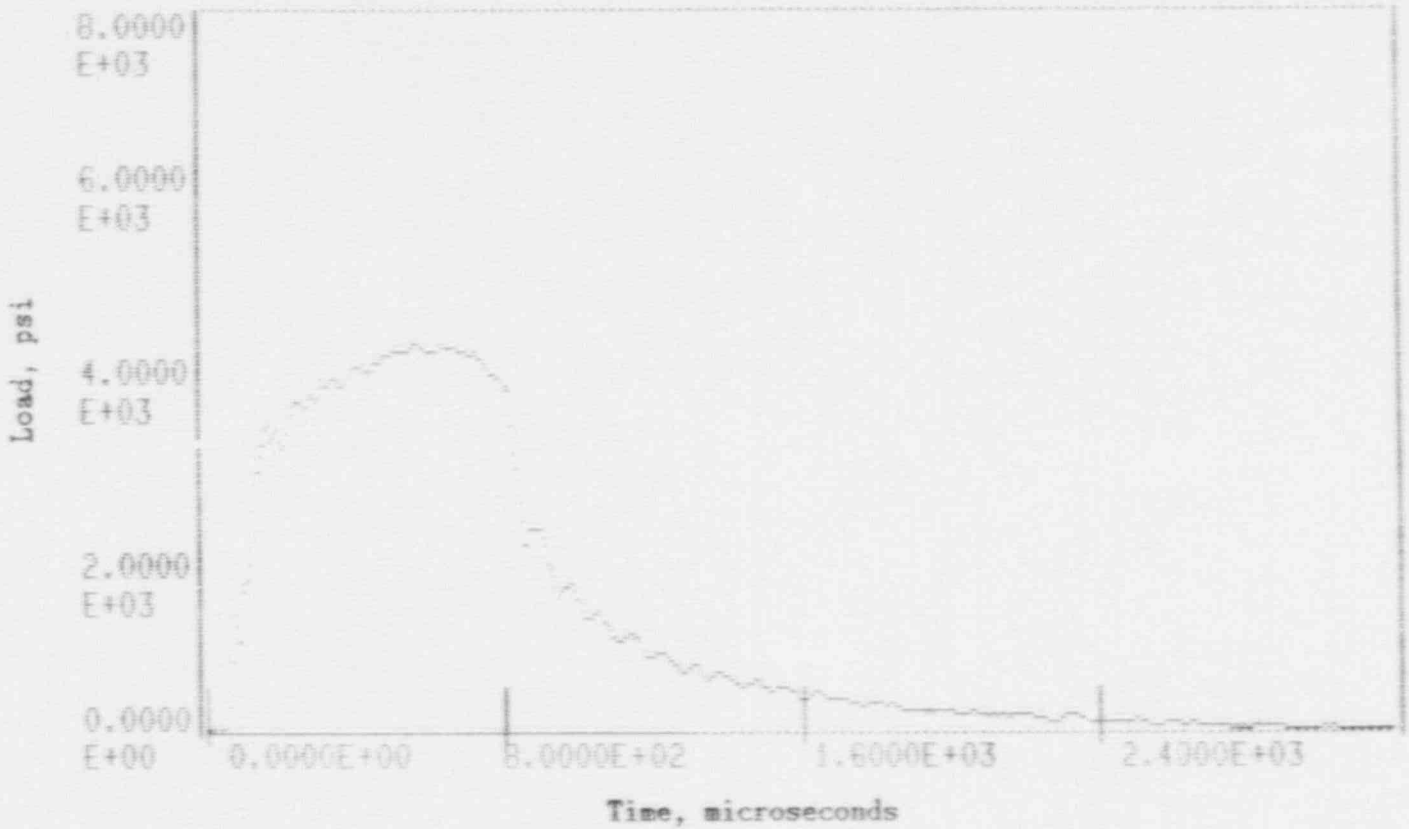

Figure A-56. Load-time record for Specimen PH60.

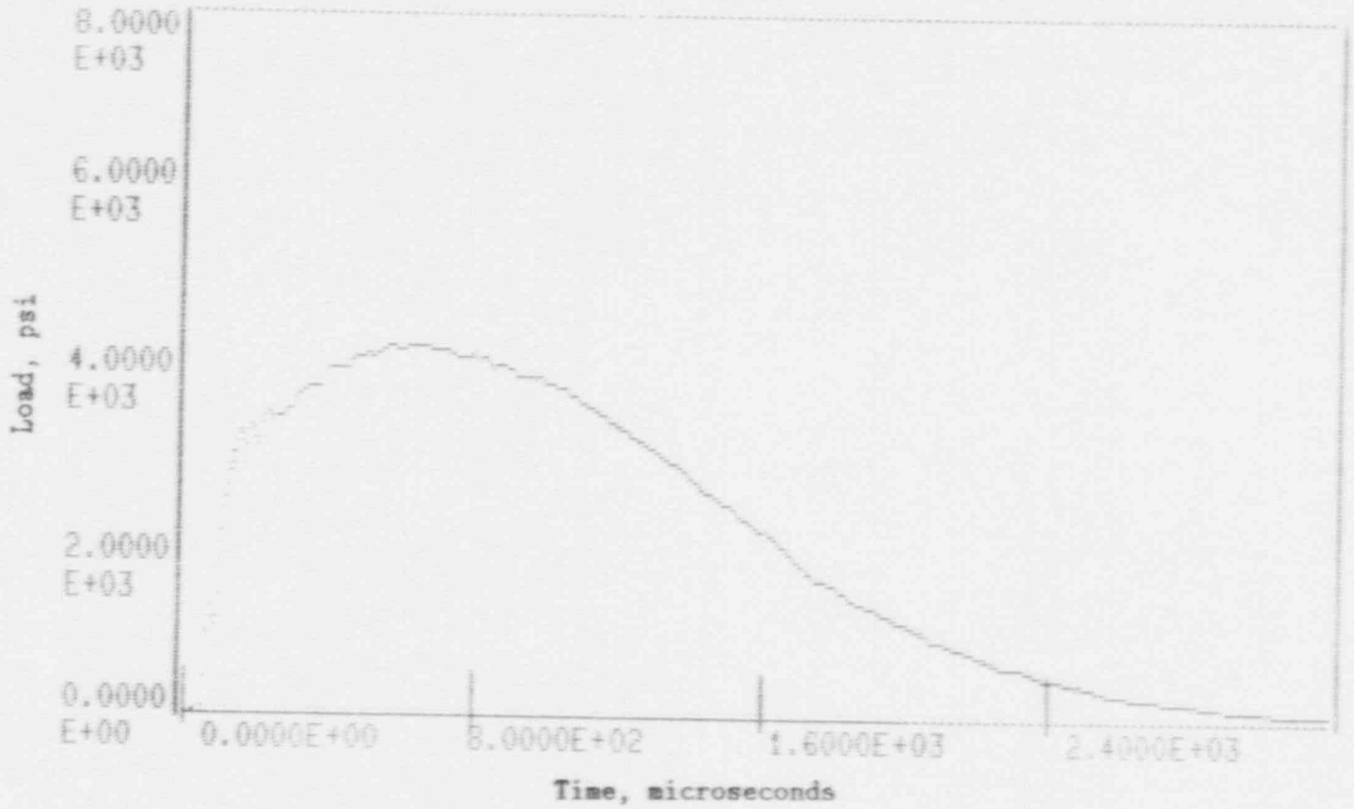

Figure A-57. Load-time record for Specimen PB47.

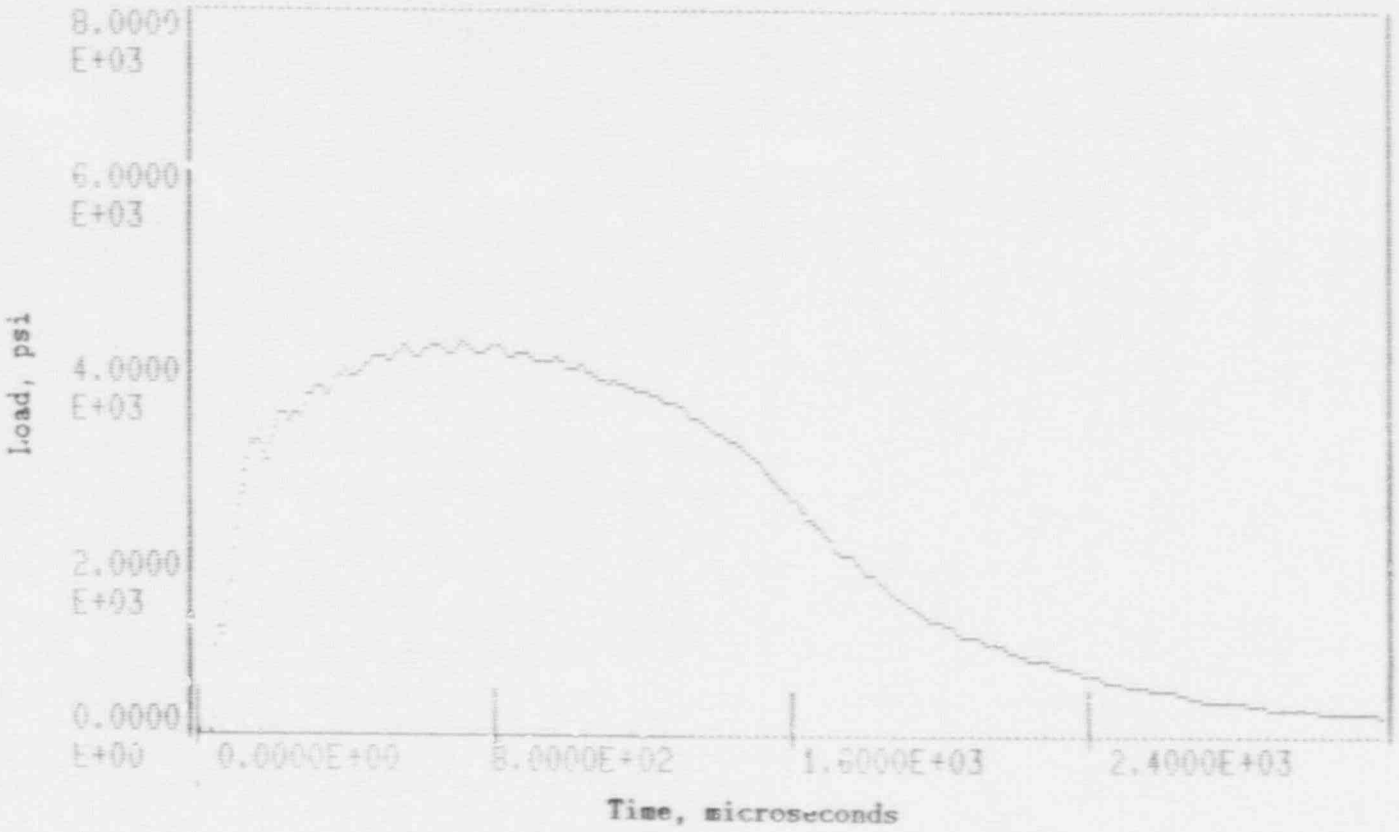

Figure A-58. Load-time record for Specimen PB49.

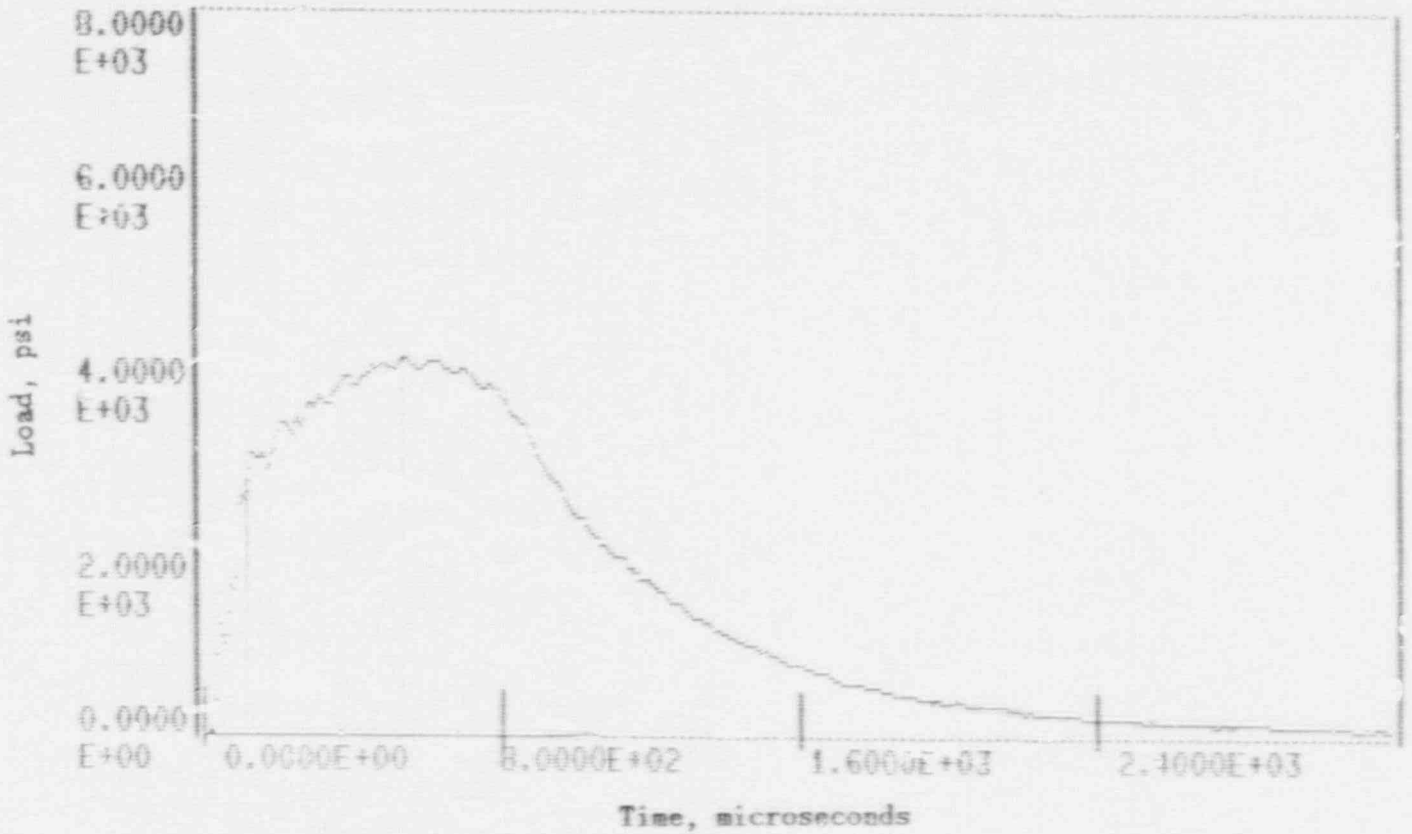

Figure A-59. Load-time record for Specimen PH56.

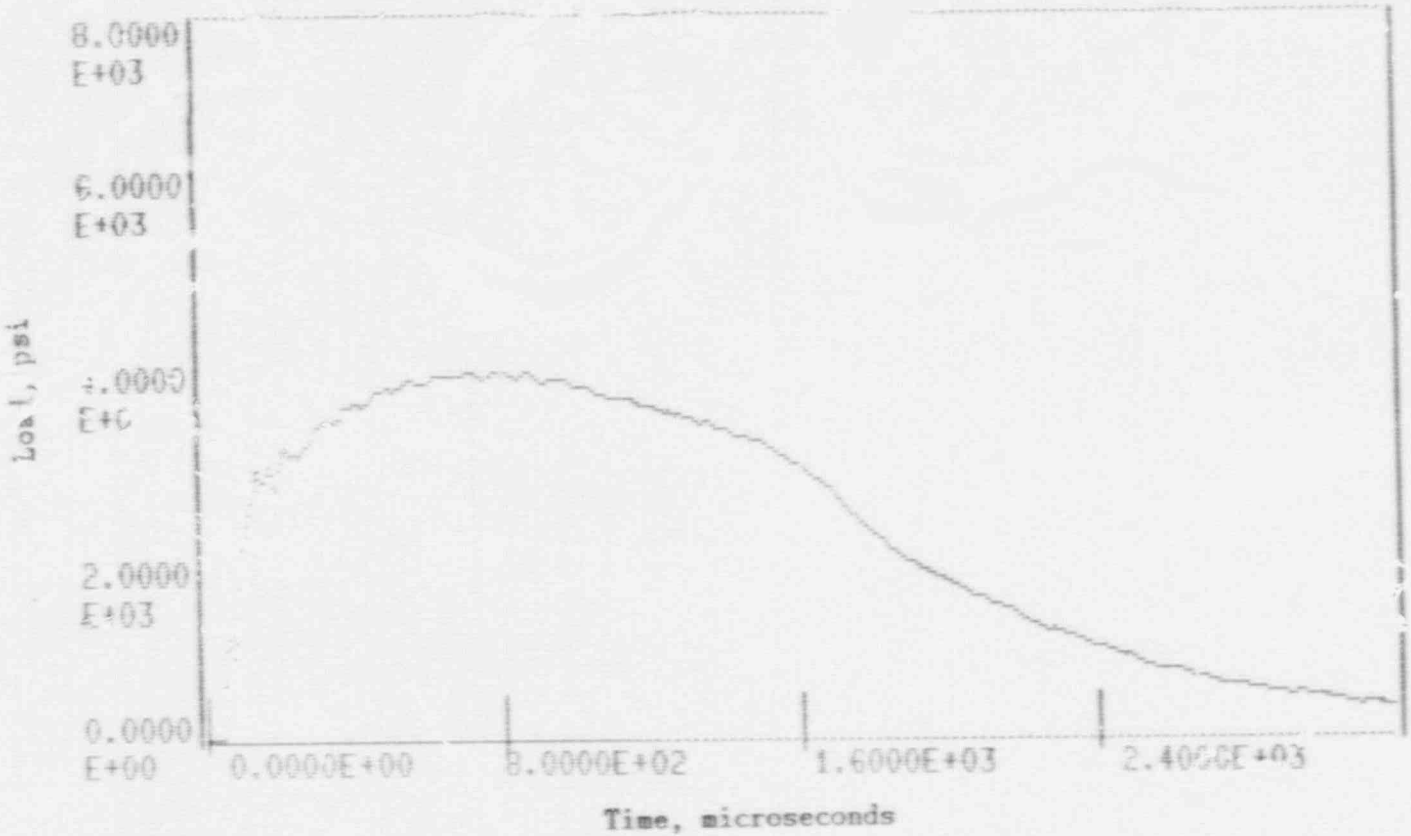

Figure A-60. Load-time record for Specimen PH48.

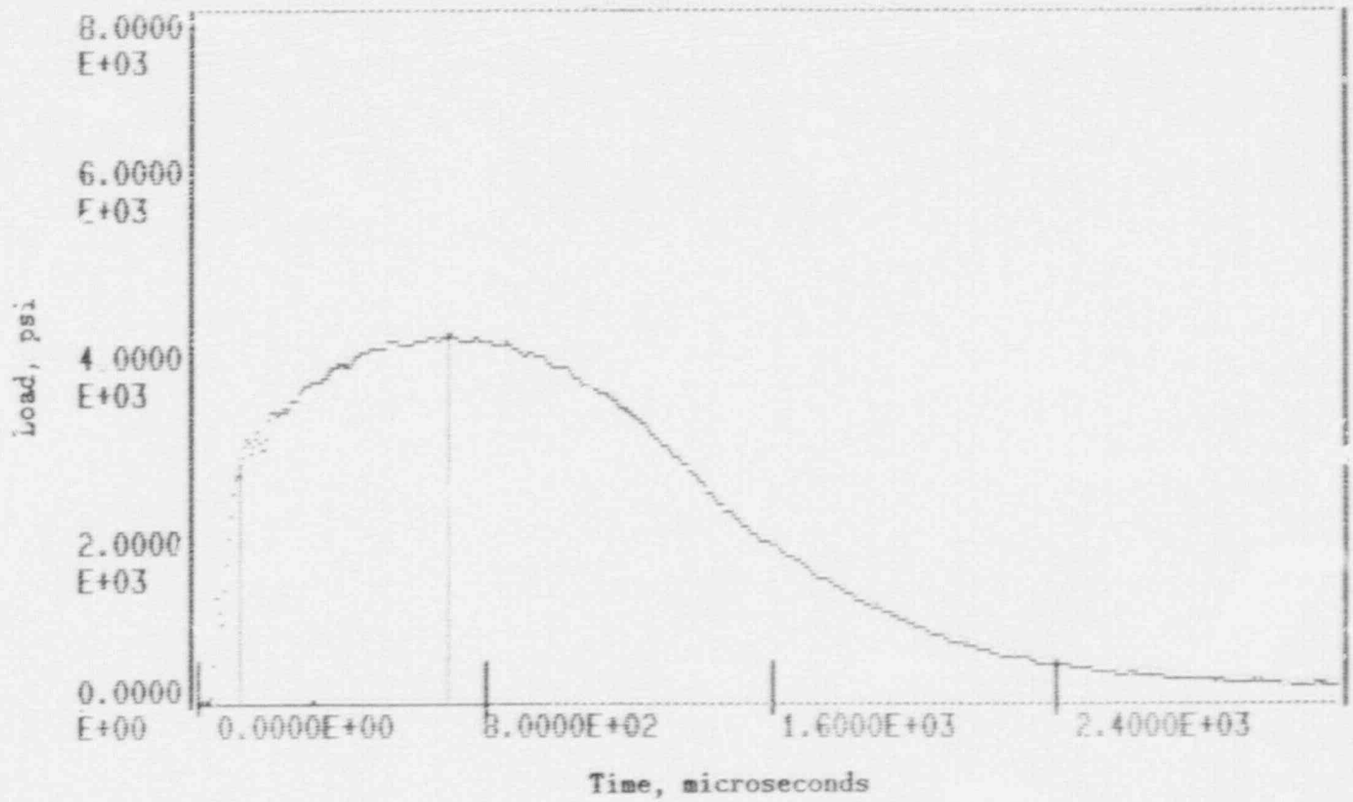

Figure A-61. Load-time record for Specimen PH50.